MEMBRANES FOR OLEFIN/PARAFFIN SEPARATIONS

A Dissertation
Presented to
The Academic Faculty

by

Mita Das

In Partial Fulfillment
of the Requirements for the Degree
Doctor of Philosophy in the
School of Chemical & Biomolecular Engineering

Georgia Institute of Technology
December 2009

MEMBRANES FOR OLEFIN/PARAFFIN SEPARATIONS

Approved by:

Dr. William, J. Koros, Advisor
School of Chemical & Biomolecular Engineering
Georgia Institute of Technology

Dr. Carson Meredith
School of Chemical & Biomolecular Engineering
Georgia Institute of Technology

Dr. Dennis W. Hess
School of Chemical & Biomolecular Engineering
Georgia Institute of Technology

Dr. Satish Kumar
School of Polymer, Textile, Fiber Engineering
Georgia Institute of Technology

Dr. Sankar Nair
School of Chemical & Biomolecular Engineering
Georgia Institute of Technology

Date Approved: August 26, 2009

To Nishant, my husband and best friend,
My parents and my brother

ACKNOWLEDGEMENTS

The last four years at Georgia Tech have been truly life-changing in many ways. Although it is difficult to do justice to everyone who helped and supported me during this period, I am especially grateful to the following individuals for their guidance, support and motivation. Combined together, they made my PhD experience possible, exciting and worthwhile.

First and foremost, I would like to express my sincerest gratitude to my advisor Dr. Bill Koros for his continuous support, encouragement and guidance throughout my entire course of study. His dedication and strong work ethic has been and will continue to be a great source of inspiration to me. I consider myself very fortunate to have him as my mentor as he has been instrumental in my growth as a person and a professional. . I would also like to thank my committee members: Dr. Dennis W. Hess, Dr. Satish Kumar, Dr. James Carson Meredith and Dr. Sankar Nair for their time and valuable insights. I am also grateful to Dr. Stephen Wilson, Dr. Douglas Galloway, Dr. Chunqing Liu and Dr. Travis Bowen from UOP for funding this research and numerous research discussions.

The members of Koros group, past and present, have been great to work with. I would like to especially acknowledge Dr. Imona Omole and Ryan Adams for their support during the early days of my work and for the numerous long and highly productive technical discussions in the laboratory. I would also like to thank Dr. Shabbir Husain, JR Johnson, Jason Ward and Dr. Madhava Kosuri for their help and support throughout my PhD work.

I must also thank others who have played a critical role and helped me stay motivated throughout my PhD program. I am extremely grateful to my family and friends for being supportive. I thank my husband, Nishant Shah, for constantly being enthusiastic about my work and career goals. He always listened to my dreams and ideas and was extremely optimistic. I cannot imagine completing my work without him. I also want to thank my parents and my brother for believing in me and providing unconditional support from the other end of the world. I am also grateful to my childhood friends Swarna Sengupta, Bibhangshu Acharya, Dr. Shiladitya Basu and my parents-in-law for being supportive.

Last but not the least, I wish to thank my Georgia Tech friends, Samirkumar Patel, Dr. Kaushik Roy Chowdhury, Mayumi Kiyono, Dr. Swasti Gupta-Mukherjee, Dr. Neetu Singh and Anwesha Roy Paladhi,, who were always there to share the good and the bad days. I will always cherish the time I spent with all of you over the last four years.

TABLE OF CONTENTS

LIST OF TABLES

Page

LIST OF FIGURES

Page

SUMMARY

The goal of this project was to develop a mixed matrix membrane with enhanced properties for propylene/propane separations. To start with the project, one of the high performance 6FDA based polyimides was identified as the polymer matrix for the rest of the project. The chosen polymer (6FDA-6FpDA) was successfully synthesized in the laboratory.

During the synthesis process the key objectives for high molecular weight and low polydispersity index polymer were identified. High molecular weight 6FDA-6FpDA was achieved via laboratory synthesis and was tested successfully.

After successful synthesis of the high performance polymer, pure polymer dense films were tested for transport properties. One problem identified with 6FDA-6FpDA polymer films for propylene/propane separations was plasticization. A major objective of this research was to develop a method for plasticization suppression. A carefully controlled annealing procedure with high temperature permeation experiments was used in this research to suppress plasticization in a mixed gas environment. To the best of our knowledge, this is for the first time plasticization suppression was achieved with pure polymeric membrane material for propylene/propane separations with pure and mixed gases. The observed mixed gas experimental selectivity was lower than the pure gas selectivity which was explained by the combination effect of dual mode and bulk flow effect.

The last objective of this project was to successfully incorporate molecular sieve materials to form a mixed matrix membrane hybrid material with enhanced transport properties First, an ideal molecular sieve for propylene/propane separation was identified and characterized. AlPO-14 was chosen for this research following its success with propylene/propane pressure swing adsorption. Mixed matrix membranes were successfully produced and tested for enhanced transport properties. Both pure and mixed gas results showed promising results with enhanced propylene permeability and propylene/propane selectivity. The experimental results were modeled with the Cussler and Maxwell models. A modified Cussler model was presented in this work. This is the first time an enhancement in the transport properties with mixed matrix membrane for propylene/propane separations has been observed. This fundamental dense film work holds a bright future for the scale up of propylene/propane separations.

CHAPTER 1

INTRODUCTION

1.1. Current Propylene Supply and Demand

Propylene is the second most important feedstock in the petrochemical industry behind ethylene [6]. Major propylene derivatives include plastics (polypropylene – PP), acrylonitrile, propylene oxide, cumene/phenol, oxo alcohols, acrylic acids, isopropyl alcohol, oligomers and other chemicals, which enable the manufacture of other chemicals and plastics. Some of these products are: propylene glycols for paints, automotive brake fluids and household detergent; polypropylene fibers for carpeting; ABS resins for telephones and automotive trim parts molded. Moreover, propylene is also consumed in refinery operations for gasoline production. Figure-1.1 shows product wise global propylene consumption.

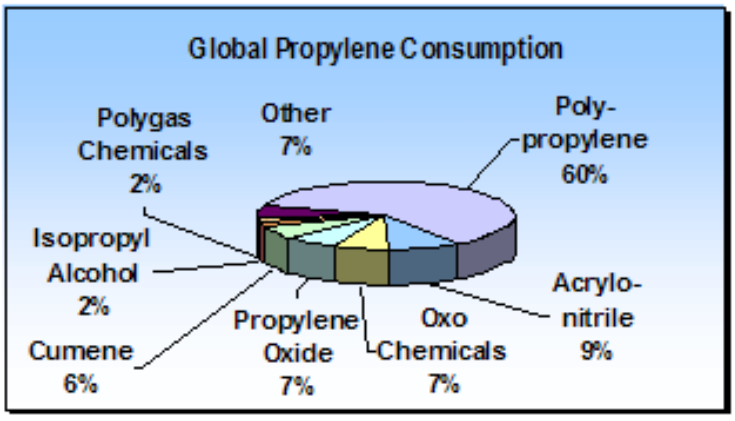

Figure-1.1: Propylene product consumption [1]

The global demand of propylene was 16.4 million tons in 1980. In 2005, it was approximately 68 million tons indicating a 6% average annual growth. This demand is expected to reach 81 million tons in 2010 (as projected by CMAI [2, 3, 4]). The increase in propylene demand is mainly driven by polypropylene demand which is expected to grow at 7%. Figure-1.2 shows the supply and demand projection by CMAI in million metric tons.

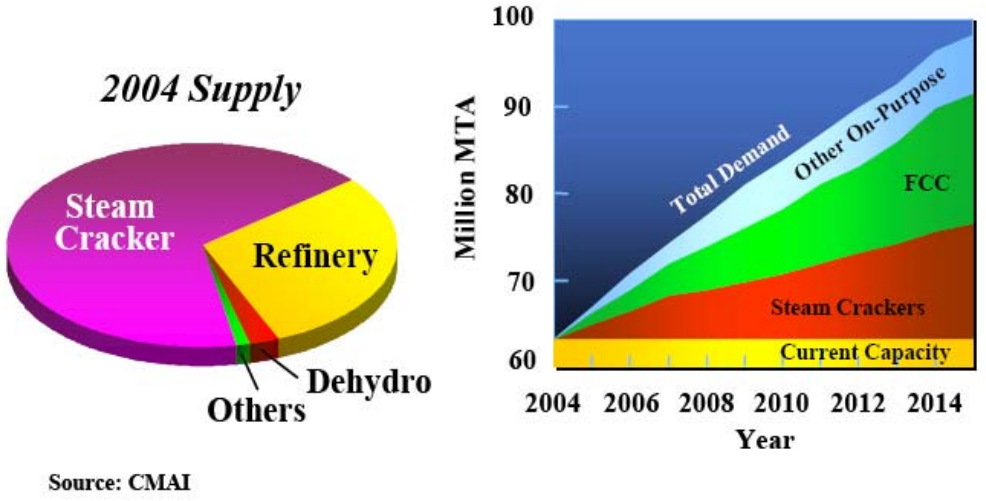

Figure-1.2: Global demand of propylene as projected by CMAI [2]

Propylene is largely a byproduct of ethylene production, which is the largest volume organic produced in the U.S. Generally, two grades of propylene are used – chemical grade (92-94 wt%) and polymer grade (99.0-99.8%). About 70 percent of this propylene is generated by steam crackers and 28 percent by refinery FCC units. Some other routes for propylene generations are propane dehydrogenation, natural gas to olefins and olefin conversions.

1.2. Propylene Production Overview

As mentioned in the previous section, propylene is mainly produced as a byproduct of steam cracking process used to produce ethylene. In this process, a hydrocarbon mixture is preheated with steam to 600^0C and then subsequently cracked at 700 ^{0}C – 900^0C. This process produces 0.67 tons of ethylene and 0.33 tons of propylene for each ton of light olefin produced. Since ethylene is the main product of this process, this process is largely influenced by the ethylene demand and hence the availability of propylene is determined by the market demand of ethylene [2, 5].

The second largest source of propylene is the FCC (fluid catalytic cracking) units, wherein the primary product of this operation is gasoline. Other co-products are dry gas, liquefied petroleum gas (LPG), decanted oil and coke. LPG is rich in light olefins. The FCC process uses partially vaporized gas oil in the presence of a zeolite catalyst around 3 atm pressure and a temperature of ~ 450^0C – 600^0C. Conventional FCC unit yields around 4-7 wt% propylene. Since in both the cases, propylene is produced as a byproduct of ethylene/gasoline production, various methods of "on-purpose" propylene production methods have been extensively investigated recently due to the continuously increasing demand of propylene [2]. Some of these processes are highlighted below.

Propane dehydrogenation is one of the most attractive options for on-purpose propylene production because propylene is the only product. Currently 2.5% of the worldwide propylene supply is produced via propane dehydrogenation. The Olefix® process developed by UOP is used mainly for this process (six out of eight currently

operating plants use Olefix® [2]). In this process, the endothermic reaction is carried out in the presence of a catalyst (for the Olefix® process it is platinum on aluminum catalyst).

Another popular on-purpose propylene production technique is the "Methanol to Olefin" (MTO) process. In this process, propylene and ethylene are the main products with trace of C_5 co-products. A second process, "methanol-to-propylene" (MTP) produces propylene and gasoline as products. MTO units can be well combined with the current FCC and steam cracking units. The UOP/HYDRO process, developed by UOP uses a silicoaluminophosphate catalyst (SAPO-34) for this conversion.

1.3. Propylene/Propane Separations

Although there is an increasing demand for on-purpose propylene production, steam cracking and FCC processes are still the main sources of propylene till date. Unfortunately none of these processes produces pure enough propylene that can be used directly. To achieve the desired grade of propylene, additional separation/purification steps are required. Currently, the separation of olefin and paraffin components is performed by cryogenic distillation, which is expensive and energy intensive due to the low relative volatilities of the components (b.p. of propylene is -47^0C and propane is -42.1^0C). The necessary columns are normally 300 feet tall and contain over 200 trays [5]. Due to the height of the column, two splitters are usually required instead of one. Around 1.2×10^{14} BTU/year energy is used for olefin/paraffin separations. The bottom product of C_3 splitter tower is propane rich, while the overhead product is high purity

propylene. A typical propylene recovery unit from the co-products of FCC unit is shown in Figure-1.3.

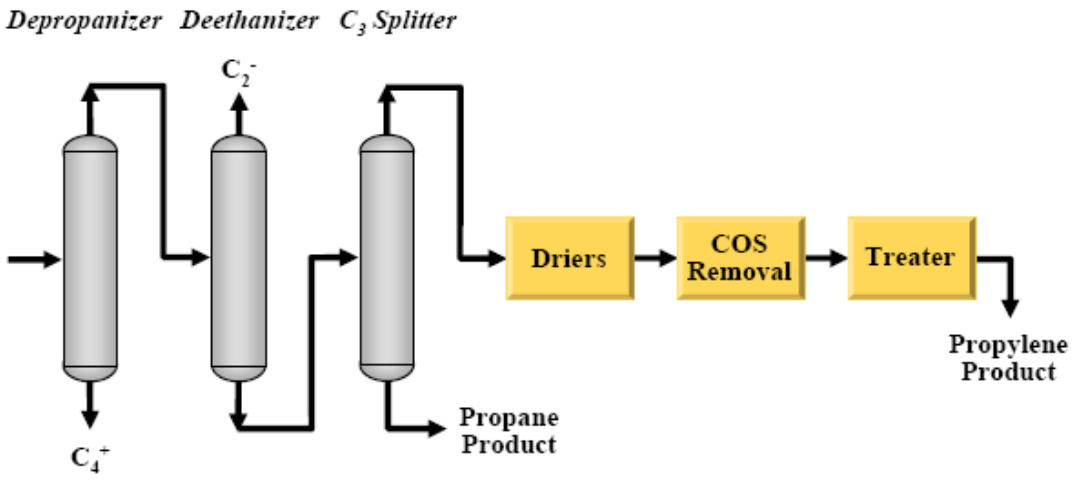

Figure-1.3: Propylene recovery unit [2]

Due to the cost and complexity of distillation, membrane separation is gradually gaining popularity for propylene/propane separations. Baker predicts that the membrane market will reach $30 million by 2010 and $125 by 2020 for vapor/vapor gas separations [6]. In the case of propylene/propane separations, it is unlikely that a membrane unit will completely replace a C_3 splitter because of the purity limitations, but it can obviously be used to debottleneck a process and increase the purity of the feed-stream of a C_3 splitter.

Another attractive application of membrane for propylene/propane separation is the use of a membrane unit in a polypropylene production plant. In a polypropylene reactor, propane enters as an impurity (99% propylene and 1% propane) and eventually builds up in the reactor. Propane buildup is controlled by continuously removing a

recycle stream which is then flared. With every mol of propane purged, 2-3 mol of propylene monomer is lost incurring a $1 million loss per plant every year [6]. A membrane unit installed before sending propane to flare is an attractive separation option. Figure-1.4 and Figure-1.5 show these two possible membrane applications for propylene/propane separations.

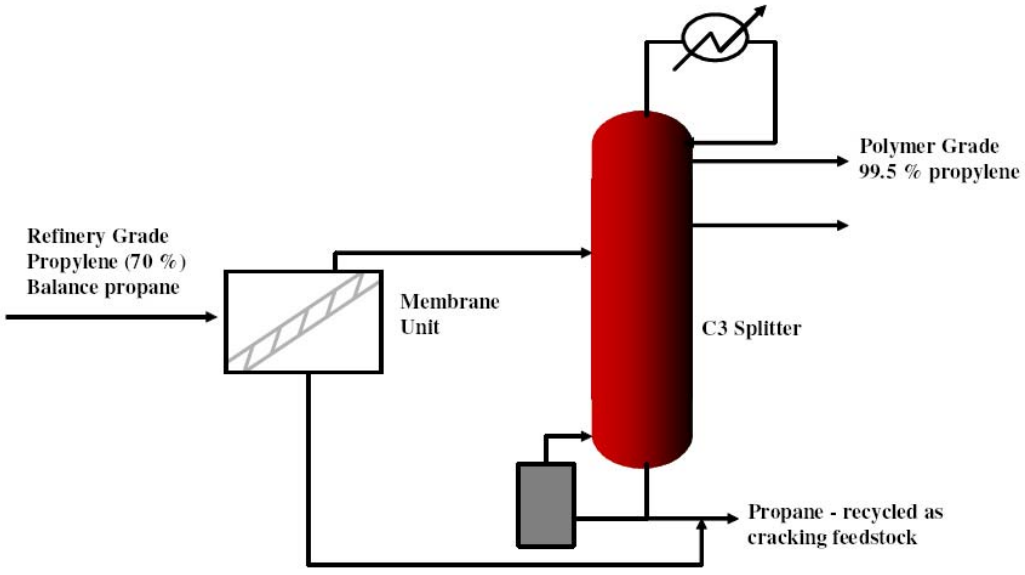

Figure-1.4: Membrane unit installed as a hybrid process for propylene/propane separations [7, 8]

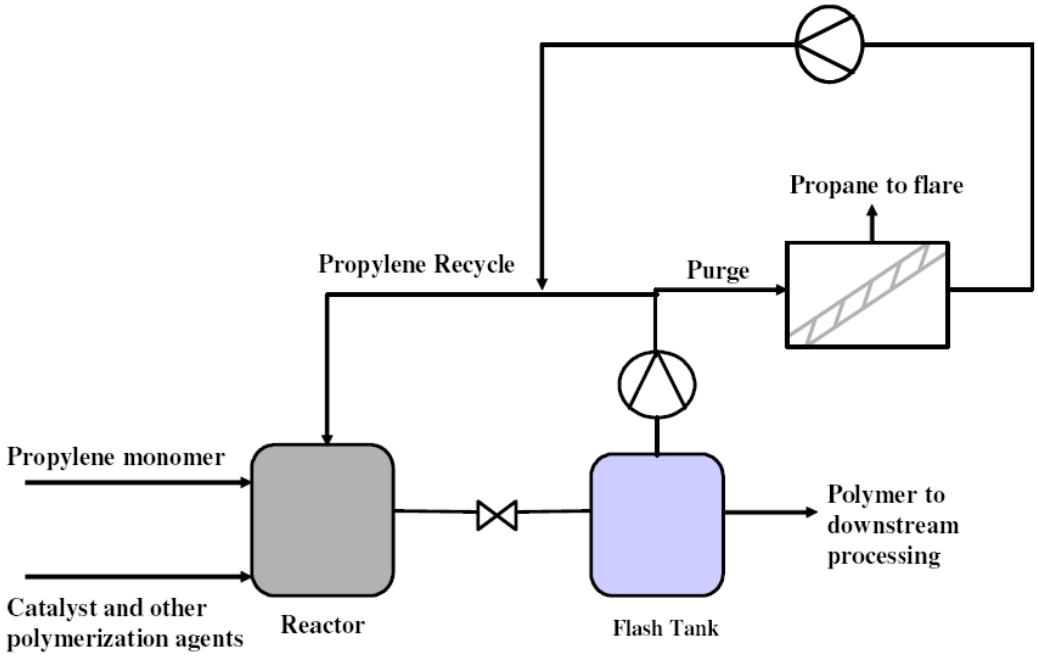

Figure-1.5: Use of membrane unit to recover propylene in a polypropylene production plant [6, 8]

Studies have shown that several polymeric membranes offer promising potential, but separation selectivity needs to be improved to be used as a cost effective separating membrane. Considerable research has been done in glassy polyimides, and polyimide-co-polypyrrolones with polyimides based on 6FDA (4,4'-(hexafluorisopropylidene)dipthalic anhydride) exhibiting the best performance [8]. On the other hand, carbon molecular sieve and zeolite membranes potentially offer superior selectivities; however, they are brittle and too costly (> $150/sq foot) to be commercially useful for large scale applications.

This research aimed to increase the selectivity of propylene/propane separation through 6FDA based polyimides. A "mixed matrix" material approach has been used in this study to create a hybrid material with superior properties to the polymer membrane. The next section describes the specific research objectives of this study.

1.4. Research Objectives

1. Identify and successfully synthesize a high performance 6FDA based polymer for propylene/propane separation.

To surpass the pure polymer permeability and selectivity upper bound line, it is wise to select a polymer with intrinsically attractive properties on or near the upper bound. An aspect of this project was to be able to synthesize high performing; high molecular weight polymer which can be used in future works as dopes for hollow fiber membranes. Commercially available polymers (e.g. Matrimid) are not on the upper bound, but three polymers 6FDA-DDBT, 6FDA-6FpDA and 6FDA-DAM respectively appear attractive [8]. The highest performing, yet easily bulk-processable, polymer from the above three materials is preferred for future hollow fiber production, since hollow fiber membranes provide high surface/area ratio. For a workable hollow-fiber dope high M_w is very desirable, since it enhances asymmetric membrane formation by increasing the chain entanglement. In addition, higher molecular weight tends to yield membranes with increased mechanical strength, compared to the relatively brittle membranes. Low molecular weight polymers therefore must be avoided by engineering the polymerization, imidization steps. In this objective an easily processable, high molecular weight polymer will be chosen and synthesized. Several parameters during the synthesis process (e.g. monomer purity, reaction temperature, precipitation method) will be explored and reported.

2. Determine the efficacy of annealing and high test temperature to suppress plasticization.

Propylene and propane tend to plasticize 6FDA based polymer at moderately high pressure at 35^0C. Plasticization occurs as a result of swelling in the polymer and as a result an upswing in the propylene permeability occurs, suppressing the selectivity. To suppress the plasticization phenomenon annealing the pure polymer dense films will be explored as an approach to stabilize the polymer and suppress excessive swelling in the presence of high pressure feeds. High temperature permeation will be performed. We are planning to perform experiments at 35^0C and 70^0C. Systematic annealing of the samples will also be explored.

This objective will cover extensive permeation characterization and analysis of the high molecular weight (low PI) 6FDA polymer based pure dense films. A detailed comparison between unannealed and annealed films will be shown. Optimization of the annealing temperature will also be explored. The effect of high and low molecular weight polymers in permeability and diffusivity will be shown via sorption and permeation dual mode model. Annealing effect in terms of plasticization suppression, permeability and selectivity will be discussed. Pure gas and mixed gas results at 35^0C and 70^0C will be discussed.

Results of pure gas sorption experiments using a pressure decay method with unannealed and annealed films at 35^0C and 70^0C will be discussed. These sorption experiments will be used to analyze the permeation data using the dual-mode model.

Mixed gas results will be explained and compared with the available literature data. Two models, dual mode model and bulk flow model will be used to analyze mixed gas data and the results will be presented.

3. Demonstrate the efficacy of dispersed molecular sieve particles to increase the permeability-selectivity tradeoff performance of mixed matrix material beyond the existing pure polymer upper bound performance under realistic feed conditions at elevated pressure (up to 400 Psia) and temperature (up to 90 °C).

The key objective in this study involves "mixed matrix" hybrid material approach with highly selective aluminophosphate molecular sieves. Aluminophosphate, AlPO-14 group materials are planned for this work. Wilson et al synthesized AlPO-14 [10], a small pore aluminophosphate molecular sieve, which selectively adsorbed propylene and essentially excluded propane [9]. AlPO-14 has various crystalline structures essentially composed of tetrahedral AlO_4 and PO_4 units. Unlike zeolites, AlPO-14 does not have framework charge balancing cations. The pore window diameter of AlPO-14 is 3.8 A with a crystalline structure which is capable of excluding the entry of propane by a steric hindrance effect which prevents the propane from entering into the internal pore/channel structure, while allowing slightly more compact propylene [9].

The efficacy of mixed matrix membrane in increasing the permeability-selectivity tradeoff performance of mixed matrix material beyond the existing pure polymer upper bound performance will be discussed. Selection of AlPO-14 and characterization of pure sieve properties will be discussed in details. Mixed matrix formation protocol will be described. Both pure and mixed gas results will be shown. Mixed gas results will be shown in two different temperatures 35^0C and 70^0C. Results from objective-2 will be

used as pure film properties for model prediction. The experimental results will be compared with Maxwell and Cussler models and any deviation will be addressed.

1.5. References

1. http://www.dow.com/productsafety/finder/pro.htm, August 12, **2009**

2. Mark Houdek, James Anderson, *"On-Purpose" propylene technology developments* Presented at the ARTC 8th Annual Meeting, 29th April **2005**, Kuala Lumpur

3. World Propylene Supply Study - *http://www.cmaiglobal.com/news/wpss.pdf (2001)*

4. *The Propylene Chain*. **1998**, U.S. Department of Energy.

5. B. R. Eldridge, *Olefin/Paraffin Separation Technology: A Review.* Ind. Eng. Chem. Res., 1993. **32**: p. 2208-2212.

6. R.B. Baker, *Future directions of membrane separation technology* Ind. Eng. Chem. Res. **41**: p. 1393-1411.

7. C. Staudt-Bickel, W.J.Koros, *Olefin/paraffin gas separation with 6FDA-based polyimide membranes*. JMS, 2000. **170**: p. 205-214.

8. R. L. Burns, W.J. Koros, *Defining the challenges for C_3H_6/C_3H_8 separation using polymeric membranes*. JMS, 2003. **211**: p. 299-309.

9. L. S. Cheng, Joel Padin, Salil U Rege, Stephen T Wilson, Ralph T Yang, *process of purifying propylene* USPTO **2002** 6,406,521

10. Wilson; Stephen T, Lok; Brent M, Flanigen; Edith M; *Crystalline metallophosphate compositions* **1982** USPTO 4,310,440

CHAPTER 2

BACKGROUND AND THEORY

2.1. Abstract

The first part of this chapter describes the essential theories of membrane gas separations used through the entire research. Permeation, sorption and dual mode gas transport properties have been described. Frame of reference model also has been described. In the later part of the chapter a summary of the polymeric gas separation background and the work so far in the field of the propylene/propane pure polymer gas separations has been described. Plasticization under the influence of condensable gases has also been discussed. Lastly, a synopsis of the ideal molecular sieves for propylene/propane has been discussed.

2.2. Membrane Transport Properties

Two different types of membrane have been studied in this research: pure polymeric membrane and mixed matrix membrane. As mentioned earlier, mixed matrix membrane is a membrane combining polymeric material and inorganic molecular sieves where molecular sieves are dispersed in a continuous polymeric phase. The basic general mechanism for gas separations via these two membranes are same and are characterized by the same parameters. The next section describes these parameters in details.

2.2.1. Permeation

Transport of gases through polymers occurs according to the solution-diffusion theory [1]. Gas molecules are introduced at the high pressure upstream side of the membrane where they "sorb" into the membrane. The amounts of sorption depend on the material and the gas penetrants. Gas molecules then diffuse through the membrane to the lower pressure side where they then desorb. Thermodynamic equilibrium on either side of the membrane is also considered during the transport process. Figure-2.1 shows the membrane solution-diffusion process schematically.

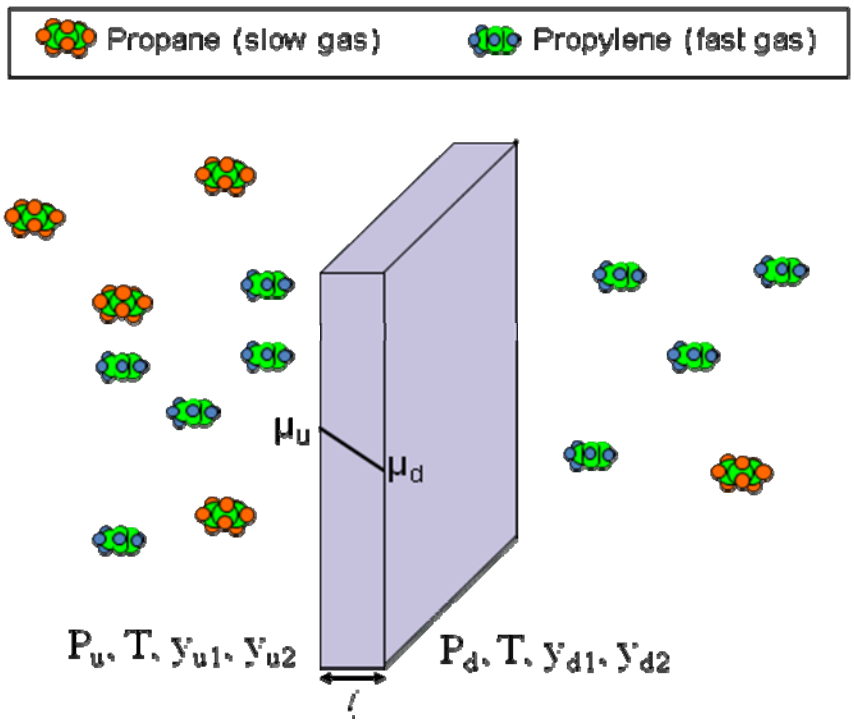

Figure-2.1: Gas separation through a polymeric film.

Fick's First Law governs the diffusion in the absence of bulk flow and is expressed as:

$$J = -D\nabla C \qquad [2.1]$$

where J is the diffusive flux, D is the diffusion constant and C is the local gas penetrants concentration. Thus diffusion of gas penetrants in one dimension is given by:

$$J_A = -D_A \frac{\partial C_A}{\partial x} \qquad [2.2]$$

Permeability of a gas is defined as the flux normalized to the pressure difference of the membrane.

$$P_A = Flux.\frac{l}{\Delta p_A} = J_A.\frac{l}{\Delta p_A} \qquad [2.3]$$

where Δp is the pressure difference across the membrane between upstream and downstream and l is the thickness of the membrane. The most common unit for permeation is Barrer where 1 Barrer = 10^{-10} $cc.(stp)/(cm^2.sec.cmHg)$.

The external penetrant pressure p_A and the equilibrium concentration within the membrane follow a linear relationship according to Henry's law and can be expressed as:

$$C_A = S_A p_A \qquad [2.4]$$

where S_A is the sorption coefficient of a penetrant. The permeability coefficient of a penetrant then can be described as the product of a kinetic parameter, D_A and a thermodynamic penetrant, S_A [2], viz,

$$P_A = Flux.\frac{l}{\Delta p_A} = -\frac{D_A(\partial C_A / \partial x)}{\Delta p / l} = \frac{D_A(C_2 - C_1)}{\Delta p} = D_A S_A \qquad [2.5]$$

For a selected gas pair, the separation factor or the selectivity (the efficiency of a membrane) can be expressed as the ratio of the mole fractions of the two gas penetrant components A and B in the downstream and upstream y_i and x_i respectively,

$$\alpha_{AB} = \frac{(y_A / y_B)}{(x_A / x_B)} \qquad [2.6]$$

with a negligible downstream pressure compared to the upstream, the selectivity is known as ideal selectivity and is expressed as,

$$\alpha^*_{AB} = \frac{P_A}{P_B} = \left(\frac{D_A}{D_B}\right)\left(\frac{S_A}{S_B}\right) \qquad [2.7]$$

In other words, the selectivity can be explained as the product of mobility selectivity and

solubility selectivity. For a particular gas pair penetration, respective permeabilities are the productivities of the particular gases and the selectivity is the efficiency of that gas pair.

2.2.2. Sorption

The sorption in glassy polymers is represented by a dual mode model, which accounts for penetrants in the normally densified and "microvoid" regions of the polymer matrix. Specifically, the model accounts for the differences in gas transport properties in both the idealized Henry's law and Langmuir domains of a glassy polymer [5-7]. The Langmuir concentration C_{HA}, for gas A, describes sorption in the "microvoid" or "holes" throughout the matrix, which are the packing defects in the non-equilibrium glassy matrix. The sorption in glassy polymers is given by [1],

$$C_A = C_{DA} + C_{HA} \qquad [2.8]$$

The pressure dependence of permeability for a single component is given by:

$$C_A = k_{DA} p_A + \frac{C'_{HA} b_A p_A}{1 + b_A p_A} \qquad [2.9]$$

where k_{DA} is the Henry's law constant, C'_{HA} is the Langmuir capacity constant, and b_A is the Langmuir affinity constant. The C'_{HA} term characterizes the amount of unrelaxed free volume in the glassy matrix accessible for additional sorption beyond that in a densified matrix, and it allows description of the non-equilibrium nature of such materials. The affinity constant, b_A is the measure of polymer's attraction for the gas penetrants to sorb into the excess unrelaxed volume. The sorption coefficient S_A is then given by combining Equations 2.8 and 2.9. Equation 2.10 represents S_A in terms of partial pressure.

$$S_A = \frac{C_A}{p_A} = k_{DA} + \frac{C'_{HA} b_A}{1 + b_A p_A} \qquad [2.10]$$

2.2.3. Diffusion In Polymers

Gas molecules diffuse through a dense polymer membrane by random jumps from one position to the other. The schematic of diffusion is shown in Figure-2.2, in which λ is the average length of random diffusion jump [3, 4].

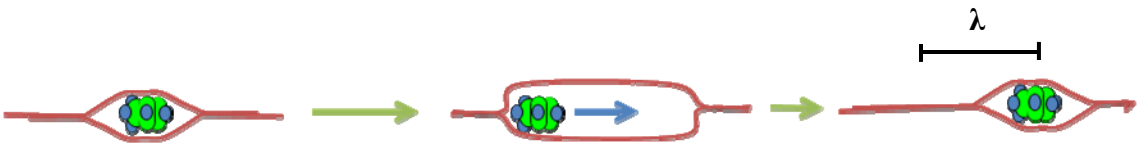

Figure-2.2: Example of diffusion through polymeric membranes. λ is the length of random diffusion jump

The rate of diffusion for a particular gas molecule depends on the frequency and the length of the random diffusion jump. In polymers, this is governed by the thermal fluctuations, which vary according to the polymeric chain structures. In case of glassy polymers, the thermal volume fluctuation is low giving much higher diffusion selectivity.

Another important parameter for polymeric gas separations is the free volume of the polymer. The specific free volume is the difference between the specific volume of the polymer and the specific volume occupied by the polymeric chain. Free volume of a polymer can be tuned by introducing bulky groups. In this case, the diffusion rate of a gas becomes faster and the flux increases. Especially in the case of rigid glassy polymers, introduction of bulky functional groups increase the diffusion of a gas, providing a way to create a high performing polymer for a particular gas pair separation (high selectivity and permeability).

Like sorption, diffusion also can be expressed as by the dual mode model. The dual mode mobility model can be written as [1]:

$$J_A = -D_{DA}\frac{\partial C_{DA}}{\partial Z} - D_{HA}\frac{\partial C_{HA}}{\partial Z} \qquad [2.11]$$

Where D_{DA} is the diffusion coefficient of A through the Henry's law environments, and D_{HA} is the diffusion coefficient of A through the Langmuir environments. Combining this flux model with the sorption model allows one to develop an expression for the permeability of A for the case with p_A upstream and a vacuum downstream, viz.

$$P = k_{DA}D_{DA} + \frac{C'_{HA}D_{HA}b_A}{1 + b_A p_A} \qquad [2.12]$$

It is possible to fit the dual mode parameter for permeability versus pressure data with sorption parameters. The sorption parameters are calculated by fitting a curve of C_A vs. p_A. Equation 2.9 is used for sorption parameters. Once the sorption parameters are known, a plot of permeability versus pressure can then be constructed. The straight line fit of the above plot then directly calculates D_{DA} and D_{HA} for a particular gas. More detailed analysis of these parameters and observations with 6FDA-6FpDA polyimide are discussed in Chapter 5.

Another important application of the dual mode model is the prediction of mixed gas behavior [8, 9]. When a mixed gas is introduced in the upstream of a membrane system, the sorption can be described as:

$$C_A = k_{DA} p_A + \frac{C'_{HA} b_A p_A}{1 + b_A p_A + b_B p_B} \qquad [2.13]$$

where, A and B are two different gases (e.g. propane and propylene). In this case we can predict the permeability of gas A in a gas mixture. The permeability equation for gas A, for the case of a vacuum downstream is then given by [8]:

$$P_A = k_{DA} D_{DA} + \frac{C'_{HA} D_{HA} b_A}{1 + b_A p_A + b_B p_B} \qquad [2.14]$$

Similarly, P_B can be calculated and finally the selectivity for a mixed gas pair can be calculated simply by taking the ratio of two permeabilities ($\alpha = P_A/P_B$). This model can be extended to the analysis of permeation data and is also known as the partial immobilization model [8]. In the above equation, two terms are introduced,

$$F_A \equiv \frac{D_{HA}}{D_{DA}} \qquad [2.15]$$

$$K_A = \frac{C'_{HA} b_A}{k_{DA}} \qquad [2.16]$$

K_A is defined as the equilibrium relationship between the dissolved mode (Henry's region) and the hole filling mode (Langmuir region). Equation 2.14 can be then rewritten as:

$$P_A = k_{DA} D_{DA} \left(1 + \frac{F_A K_A}{(1 + b_A p_A + b_B p_B)} \right) \qquad [2.17]$$

2.2.3.1. Frame of reference/bulk flow model

In all of the above derivations from Fick's law, the frame of reference terms were not considered. In a mixed gas environment, the flux of each component can be very dependent of each other which are not considered in Equation 2.17 [10, 11]. In this environment, the flux of each component is the sum of the diffusive flux and the bulk or convective flux in a polymer. Equations 2.18-2.21 are the bulk flow contribution expressions in case of a mixed gas. In other words, when a mixture of propylene and propane is introduced in the membrane upstream, if the flux of propylene is large enough, its coupling with propane causes the diffusive and convective flux of propane to be of the same order of magnitude [10].

$$n_A = n_A^{bulk} + n_A^{diffusion} \qquad [2.18]$$

$$n_A = (n_A^k + n_B + n_P)\omega_A - \rho D_{A,m}\frac{d\omega_A}{dx} \quad [2.19]$$

$$n_B = (n_A^k + n_B + n_P)\omega_B - \rho D_{B,m}\frac{d\omega_B}{dx} \quad [2.20]$$

$$n_P = (n_A^k + n_B + n_P)\omega_P - \rho D_{P,m}\frac{d\omega_P}{dx} \quad [2.21]$$

In the normal case of a stationary membrane, the polymeric flux term is zero (n_P). Replacing n_p with zero in Equations 2.19-2.21, the mutually dependent flux for each gas component (A and B) can be derived and consequently expressed by Equations 2.22-2.24:

$$n_A = \frac{-\rho D_{DA}\frac{d\omega_A}{dx}}{\left[1-\left(1+\frac{1}{r}\right)\omega_A\right]} \quad [2.22]$$

$$n_B = \frac{-\rho D_{DB}\frac{d\omega_B}{dx}}{\left[1-(1+r)\omega_B\right]} \quad [2.23]$$

$$r = \frac{n_A}{n_B} \quad [2.24]$$

In the above equations, ω is the mobile concentrations of the penetrants A and B. ω_A and ω_B are defined by Equations 2.25-2.26.

$$\omega_A = \omega_A^{mobile} = \frac{k_{DA} p_A M_A}{22400\rho}\left(\frac{1+F_A K_A}{1+b_A p_A + b_B p_B}\right) \qquad [2.25]$$

$$\omega_B = \omega_B^{mobile} = \frac{k_{DB} p_B M_B}{22400\rho}\left(\frac{1+F_B K_B}{1+b_A p_A + b_B p_B}\right) \qquad [2.26]$$

Once ω_A and ω_B are calculated, the following boundary conditions are then defined for the pressure and mobile concentrations for A and B for upstream and downstream of the membranes.

$$at\ x = 0;\ p_A = p_{A,up};\ p_B = p_{B,up};\ \omega_A = \omega_{A,up};\ \omega_B = \omega_{B,up}$$

$$at\ x = l;\ p_A = p_{A,d};\ p_B = p_{B,d};\ \omega_A = \omega_{A,d};\ \omega_B = \omega_{B,d}$$

The following flux expressions (accounting for the bulk flow effect) are then obtained using the above boundary conditions for penetrants A and B:

$$n_A = \frac{\rho D_{DA}}{l} . \frac{\ln\left(\frac{1-\omega_{A,d}\left(1+\frac{1}{r}\right)}{1-\omega_{A,up}\left(1+\frac{1}{r}\right)}\right)}{\left(1+\frac{1}{r}\right)} \qquad [2.27]$$

$$n_B = \frac{\rho D_{DB}}{l} . \frac{\ln\left(\frac{1-\omega_{B,d}\left(1+r\right)}{1-\omega_{B,up}\left(1+r\right)}\right)}{\left(1+r\right)} \qquad [2.28]$$

The above equations can be used to obtain the permeability using the frame of reference (Equation – 2.29). The process is an iterative where an initial guess value of r is guessed and then used to solve for n_A and n_B iteratively. A good guess value of r is the ratio of n_A and n_B neglecting the r term in the Equations 2.27 and 2.28 [10].

$$\frac{P_A}{l} = \frac{22400 . n_A}{M_A . \Delta p_A} \qquad [2.29]$$

2.2.4. Sorption and Diffusion Through Molecular Sieves

Zeolite and other aluminosilicate and carbon molecular sieves consist of ultra-micropores. They are promising due to the discrimination capabilities of small molecules [12-17]. The sorption process follows the Langmuir sorption model and is similar to the Langmuir sorption in the polymer. In case of a molecular sieve, since there is no Henry's densified region, solubility only comes from Langmuir sorption site. In this case, Equation-2.9 can be re-written as:

$$C_A = \frac{C'_{HA} b_A p_A}{1 + b_A p_A} \qquad [2.30]$$

At high pressure, the sorption sites become saturated. At steady state, the sorbed molecules diffuse through the molecular sieves via random jumps through the interconnecting channels. Zeolites separate gas pairs depending on the relative differences in the shapes and the sizes of the molecules. Figure-2.3 illustrates the molecular sieving nature.

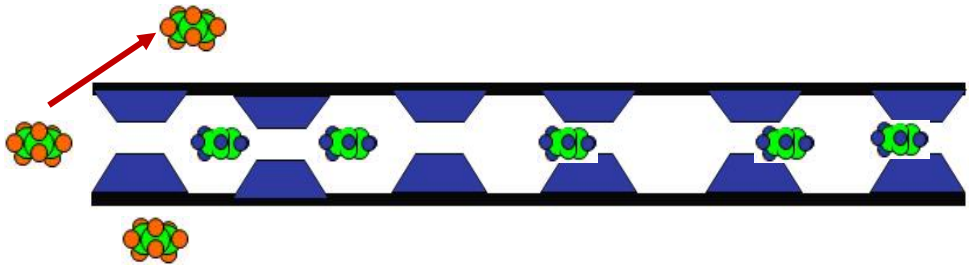

Figure-2.3: Molecular sieving process for propylene/propane separations.

2.3. Temperature Dependence of Gas Transport

The temperature dependence of permeability for a given feed partial pressure is typically represented by an Arrhenius relationship [3].

$$P = P_o \exp\left[\frac{-E_p}{RT}\right] \qquad [2.31]$$

where Po is a pre-exponential factor, Ep is the apparent activation energy for permeation, T is the temperature in Kelvin, and R is the universal gas constant. The temperature dependence of diffusion is also represented by an Arrhenius relationship.

$$D = D_o \exp\left[\frac{-E_d}{RT}\right] \qquad [2.32]$$

D_o is the pre-exponential factor, and Ed is the apparent activation energy for diffusion, which represents the energy required for a gas penetrant to jump between sorption sites within the polymer matrix. The Van't Hoff equation is used to describe the temperature dependence of sorption coefficient S.

$$S = S_o \exp\left[\frac{-\Delta H_S}{RT}\right] \qquad [2.33]$$

So is the pre-exponential factor, and ΔHs is the apparent heat of sorption which reflects contribution from the temperature dependence in both the Henry's region and the Langmuir regions.

As mentioned earlier, the permeability is the product of the diffusion and the sorption coefficients. Equation 2.32 and 2.33 can be combined to express permeability in an Arrhenius expression:

$$P = D_0.S_o \exp\left[\frac{-(E_d + \Delta H_S)}{RT}\right] \qquad [2.33]$$

$$P = P_o \exp\left[\frac{-Ep}{RT}\right] \qquad [2.34]$$

where, $Ep = E_D + \Delta H_S$

and $Po = Do.So$

2.4. Plasticization In Polymeric Membranes

Propylene and propane tend to plasticize glassy polymers even at a very low pressure (p = 2 bar) [18]. Plasticization occurs as a result of swelling in the polymer, leading to a result an upswing in the propylene or propane permeability. Plasticization usually undermines the selectivity. It is believed that as the sorption uptake in dissolved mode increases leading to a significant swelling in the matrix [19-28]. This swelling causes an increase in the fractional free volume (FFV) of the polymer. Due to this swelling, a significant increase in segmental motion is observed. This is reflected by an upturn in the permeability-pressure plot for a particular gas pair and both sorption and diffusion coefficients may deviate from the simple dual mode expressions described earlier in such case. The upturn pressure is known as the plasticization pressure. Although the permeability increases for a plasticized membrane, the selectivity decreases significantly due to the loss of diffusivity selectivity. In other words a plasticized membrane becomes less size selective. Figure-2.4 shows the response of a typical plasticized membrane. As shown in Figure-2.4, the permeability takes an upturn (propylene permeability is the red curve) and the selectivity decreases beyond the plasticization pressure. Propylene and propane, both being condensable, tend to plasticize polymeric membranes in case of a condensable membrane, since the amount of sorbed gases is much higher, the swelling of a matrix occurs at much lower partial pressures.

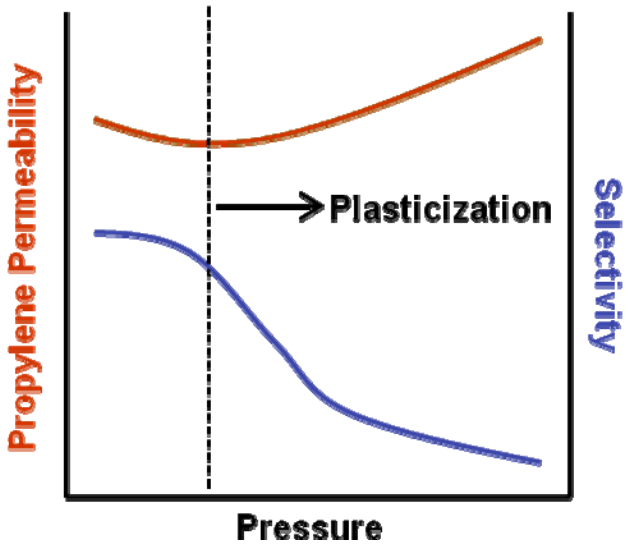

Figure-2.4: Plasticization response of a membrane

The dual mode model does predict increase in diffusion coefficients with higher pressure, not associated with the swelled matrix [2]. This is shown in Equation-2.35.

$$D_{eff} = D_D \frac{\left[1 + \frac{FK}{\left(1 + C_D \frac{b}{K_D}\right)^2}\right]}{\left[1 + \frac{K}{\left(1 + C_D \frac{b}{K_D}\right)^2}\right]} \qquad [2.35]$$

In a non-ideal situation, the observed Deff is much higher than the predicted Deff, calculated by Equation-2.35 due to the swelling and plasticization processes. Plasticization signifies a deterioration of the membrane ultimately making the membrane inefficient. In mixed gas feeds, as soon as the membrane plasticizes, the selectivity suffers heavily; thus it is important to test membranes with mixed gas compositions. An example of plasticization behavior is shown below [28], where Figure-2.5 shows the plasticization behavior of 6FDA-6FpDA with propylene observed by Staudt-Bickel and Koros. An upturn in permeability values around 3 atm propylene upstream pressure onwards was observed. Permeation tests were performed with pure gases in Figure-2.5.

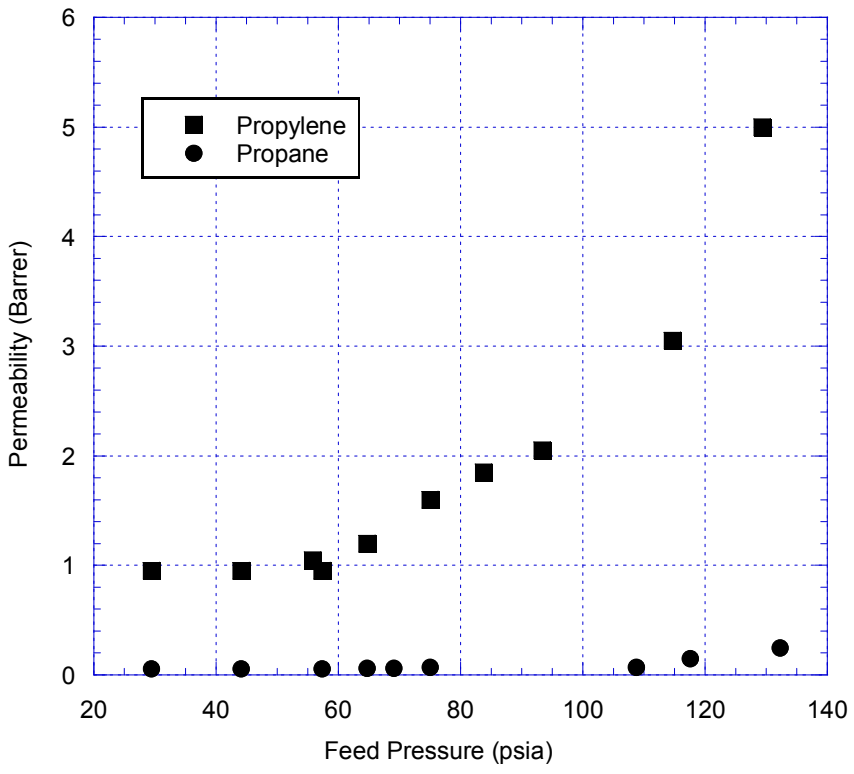

Figure-2.5: 6FDA-6FpDA plasticization behavior with pure gas. Tested at 35^0C [28]. ■ – Propylene permeability, ● - Propane permeability.

Figure-2.6 demonstrates this effect with a mixed gas propylene/propane permeation test done with a 50/50 propylene/propane gas mixture. The mixed gas selectivity in this case drops down to 7 from an originally starting value of 13 (around 50% decrease in selectivity) [28].

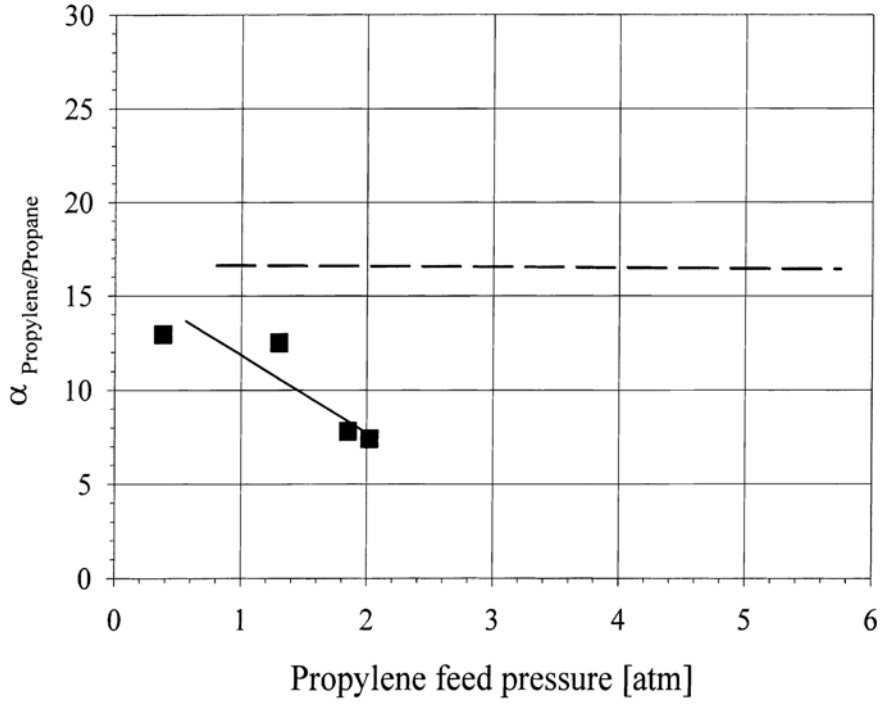

Figure-2.6: 6FDA-6FpDA plasticization behavior with mixed gas (50:50). Tested at 35^0C. ■ – Experimental mixed gas selectivity, ---- - Ideal propylene/propane selectivity.

As seen from the above example, it is very important to have a stable polymeric membrane, which doesn't plasticize under a mixed gas environment. In this research a post treatment annealing approach has been taken to suppress plasticization and is discussed in Chapter 5 in detail.

2.5. Polymeric Membrane Propylene/Propane Separations

Polymers provide a range of desirable properties that are important for gas separation processes including low cost, high permeability, good mechanical stability, and ease of processing. However, polymeric membranes based on rubbery polymers have very low selectivity for olefin/paraffin (especially propylene/propane) separations. Tanaka et al. reported a selectivity of 1.7 for a polybutadiene membrane at 50^0C permeation temperature [29]. Ito et al reported a propylene/propane selectivity of 1.0 with silicone rubber membrane [30].

A polymer material with a high glass-transition temperature (Tg), high melting point, and negligible crystallinity is generally preferred. Glassy polymers (i.e., polymers below their Tg) have stiffer polymer backbones and therefore force relatively larger molecules permeate the membrane more slowly. To increase the membrane selectivity, either the diffusivity or the solubility needs be enhanced. A rather general trade-off exists between permeability and selectivity is known as a polymer upper bound limit. Robeson, in 1991, defined the upper-bound of polymeric membranes for gas pairs such as O_2/N_2, CO_2/CH_4, H_2/CH_4, and others. In 2001, Burns and Koros identified the upper bound for C_3H_6/C_3H_8 separation at 35°C (Figure 2.7) [31]. The data were taken from a number of research studies and matched with a mathematical model. Table-2.1 shows a selected summary of pure polymer permeabilities and selectivities for this particular gas pair [31].

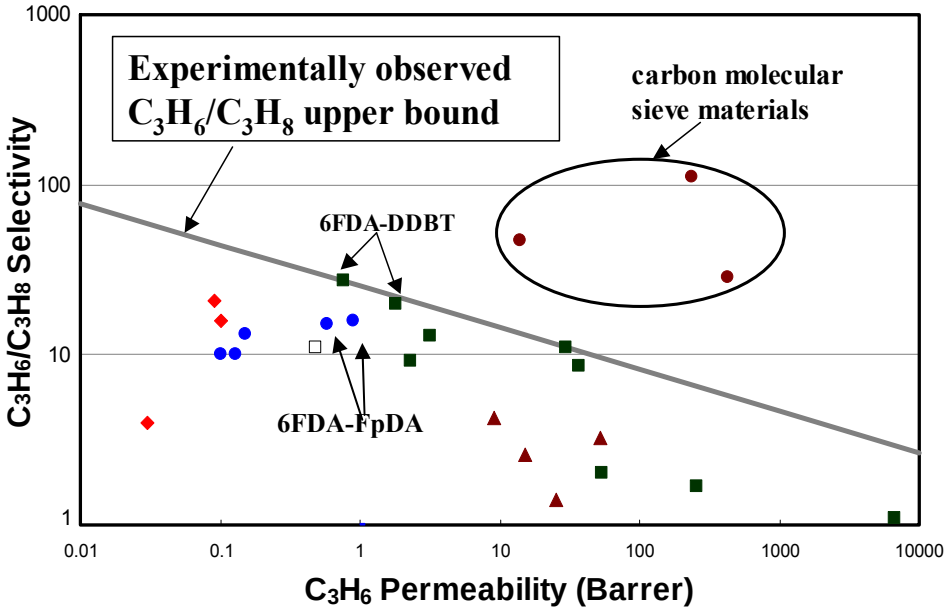

Figure-2.7: C_3H_6/C_3H_8 experimental upper bound based on pure gas permeation data over the range 1 – 4 atm feed pressure.□ = 100°C, ■ = 50°C, ● = 35°C, ▲= 30°C, ♦ = 26°C [31].

Table-2.1: C_3H_6/C_3H_8 permeability and selectivity for different polymers

Ref#	Author	Polymer	Temp (^oC)	Feed Pressure	P_{C3H6} (Barrer)	C_3H_6/C_3H_8
[28]	Staudt-Bickel and Koros	6FDA-mPD	35	3.8 atm	0.13	10
[28]	Staudt-Bickel and Koros	6FDA-IpDA	35	3.8 atm	0.58	15
[28]	Staudt-Bickel and Koros	6FDA-6FpDA	35	3.8 atm	0.89	16
[31]	Burns and Koros	Matrimid®	35	2 atm	0.10	10
[31]	Burns and Koros	6FDA-33'DMDB	35	1.1 atm	0.15	13.2
[29]	Tanaka et al.	6FDA-TrMPD (DAM)	50	2 atm	**30**	**11**
[32]	Okamoto et al.	6FDA-DDBT	50	2 atm	**1.8**	**20**
[29]	Tanaka et al.	6FDA-DDBT	50	2 atm	**0.76**	**27**

A significant amount of research has been done on glassy polyimides for propylene/propane separations [28-32]. Among all these, polyimides based on 4,4'-(hexafluorisopropylidene)dipthalic anhydride (6FDA) have exhibited the best performance. The upper bound is currently defined by the 6FDA-based polymers prepared from the TrMPD (DAM) and DDBT. The ideal selectivities of these polymers are 11, 20 respectively at 50˚C. For 6FDA-DDBT, Tanaka et al. reported a selectivity of 27 @ 50˚C and 15 @100˚C [29], which were thereafter clarified to be for aged films (2.5 yrs) [33]. As mentioned earlier, Staudt-Bickel and Koros [28] also reported an ideal selectivity of 16 for the polyimide 6FDA-6FpDA. The report showed an increase in selectivity with a decrease of temperature from 308K to 298K; however, as noted earlier strong plasticization effects were seen at very low pressure for propylene at lower temperature. In 50:50 propane/propylene mixed gas experiments, the selectivity

decreased with increasing feed pressure by as much as 50% from ideal selectivity. Similarly most of the membranes for propylene/propane separations exhibit plasticization at a very low pressure (2-4 bar).As mentioned in the previous section, a successful systematic annealing approach has been taken in this research to suppress plasticization and is reported in Chapter-5.

2.6. Separations With Mixed Matrix Membranes

As mentioned in Chapter 1, to be able to successfully produce at least chemical grade propylene (~94% purity), propylene/propane selectivity of at least 16 is needed in a mixed gas environment [4]. None of the above mentioned polymeric materials demonstrates that high separation efficiency with propylene/propane for commercial use. All the numbers in Table-2.1 are for pure gas experiments. The selectivity is expected to reduce further in case of a mixed gas environment, resulting in a low performing pure polymeric membrane material.

To achieve high enough permeability and selectivity, a mixed matrix membrane approach is proposed in this research. It is noticeable from Figure-2.8 that pure polymers selectivity/permeability points lay on or below the upper bound line. On the other hand, inorganic materials have excellent membrane separation properties (carbon molecular sieve points on the upper-bound curve). Hybrid or “Mixed Matrix” materials comprising a mixture of inorganic domains in a traditional organic polymer are excellent candidates to overcome the “upper-bound” constraint associated with pure polymers. The most

common description of the performance of such materials is given by the so-called "Maxwell model" (Equation-2.36), viz. [34]

$$P_{MM} = P_M\left(\frac{P_D + 2P_M - 2\Phi_D(P_M - P_D)}{P_D + 2P_M + \Phi_D(P_M - P_D)}\right) \qquad [2.36]$$

where P is the permeability, Φ_D is the volume fraction of the dispersed phase, the MM subscript refers to the mixed matrix membrane, the M subscript refers to the continuous matrix, and the D subscript refers to the dispersed phase present at a volume fraction of Φ_D. The selectivity of the hybrid for component A vs. B is simply the ratio of the composite permeability of component A vs. B, e.g. P_{CA}/P_{CB}, determined using P_{CA} and P_{CB} from Equation 2.36.

For an ideal polymer-sieve matching, addition of a small volume fraction of sieves to the polymer matrix increases the overall separation efficiency significantly. The ideal polymer-sieve matching criteria have been described in Chapter-6 in detail. The interfacial region, which is a transition phase between the continuous polymer and dispersed sieve phases, is of particular importance in successful mixed matrix membrane formation [35-43]. Zeolites have been the most commonly used solid fillers in mixed matrix work. Almost all of the studies on zeolite/polymer mixed matrix membranes use commercially available large zeolite particles with particle sizes in the micron range as solid fillers. Recently use of nano-sized particle in mixed matrix membranes has been reported [37-38].

The type of morphology which forms at the interfacial region impacts a membrane's separation properties. The Maxwell model is illustrated in Fig. 2.8. As shown in Figure 2.8, the ideal mixed matrix membrane will exhibit both an increase in selectivity and permeability as the solid phase volume fraction is increased, and the Maxwell model can be used to estimate these separation properties [35]. For example, if we start with pure 6FDA-6FpDA polymer, which lies under the upper-bound curve, and a molecular sieve with a propylene permeability of 4 Barrer and a propylene/propane selectivity of 100, the mixed matrix permeability and selectivity will follow a Maxwell Model as shown (for 20, 30 and 40 wt% loading).

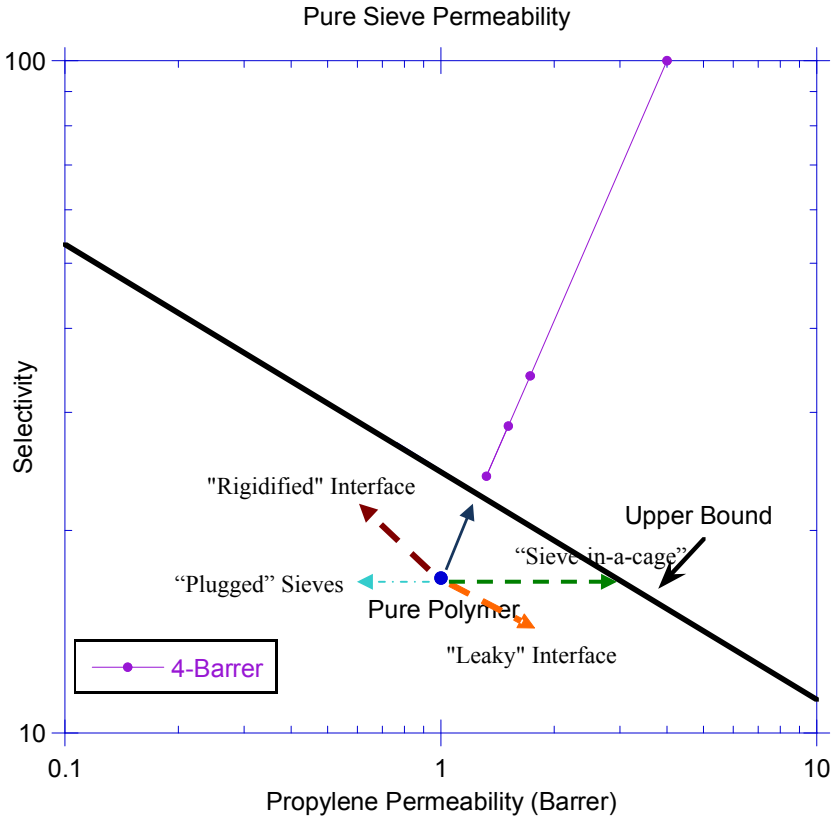

Figure-2.8: A graphical representation of interfacial morphologies for MMM and their effect on C_3H_6/C_3H_8 gas transport properties.

It is clear from the figure that a selectivity and permeability enhancement will be observed in the ideal case. Poor interfacial adhesion ("Sieve in a cage" or "Leaky interface") can result in interfacial voids that are much larger than the penetrating molecules [43, 44]. Such voids destroy the selectivity enhancement due to addition of the sieving phase, reducing the overall selectivity of the mixed matrix membrane to the pure polymer value, and increasing the permeability due to transport through the interfacial voids (Figure 2.8). Another nonideal behavior corresponds to total plugging of the dispersed phase, so significant reductions in permeability with no change in selectivity results. On the other hand, if a nanoscopic zone near the surface of the sieve has reduced permeability with equivalent or better selectivity to that of the intrinsic matrix; selectivity enhancement, along with reduced effective permeability relative to the Maxwell predictions is observed. This situation is typically referred to as a "Rigidified Interface".

2.6.1. AlPO-14 for propylene/propane separations

AlPO-14 has been successfully used for propylene propane separations via pressure and vacuum swing adsorption experiments by UOP [45, 47]. Padin et al demonstrated that propylene/propane separation is favorable with equilibrium isotherm since almost no amount of propane was sorbed by AlPO-14 [46]. Following the success of AlPO-14 with commercial PSA application, AlPO-14 group materials has been used for this work. Wilson et al synthesized AlPO-14 [10], a small pore aluminophosphate molecular sieve, which selectively adsorbed propylene and essentially excluded propane [45]. AlPO-14 has various crystalline structures essentially composed of tetrahedral AlO_4

and PO_4 units. Unlike zeolites, AlPO-14 does not have framework charge balancing cations. The pore window diameter of AlPO-14 is 3.8 A with a crystalline structure which is capable of excluding the entry of propane by a steric hindrance effect which prevents the propane from entering into the internal pore/channel structure, while allowing slightly more compact propylene [45]. Figure-2.9 shows the structure of AlPO-14 with the diffusion paths for propylene. Table-2.2 shows that even for propylene diffusion is possible only via one direction ([1, 1, -1]).

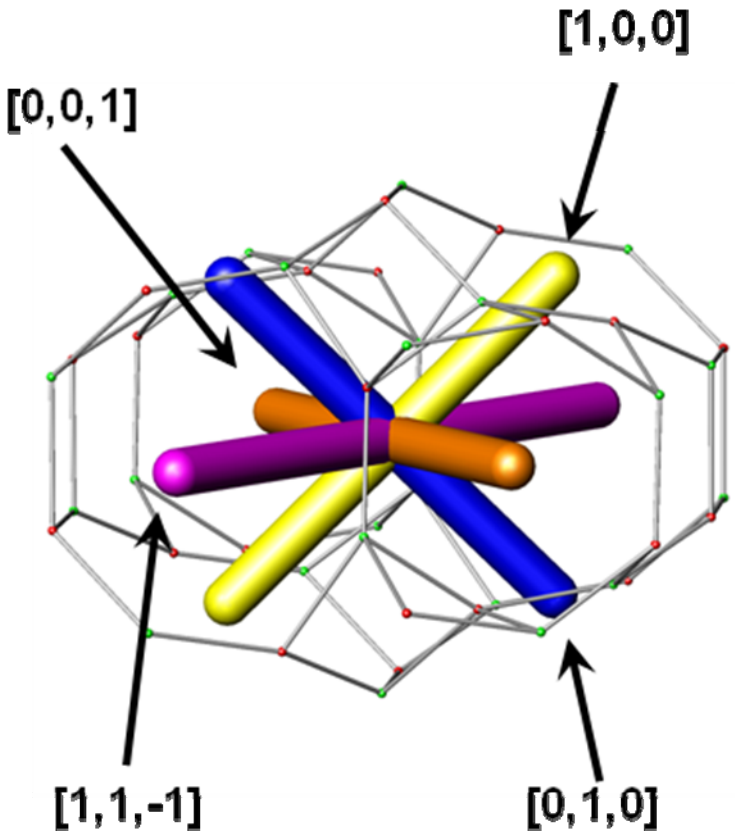

Figure-2.9: AlPO-14 diffusion paths. Single cage bounded by eight 8-rings, consisting of 4 pairs oriented along the four shown crystallographic directions [49]

Table-2.2: AlPO-14 Structure Data [49]

Channel direction	Color (Figure-2)	8-ring pore dimensions
[1,1,-1]	**Magenta**	**3.4 x 3.5**
[0,0,1]	**Gold**	**2.8 x 4.1**
[0,1,0]	**Blue**	**2.1 x 4.9**
[1,0,0]	**Yellow**	**1.9 x 4.9**

It is also worth mentioning that AlPO-14 has a high aspect ratio structure. The Maxwell model described in the previous section is not applicable in case of AlPO-14 molecular sieves due to the high aspect ratio. In this case, another model is used for this research. This model is called the Cussler model and is used for the molecular sieves with aspect ratio higher than one [50]. Cussler model considers the enhancements in diffusivity for permeable sieves and is expressed by, viz:

$$\frac{J_0}{J} = 1 - \phi + \left[\frac{1}{\frac{1}{\delta\phi} + \frac{4(1-\phi)}{A_R{}^2\phi^2}} \right] \qquad [2.37]$$

where J_0 is pure polymer flux across the membrane, J is the flux across the mixed matrix membrane. Φ is the volume fraction of the sieve in the mixed matrix membrane, A_R is the sieve aspect ratio (defined as width/length) and δ is the ratio of diffusivity coefficient

of polymer to sieve. Please note that in the original Cussler equation, a term α was used instead of A_R and was defined as $\alpha = A_R/2$. Since throughout this work α has been used to describe the selectivity, hence the new term A_R was introduced to avoid any confusion. The above equation was then used to calculate the Cussler model prediction for this research.

2.7. References

1. Koros and Chern, *Separations of gaseous mixtures using polymer membranes,* Handbook of Separation Process Technology, R.W. Rousseau, Editor, 1987, John Wiley & Sons. P. 862-953

2. Crank, *The Mathematics of Diffusion*. 2nd Edition, 1975. Oxford: Clarendon Press

3. Koros and Fleming, *Membrane Based Gas Separations*. JMS, 1993, **83**:p. 1-80

4. Baker, R.W. *Future of Gas Separation Technology.* Ind. Eng. Chemical. Res., 2002. **41**, p: 1393-1411

5. Vieth, W.R., J.M. Howell, and J.H. Hsieh, *Dual sorption theory.* Journal of Membrane Science, 1976. **1**: p. 177-220.

6. Barrer, R.M., J.A. Barrie, and J. Slater, *Sorption and Diffusion in Ethyl Cellulose. Part III. Comparison Between Ethyl Cellulose and Rubber.* Journ. Polymer Sci., 1958. **27**: p. 177-197.

7. Koros, W.J., *Sorption and Transport in Glassy Polymers*, in *Department of Chemical Engineering*. 1977, The University of Texas at Austin: Austin.

8. Koros, W.J., et al., *Model For Permeation of Mixed Gases and Vapors in Glassy Polymers.* Journal of Polymer Science, Polymer Physics Edition, 1981. **19**(10): p. 1513-1530.

9. Koros, W.J., *Model for sorption of mixed gases in glassy polymers.* J. Polym. Sci., Polym. Phys. Ed., 1980. **18**(5): p. 981-92.

10. Kamaruddin, H.D., *Analysis of methanol/methyl tert-butyl ether (MTBE) separations using pervaporation*, in *Department of Chemical Engineering*. 1997, The University of Texas at Austin: Austin, TX. p. 215.

11. Kamaruddin, H.D. and W.J. Koros, *Some observations about the application of Fick's first law for membrane separation of multicomponent mixtures.* Journal of Membrane Science, 1997. **135**: p. 147-159.

12. Bird, A.J. and D.L. Trimm, *Carbon molecular sieves used in gas separation membranes*, in *Carbon*. 1983. p. 177-80.

13. Barton, T.J., et al., *Tailored Porous Materials.* Chem. Mater., 1999. **11**(10): p. 2633-2656.

14. Chen, Y.D. and R.T. Yang, *Preparation of Carbon Molecular Sieve Membrane and Diffusion of Binary Mixtures in the Membrane.* Ind. Engr. Chem. Ress, 1994. **33**(12): p. 3146-53.

15. Vu, D.Q., *Formation and Characterization of Asymmetric Carbon Molecular Sieve and Mixed Matrix Membranes for Natural Gas Purification*, in *Chemical Engineering*. 2001, The University of Texas at Austin: Austin, Texas. p. 334.

16. Ruthven, D.M., *Diffusion of oxygen and nitrogen in carbon molecular sieve.* Chemical Engineering Science, 1992. **47**(17-18): p. 4305-8.

17. Auerbach, S.M., K.A. Carrado, and P.K. Dutta, *Zeolite Science and Technology*. 2003, New York: Marcel Dekker, Inc.

18. Sanders et al. *Systems and Methods for the Separations of Propylene and Propane*. US Patent. 2008/**0167512**, Jul. 10 2008.

19. Ismail, A.F. and W. Lorna, *Penetrant-induced plasticization phenomenon in glassy polymers for gas separation membrane.* Separation and Purification Technology, 2002. **27**(3): p. 173-194.

20. Sanders, E.S., S.M. Jordan, and R. Subramanian, *Penetrant-plasticized permeation in polymethylmethacrylate.* Journal of Membrane Science, 1992. **74**(1-2): p. 29-36.

21. Wessling, M., M. Lidon Lopez, and H. Strathmann, *Accelerated plasticization of thin-film composite membranes used in gas separation.* Separation and Purification Technology, 2001. **24**(1-2): p. 223-233.

22. Wind, J.D., et al., *Carbon Dioxide-Induced Plasticization of Polyimide Membranes: Pseudo-Equilibrium Relationships of Diffusion, Sorption, and Swelling.* Macromolecules, 2003. **36**: p. 6433-6441.

23. Houde, A.Y., S.S. Kulkarni, and M.G. Kulkarni, *Permeation and plasticization behavior of glassy polymers: a WAXD interpretation.* Journal of Membrane Science, 1992. **71**(1-2): p. 117-128.

24. Wessling, M., et al., *Plasticization of gas separation membranes.* Gas Separation & Purification, 1991. **5**(4): p. 222-228.

25. Zhou, S. and S.A. Stern, *The effect of plasticization on the transport of gases in and through glassy polymers*, in *J. Polym. Sci., Part B: Polym. Phys.* 1989. p. 205-22.

26. Sejour, H., *Investigation of dithiolenes for propylene/propane membrane separation,* 2007, Georgia Institute of Technology, GA.

27. Omole, Imona, *Crosslinked Polyimide Hollow Fiber membranes for Aggressive Natural Gas Feed Streams*, 2008, Georgia Institute of Technology, GA.

28. C. Staudt-Bickel, W.J.Koros, *Olefin/paraffin gas separation with 6FDA-based polyimide membranes*. JMS, 2000. **170**: p. 205-214.

29. K. Tanaka, A.T., Jianqiang Hao, H. Kita, K. Okamoto, *Permeation and separation properties of polyimide membranes to olefins and paraffins.* JMS 1996. **121**: p. 197-207.

30. Ito Akira et al. *Permeation of propane and propylene through cellulosic polymeric membrane*. J. Applied polymer Science. 1989, **38**, 483-490.

31. R. L. Burns, W.J. Koros, *Defining the challenges for C_3H_6/C_3H_8 separation using polymeric membranes*. JMS, 2003. **211**: p. 299-309.

32. K. Okamoto, K.N., Jinaquiang Hao, Kazuhiro Tanaka, Hidetoshi Kita, *Permeation and separation properties of polyimide membranes to 1,3-butadiene and n-butane.* JMS, 1997. **134**: p. 171-179.

33. M. Yashino et al., *Olefin/paraffin separation performance as asymmetric hollow fiber membrane of 6FDA/BPDA-DDBT copolyimide*. JMS, **2003**, 212: p-13-27

34. Mahajan, R. and W.J. Koros, *Mixed matrix membrane materials with glassy polymers Part 1.* Polymer Engineering and Science, 2002. **42**(7): p. 1420.

35. L. Chunqing, Hillock A.M., Husain S., Koros, W. J. ,Kulprathipanja, S. *Review of Recent Progress in Mixed Matrix Membranes, Chapter in Advances in Membrane* Science, Wiley & Sons Publishers, N. L. Li Editor

36. Kulprathipanja, S.; Neuzil, R. W.; Li, N. N. *Separation of fluids by means of mixed matrix membranes.* US 4,740,219, **1988**.

37. Moermans, B.; Beuckelaer, W. D.; Vankelecom, I. F. J.; Ravishankar, R.; Martens, J. A.; Jacobs, P. A., *Incorporation of nano-sized zeolites in membranes*. Chemical Communications **2000**, 2467-2468

38. Wang, H.; Holmberg, B. A.; Yan, Y., *Homogeneous polymer-zeolite nanocomposite membranes by incorporating dispersible template-removed zeolite nanocrystals.* Journal of Materials Chemistry **2002**, 12, 3640-3643

39. Okamoto, Kenichi; Noborio, Kenji; Hao, Jianqiang; Tanaka, Kazuhiro; Kita, Hidetoshi, *Permeation and separation properties of polyimide membranes to 1,3-butadiene and n-butane.* JMS, **1997,** 134(2), 171-179

40. Christopher J. Cornelius; *Physical and Gas permeation properties on a series of Novel hybrid inorganic-organic composites based on a synthesized fluorinated polymer.* PhD -Virginia Tech **2000**

41. Cornelius, C. J.; Marand, E., *Hybrid silica-polyimide composite membranes: gas transport properties.* JMS **2002**, 202, (1-2), 97-118.

42. Maria Coleman; *Isomers of fluorine-containing polyimides for gas separation membranes (glassy polymers)*, Ph.D., University of Texas - Austin, **1992**

43. Mahajan, R.; Burns, R.; Schaefer, M.; Koros, W., *Challenges in forming successful mixed matrix membranes with rigid polymeric materials*. Journal of Applied Polymer Science **2002**, 86, 881-90.

44. Moore, T. T.; Mahajan, R.; Vu, D. Q.; Koros, W. J., *Hybrid membrane materials comprising organic polymers with rigid dispersed phases.* AIChE Journal **2004**, 50, (2), 311-321.

45. Cheng L, Padin J, Rege S. U., Wilson S. T., Yang R T. *Process for purifying propylene*. **US 6,406,521**, 2002

46. Padin J, Rege S. U., Yang R. T., Cheng L. S., *Molecular sieve sorbents for kinetic separation of propane/propylene.* Chemical Engineering Science, **55**, 4525.

47. Cheng L, Wilson S.T., *Vacuum swing adsorption process for separating propylene from propane.* **US 6,296,688,** 2001

48. Wilson; Stephen T, Lok; Brent M, Flanigen; Edith M; *Crystalline metallophosphate compositions* **1982** USPTO 4,310,440

49. Data Supplied by UOP

50. Cussler E. L., *Membranes containing selective flakes,* JMS, 1990. **52:** p. 275-288

CHAPTER 3

MATERIALS AND EXPERIMENTAL METHODS

3.1. Polymeric Materials

Polymeric materials studied in this work were synthesized in the laboratory. The material selection process was based on the transport properties of the polyimide for propylene/propane separations. Previous researches have shown initial promising results with 6FDA-6FpDA polymer [1, 2] that were promising. Bulky CF_3 groups of these monomers provide molecular spacing, which is necessary to tune the selectivity of the polymer.

Moreover, this was also one of the highest performing polymers in the upper-bound curve for propylene/propane separations [1]. Figure-3.1 shows the upper bound curve for this particular gas separation. In the case of 6FDA-DDBT polymer (Figure-3.1), Tanaka et al. reported a selectivity of 27 @ 50˚C and 15 @100˚C [3], which were thereafter clarified to be for aged films (2.5 yrs) [4]. The 6FDA-6FpDA data shown in Figure-3.1 were measured at 35^0C. Initially, research was pursued with 6FDA-DDBT by Burns [1]; however, the work indicated that this material is not the preferred matrix material. The potential reasons have been described in details in Chapter-4.

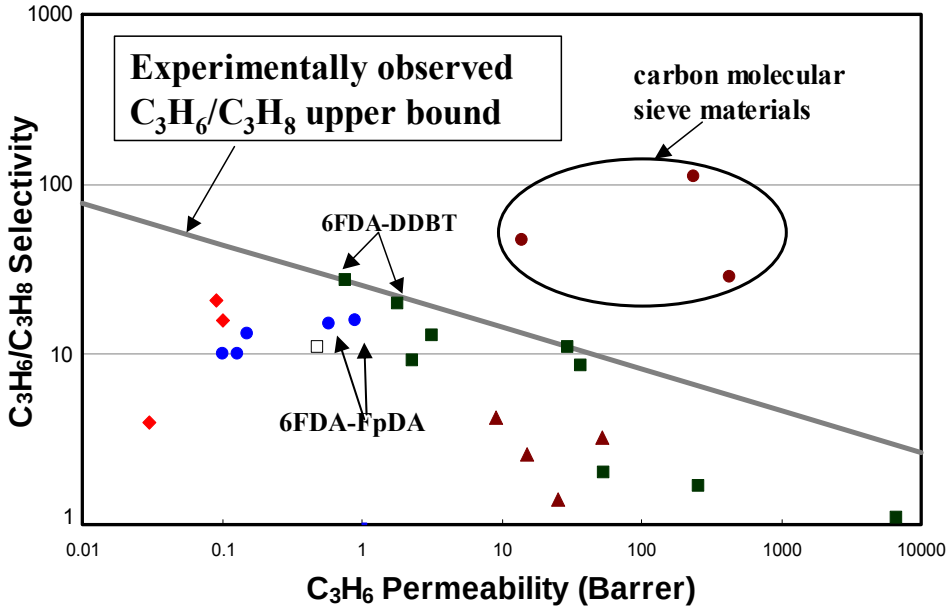

Figure-3.1: C_3H_6/C_3H_8 experimental upper bound based on pure gas permeation data over the range 1 – 4 atm feed pressure.□ = 100°C, ■ = 50°C, ● = 35°C, ▲= 30°C, ♦ = 26°C [31].

Following in the difficulty with 6FDA-DDBT, 6FDA-6FpDA was chosen for this entire research. A polycondensation reaction method was used for the synthesis process. To increase the molecular weight and the polydispersity index of the polymer, synthesis conditions were modified. The monomers, along with the catalysts and solvents, used for the synthesis processes (thermal and chemical imidization) are listed in Table-3.1. Figure-3.2 shows the structures of 6FDA-DDBT and 6FDA-6FpDA. Polyimide synthesis process is described in the next section.

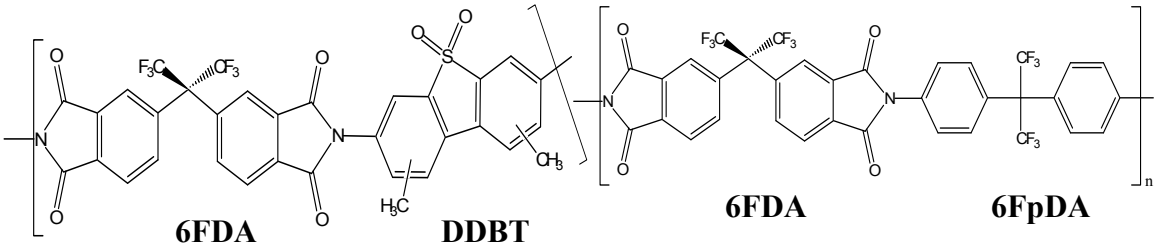

Figure-3.2: 6FDA-DDBT and 6FDA-6FpDA polymer structures.

Table-3.1: List of materials for polymer synthesis

Structure	***Abbreviation***	***Chemical Name***
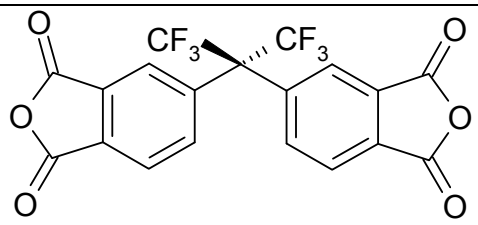	6FDA (dianhydride)	4,4'-(hexafluoroisopropylidene) diphthalic anhydride
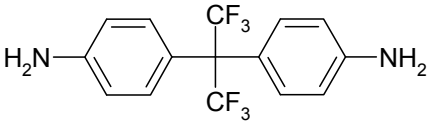	6FpDA (diamine)	4,4'-(hexafluoro-isopropylidene) dianiline
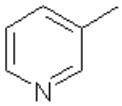	Beta – Picoline	Beta-Picoline chemical imidization catalyst
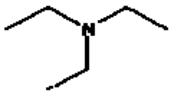	TEA	Triethylamine chemical imidization catalyst
	(ODCB)	1,2-Dichlorobenzene thermal imidization catalyst
	NMP	*N*-Methyl-2-pyrrolidone solvent for synthesis process
CH_3-OH	Methanol	Methanol (phase separation)

3.1.1. Polymer Synthesis

The 6FDA and 6FpDA monomers were purified by sublimation process before synthesis. The 6FDA monomer usually is more impure than the 6FpDA monomer. The importance of monomer purification has been described in detail in Chapter-4. Generally, sublimed monomers yield a higher molecular weight and lower polydispersity index polymer. Figure-3.3 shows the sublimation set-up used for this work. The synthesis schematic for 6FDA-6FpDA is shown in Figure-3.4.

Figure-3.3: Sublimation set-up used for monomer purification process.

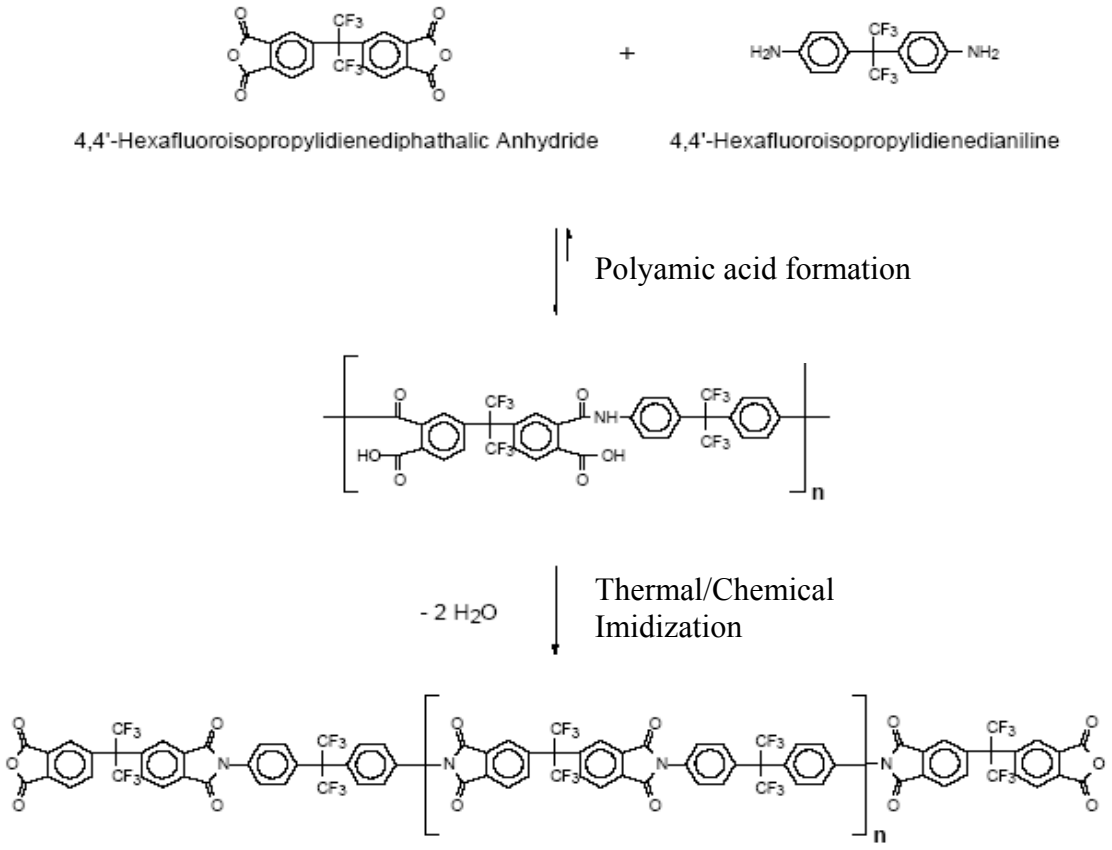

Figure-3.4: Schematic of 6FDA-6FpDA synthesis reaction

The polyimide was synthesized by a two step polycondensation reaction. In the first step a polyamic acid was formed by reacting dianhydrides and diamines (6FDA and 6FpDA were added in a 1:1 stoichiometric ratio). The 6FpDA monomer was first dissolved in NMP solution (total NMP: monomer ratio is ~ 4:1) with the help of a stirrer. Once the 6FpDA was completely dissolved, the 6FDA monomer was added portion wise in 3-4 steps. This solution was then stirred under nitrogen a purge for ~18 hours for polyamic acid formation. For very high molecular weight polymer, the solution turned highly viscous within the first couple of hours of the reaction. Once the polyamic acid

was formed, the ring structure of the polyamic acids is closed via a condensation reaction. This was done by thermal or chemical imidization methods, which are discussed in detail in the next.

3.1.2. Imidization

Imidization process involves the dehydration of polyamic acids to form a polyimide (step 2 in Figure-3.4). This is generally carried out either thermally or chemically. In case of the thermal imidization process, the reaction solution was heated to a high temperature in the presence of a catalyst (ortho-dichlorobenzene). ODCB forms an azeotrope with water, which was then removed from the solution with a Dean-Stark trap. The temperature was maintained at 180^0C for 18 hours. Omole et al. observed a molecular build up even after 18 hours of the imidization reaction (the molecular weight (Mw) rose from ~92,000 (at 18 hrs) to 103,000 (at 26 hrs)) [5]. The heat treatment of the thermal imidization process dehydrates the solution thus helping to remove all of the water molecules. However, there is a tendency to form chemical crosslinks between the polymeric or oligomeric chains at high temperatures; affecting the solubility of the polymers. This has been discussed in detail in the next Chapter.

Chemical imidization is another way to complete the cyclization reaction of the polyamic acid. Researchers have typically used TEA (tri-ethyl-amine)/ pyridine as catalyst for this cyclization reaction with acetic anhydride as a dehydrating agent. In this process, the catalyst was added in the polyamic acid solution at room temperature. Once the catalyst was dissolved completely, the acetic anhydride was then added to the same solution. The amount

of acetic anhydride was determined by calculating the moles of water to be removed from the reaction (for each mole of 6FDA-6FpDA produced, two molecules of water were to be removed). For this particular case, a 10% excess of acetic anhydride was added to the solution to ensure the complete ring closure. The catalyst and the dehydrating agent were added in a 1:1 ratio. In general, TEA or pyridine are used as the catalyst for cyclization reaction. The reaction was performed for ~18 hours and then the resultant polyimide solution was precipitated in methanol.

TEA is a stronger base than pyridine (pKa of TEA is 10.7 and pKa of pyridines range from 4.9-6.6). Kudryavtsev observed a slower rate of imidization and longer induction period for TEA catalyst as compared to pyridine catalyst [7]. Additionally, triethylamine can react with polyamic acid carboxyls to form "salt-type" structures. To avoid any of the complexities mentioned here, beta-picoline (a derivative of pyridine) was used as a catalyst in this research. A detailed description of the complete procedure can be found in Appendix A.

After successful imidization, the polyimide was precipitated in pure methanol. Previous researchers have used a mixture of methanol/water, but in this research pure methanol was used to avoid any hydrolyzing effects. The precipitate was then dried in the fume hood for one day before drying under vacuum for 12-16 hours at 200^0C. Figure-3.5 shows the different steps of synthesis process.

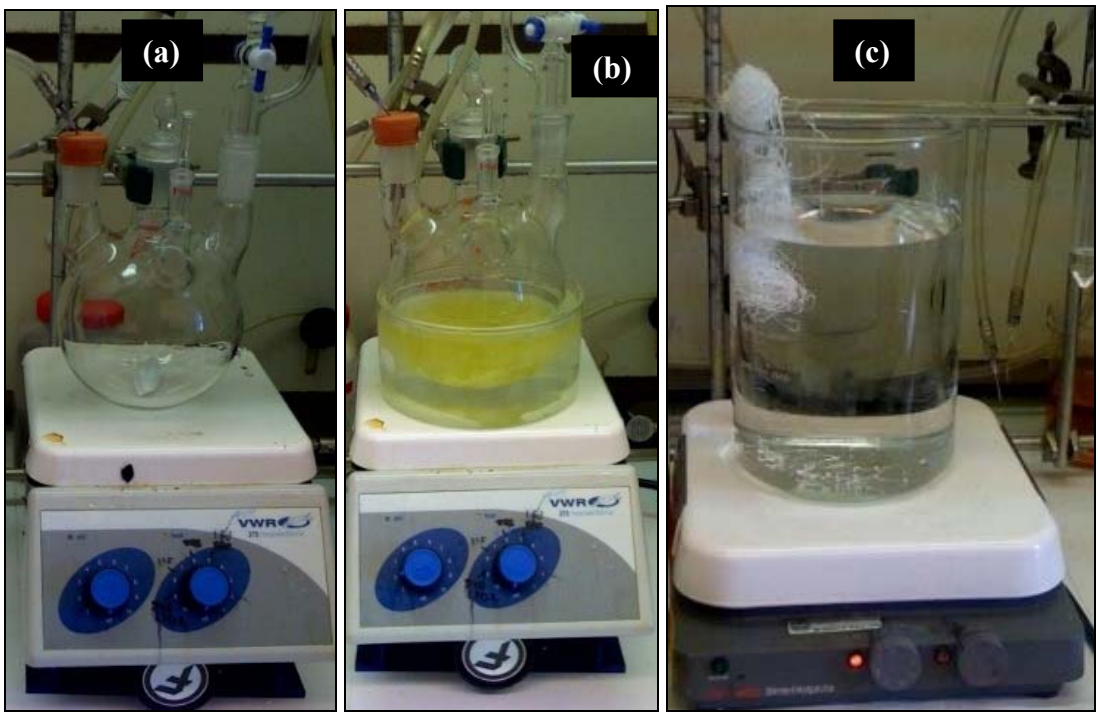

Figure-3.5: Synthesis process – (a) the whole set-up is purged prior to polyamic acid formation, (b) chemical imidization process in progress (c) precipitation in methanol

3.2. Molecular Sieve Materials

As mentioned in Chapter-2, AlPO-14 was used in this research as the sieve material for mixed matrix membrane formation in this work. AlPO-14 was graciously supplied by UOP. The sieves were dried at 150^0C under vacuum for 12 hours to remove any moisture before use. Figure-3.6 shows the SEM pictures of AlPO-14 used in this work.

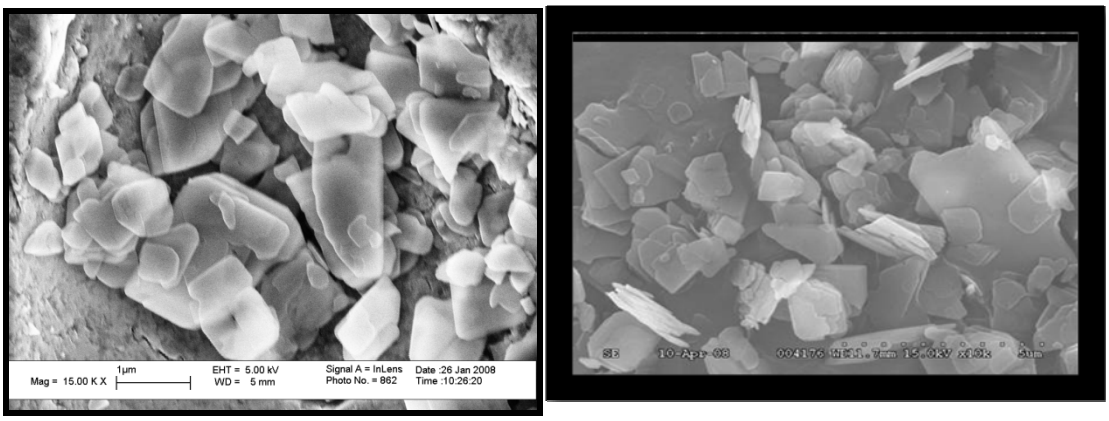

Figure-3.6: SEM images of AlPO-14 used in this work.

3.3. Experimental Methods

3.3.1. Permeation

Dense film permeation experiments were performed in this work. Both pure and mixed gases were tested with dense films.

3.3.1.1. Dense film preparation – solution casting

Dense films were prepared by dissolving the polymer in dichloromethane solution at 3 to 4 wt%. Polymers were dried in a vacuum oven for 12 hours at 110^0C to remove any trace of moisture prior to solution preparation. The solution was extruded through a 0.25 micron filter onto a Teflon® casting dish or inside a metal casting ring, on top of a level glass plate. The syringe was used to remove any contaminants from the polymer solution before casting. The dish with the polymer solution was covered with an inverted glass funnel and capped with a Kimwipe® (Kimberly-Clark Corporation; Roswell, Georgia), which acts as a plug to control the rate of evaporation of dichloromethane from

the membrane. Rapid solvent evaporation can result in uneven evaporation and thickness variations in the membrane. Moreover, the funnel used to cover the glass plate also prevented any small contaminant particle from being trapped in the membrane at a nascent stage. Figure-3.7 shows the solution cast process [6].

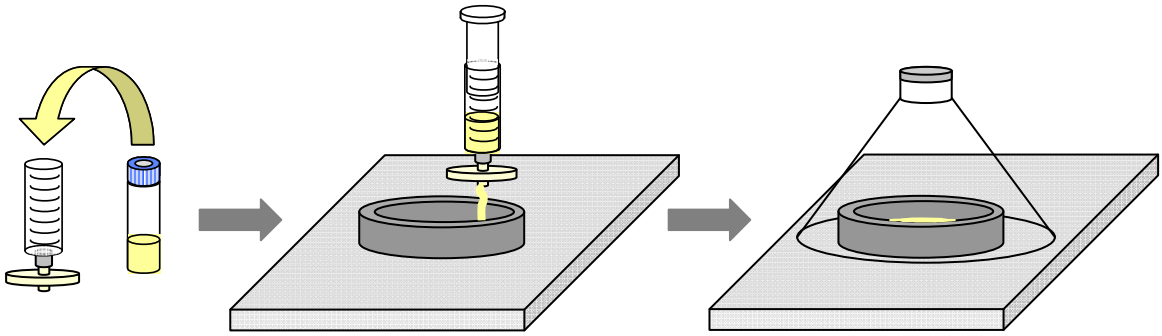

Figure-3.7: Pure polymer membranes were solution cast on a glass surface. Adapted from [6]

Once the membrane was covered with the funnel, it was left for 12-24 hours. Solvent was allowed to evaporate until the membrane was fully vitrified. The membrane was then removed from the glass plate and dried under vacuum oven at 200^0C – 210^0C for 12-18 hours. The choice of the drying temperature has been described in details in Chapter-5.

3.3.1.2.Dense film preparation – draw casting

Draw casting method was used for mixed matrix membrane preparation. The polymer was dried at 100^0C for overnight to remove any trace of water. AlPO-14 was dried in a vacuum oven at 150^0C for 12-16 hours. A 15-20 wt% polymer dope solution was prepared in dichloromethane solution in a 20 ml I-CHEM™ vial. To ensure the homogeneity of the polymer dope solution, the vial was rolled slowly overnight for a day. The dry sieves were placed in a 20ml I-CHEM™ vial and then dispersed in dichloromethane. Around 2 ml of dichloromethane was used per 100 mg of AlPO-14 sieves. The solution was sonicated three times in 30 seconds intervals (Vibracell, Sonics & Materials). An ice bath was used to prevent a temperature rise during the sonication process. Once the sieves were well dispersed, they were primed with polymer. The priming process helped the interaction of polymer and the sieve by coating with a small amount of polymer at a very dilute stage. The amount of polymer added was typically 10% of the total polymer used in the final dope. This solution was then placed on a roller and allowed to mix overnight. Following the priming stage, the remainder of the polymer dope was then added to the solution and the solution was then rolled for one day before draw casting. The final dope had typically 13 to 17 wt% AlPO-14 in polymer. The final, viscous casting dope was used to draw cast with a casting knife on a glass plate surface. If the dope was too dilute for draw casting, the vial was purged by nitrogen gas to evaporate some of the solvent [6].

The casting process was carried out in a glove bag (Two-hand AtmosBag, Aldrich). First, the glove bag was saturated with dichloromethane, which reduces the

rate of solvent evaporation of the membrane drastically. The bag was then allowed to equilibrate for around one hour and then the film was cast by pouring the viscous solution on the casting plate and drawing it with a casting knife. This process is illustrated by Figure-3.8. The film was left in the glove bag until all of the solvent in the film had evaporated (12-24 hours). Films were removed using water and dried similarly as described in the solution casting process.

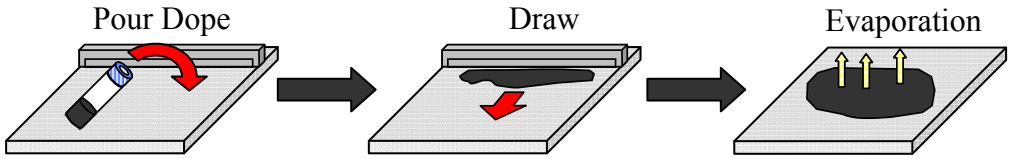

Figure-3.8: Hybrid membranes were draw cast in a glove-bag saturated with solvent vapor [6].

3.3.1.3. Pure gas permeation experiments

All dense films were tested for their permeation properties by a constant volume, variable pressure permeation system. Gases were introduced in the upstream ballast and were allowed to permeate through a membrane. The downstream ballast was used to collect the permeate gas. Pressure increase in was recorded and a permeability coefficient in Barrer was calculated using Equation-3.1.

$$P_A = \frac{2.939x10^4 \bullet \left(\frac{dp}{dt}\right) \bullet V \bullet l}{T \bullet A \bullet \Delta p_A} \qquad [3.1]$$

Where, for a given gas A, (dp/dt) was in torr/min, was measured using a MKS Baraton® transducer. The permeation rate was adjusted for leaks by subtracting out a measured leak rate. Leak rates were measure for at least 12 hours. Before the leak test, the assembled membrane system was evacuated for 2-3 days. The volume, V (in cm^3), is that of the downstream ballast and the driving force, p_A, was the upstream pressure, since the downstream was maintained under vacuum prior to the test. The thickness, *l* (mils) of the film was measured using a micrometer (B.C. AMES Co.) and the area (cm^2) was scanned using ScionImage® software package. The temperature of the permeation system was constant throughout the experiment. In addition to propylene and propane, oxygen and nitrogen permeabilities were also measured as benchmark gases. Figure-3.9 shows the high temperature permeation system setup used for this research.

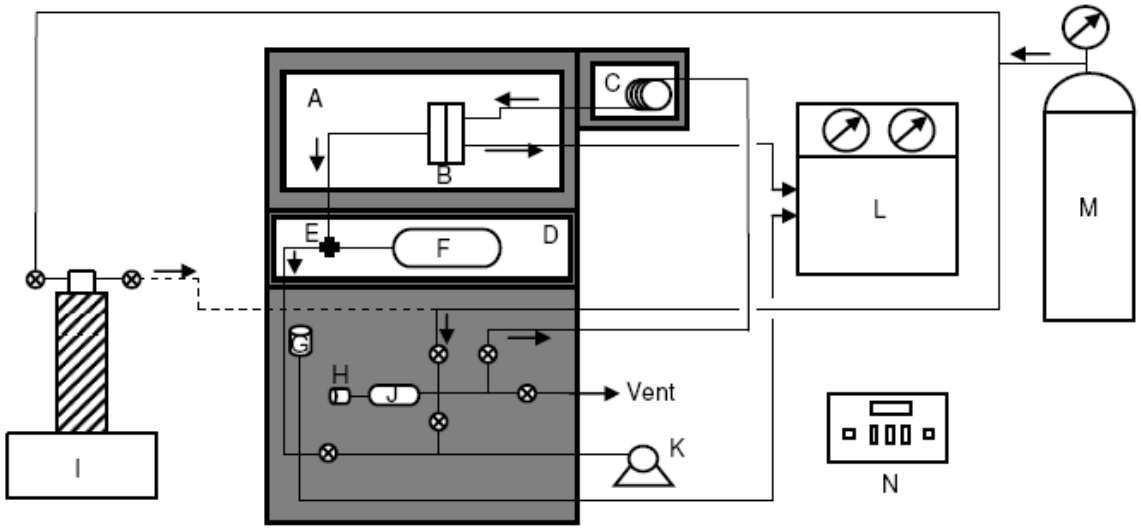

A. Main Oven
B. Permeation Cell
C. Preheat Chamber
D. Lower Oven
E. Rupture Device
F. Downstream Volume
G. Downstream Pressure Transducer
H. Upstream Pressure Transducer
I. ISCO Pump
J. Upstream Volume
K. Vacuum Pump
L. Gas Chromatograph
M. Gas Cylinder
N. Temperature Controller

Figure-3.9: Diagram of the high temperature high pressure system used for this research.

Figure-3.10 and 3.11 show diagrams of the permeation cell used and the masking technique used in this research. The masking technique was developed by Cathy Zimmerman and Zen Mogri and is discussed in details by Burns and Perry [8, 6].

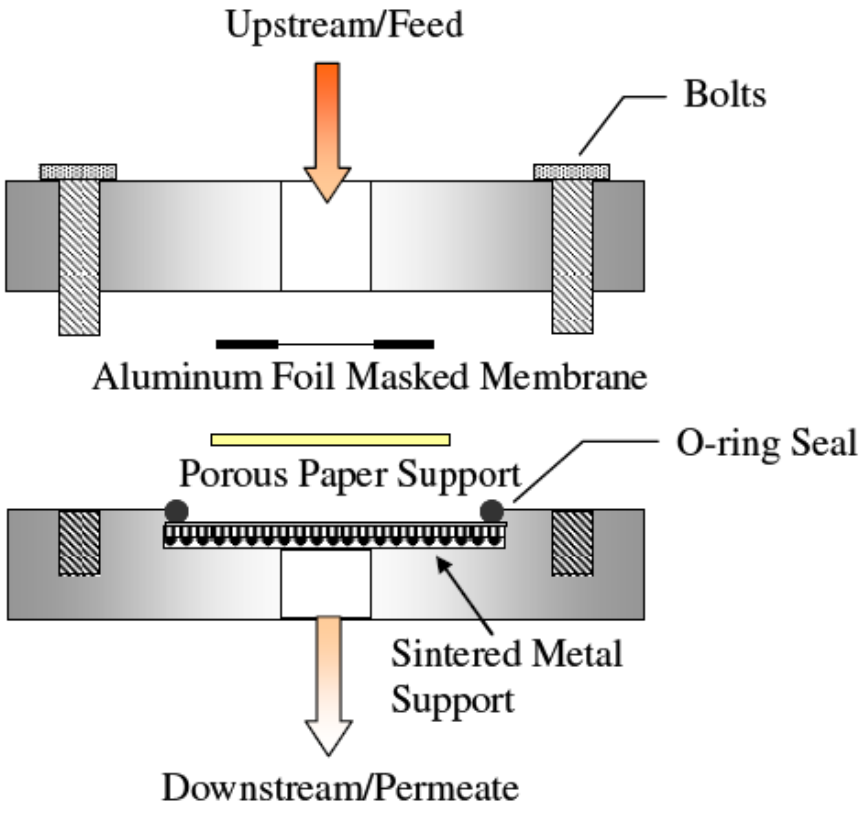

Figure-3.10: Permeation cell. Adapted from [8]

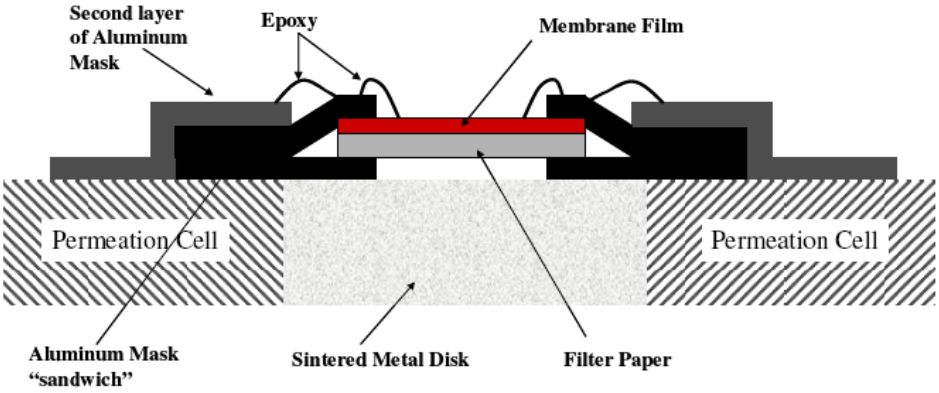

Figure-3.11: Masking technique for rigid materials. Adapted from [8]

3.3.1.4. Mixed gas permeation experiments

Mixed gas experiments were performed with 50/50 and 75/25 propylene/propane gas mixtures. The gas cylinders were obtained from AirGas. In the case of mixed gas experiments, a stage cut of less than 1% was used to avoid concentration polarization [5]. The percentage of the feed that permeates through the membrane is called the stage cut. Permeate collected in the downstream ballast was sent to the GC (gas chromatograph) for further analysis. Areas obtained from the GC were then used to calculate the selectivity. Permeabilities of propylene and propane were calculated from the permeate flux.

3.4. Sorption

A pressure decay method was used for gas sorption measurements. In this method, the equilibrium sorbed concentration at a given pressure can be used to calculate the solubility coefficient. Before the sorption experiments the films or the molecular sieves were dried in a vacuum oven at 110^0C to remove any trace moisture (sieves were dried at 150^0C). After loading the sample in the sorption cell, the system was evacuated for 1-2 days. A known amount of the sorption gas was introduced in the reservoir cell of known volume. The reservoir cell was equilibrated thermally for around 2 hours. A water bath with a circulator was used to maintain the system at a constant temperature. A pressure valve between the feed reservoir and the sample cell was briefly opened and then closed in order to introduce the reservoir gas into the sample cell. The pressure in both chambers was monitored via pressure transducers. Once the gas reached

equilibrium, a mole balance was used to calculate the amount of gas absorbed by the sample. The pressure in the cell will decay progressively indicating gas sorption into the sample in the cell. Figure-3.12 shows the schematic of the pressure decay sorption apparatus used in this research. The compressibility factors were obtained from NIST.

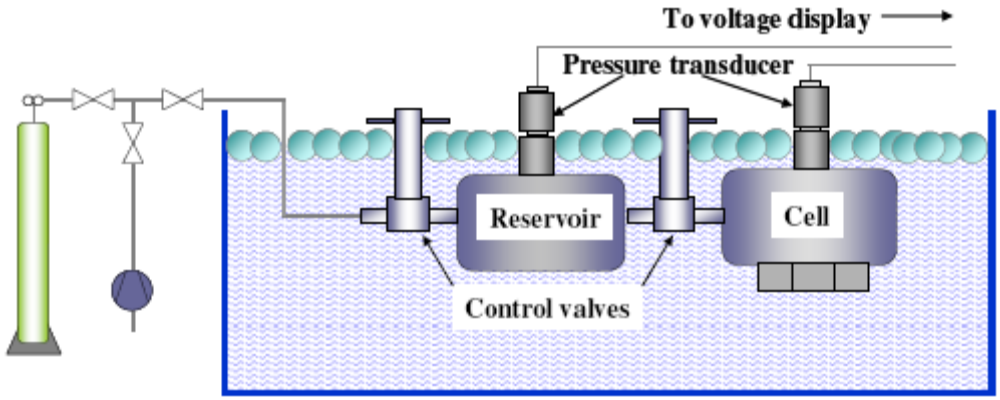

Figure-3.12: Schematic diagram of the pressure decay sorption system [1].

3.5. Characterization Techniques

3.5.1. Gel permeation chromatography (GPC)

Gel permeation chromatography was used to analyze the molecular weight and polydispersity index of the various polymer samples synthesized in this work. The samples were prepared as 5 wt% polymer in THF. The tests were performed in Dr. Chris Jones's laboratory (Viscotek – GPCmax).

3.5.2. Fourier Transform Infra-red Spectroscopy (FTIR)

Fourier transform infrared spectroscopy provides information about the functional groups present in a sample. More specifically, bonds in a sample that can generate a dipole-dipole moment will be active to FTIR spectroscopy. A Bruker Tensor 27 FTIR spectrometer was used for these measurements. Polymer powder samples were analyzed using a Harrick MVP_2 micro ATR with at least 256 scans at a resolution of $1cm^{-1}$.

3.5.3. Nuclear Magnetic Resonance Spectroscopy (NMR)

^{1}H NMR (also known as proton NMR) experiments were conducted in deuterated solution. The samples were prepared by dissolving polymer into deuterated THF/DMSO (Dimethyl Sulfoxide) at 2 – 2.5 wt%. The solutions were analyzed using a Varian Mercury Vx 300 spectrometer to determine the characteristics polyimide peaks. ^{13}C NMR experiments were conducted in solid state using a Bruker DSX 300 with the following specifications: 7 mm MAS rotor, 300 MHz 1H, pulse sequence: CP-MAS with TOSS to suppress spinning side bands, spinning speed: 5 kHz, repetition delay of 4 s, contact time of 1 ms, 90 degree pulse length: 5 microseconds, number of scans: 10K.

3.5.4. Scanning Electron Microscopy (SEM)

Scanning electron microscopy (SEM) was used to directly observe some of the morphological characteristics of hybrid membranes. While the resolution is not small enough to clearly show the presence of angstrom scale defects believed to exist in some membranes, it can show larger voids that may occur in the film. Mixed matrix membrane interfacial morphology with 6FDA-6FpDA and AlPO-14 were examined under a high resolution scanning electron microscope (Leo 1530 thermally assisted field emission (TFE), Cambridge, UK). The SEM samples were prepared by fracturing the mixed matrix films cryogenically in liquid nitrogen using two tweezers. The samples were sputter coated with gold. In the case of AlPO-14 molecular sieves, a very dilute solution of AlPO-14 in methanol was prepared (~1 wt% solution). One to two drops of this dilute solution was allowed to dry on the sample holder surface before examining the powders for their geometric characteristics.

3.5.5. Dynamic Scanning Calorimetry (DSC)

The glass transition temperature (Tg) of the polymers was determined using a DSC (Q200, TA instrument). The sample is heated beyond its expected glass transition temperature point but below the thermal degradation point. Energy flux required to heat the sample is continuously monitored in this experiment. The glass transition temperature is determined by the step increase of the energy flux because at temperatures above the Tg, the polymer enters the rubbery state, and in the rubbery state, more chains are flexible and so more energy is required to raise the temperature of the sample. DSC experiments

were done with 6FDA-6FpDA films and a white solid precipitate from 6FDA-6FpDA thermal imidization process. In all the DSC experiments, the samples were heated to 350^0C at a ramp rate of 10^0C per min.

3.5.6. Gas Chromatograph (GC)

As mentioned earlier, mixed gas permeation measurements were conducted in a similar manner as pure gas measurements. Feed gas was swept over the membrane using less than a 1% stage cut (ratio of permeate flow / feed flow) to ensure a constant composition on the upstream side (to avoid concentration polarization [5]). Flow rate was verified with a bubble flow meter at the feed line outlet. Flow was controlled with a needle valve. At steady state, the sample was collected in the downstream and the permeation rate was measured. The sample was sent to the GC (HP 5880) loop, and automatically injected. The GC is equipped with a TCD detector, and a HP-Plot / Al_2O_3 (30m) column.

3.6. References

1. Burns R. L., Koros W.J., *Defining the challenges for C_3H_6/C_3H_8 separation using polymeric membranes*. JMS, 2003. **211**: p. 299-309.

2. Staudt-Bickel C, Koros W.J., *Olefin/paraffin gas separation with 6FDA-based polyimide membranes*. JMS, 2000. **170**: p. 205-214.

3. Tanaka K, A.T., Jianqiang Hao, H. Kita, K. Okamoto, *Permeation and separation properties of polyimide membranes to olefins and paraffins.* JMS 1996. **121**: p. 1997-207.

4. Okamoto, K., Jinaquiang Hao, K Tanaka, H Kita, *Permeation and separation properties of polyimide membranes to 1,3-butadiene and n-butane*. JMS, 1997. **134**: p. 171-179.

5. Omole, Imona, *Crosslinked Polyimide Hollow Fiber Membranes for Aggressive Natural Gas Feed Streams*, PhD dissertation, Georgia Tech, 2008

6. Perry, John D, *Formation and Characterization of Hybrid Membranes Utilizing high Performance Polyimides and Carbon Molecular Sieves*, PhD Dissertation, Georgia Tech, 2007

7. Kudryavtsev, V.V., *Polyamic Acids and Polyimides – Synthesis, Transformations and Structure*, Edited by Bessonov and Zubkov, CRC press, **1993**. p. 13-17.

8. R. L. Burns, W.J. Koros, *Defining the challenges for C_3H_6/C_3H_8 separation using polymeric membranes*. JMS, 2003. **211**: p. 299-309.

CHAPTER 4

HIGH MOLECULAR WEIGHT 6FDA-6FPDA SYNTHESIS AND CHARACTERIZATION

4.1. Abstract

The first section of this chapter describes the main criteria for selecting high performing polymer as a first step for propylene/propane separations. The reasons for these selections are described in detail. After identifying best polymer, the main challenge in this research was to synthesize high molecular weight polymer consistently. A modified synthesis method has been described here. A closer look on different imidization methods (chemical and thermal) has also been described in detail. One main problem with the thermal imidization approach was the formation of a white solid precipitate in polymer solution. This has been addressed and the white precipitate was successfully eliminated. GPC, FTIR and solution NMR was used to characterize synthesized polymers.

4.2. Upper Bound Polymers for Propylene/Propane Separations

As mentioned in Chapter 2, Burns and Koros introduced the C_3H_6/C_3H_8 separation upper bound curve at 50^0C based on pure gas separation performances (Figure-4.1). Data were taken from a number of research studies and matched with a

mathematical model [1]. Staudt-Bickel and Koros [2] also reported an ideal selectivity of 16 for the polyimide 6FDA-6FpDA. The report showed an increase in selectivity with a decrease of temperature from 308K to 298K. Table-2.1 shows a selected summary of pure polymer permeabilities and selectivities for this particular gas pair used to construct the upper bound [1].

Table-4.1: C_3H_6/C_3H_8 permeability and selectivity for different polymers (pure gas)

Ref#	Author	Polymer	Temp (^oC)	Feed Pressure	P_{C3H6} (Barrer)	C_3H_6/C_3H_8
[2]	Staudt-Bickel and Koros	6FDA-mPD	35	3.8 atm	0.13	10
[2]	Staudt-Bickel and Koros	6FDA-IpDA	35	3.8 atm	0.58	15
[2]	Staudt-Bickel and Koros	6FDA-6FpDA	35	3.8 atm	0.89	16
[1]	Burns and Koros	Matrimid®	35	2 atm	0.10	10
[1]	Burns and Koros	6FDA-33'DMDB	35	1.1 atm	0.15	13.2
[3]	Tanaka et al.	6FDA-TrMPD (DAM)	50	2 atm	**30**	**11**
[4]	Okamoto et al.	6FDA-DDBT	50	2 atm	**1.8**	**20**
[3]	Tanaka et al.	6FDA-DDBT	50	2 atm	**0.76**	**27**

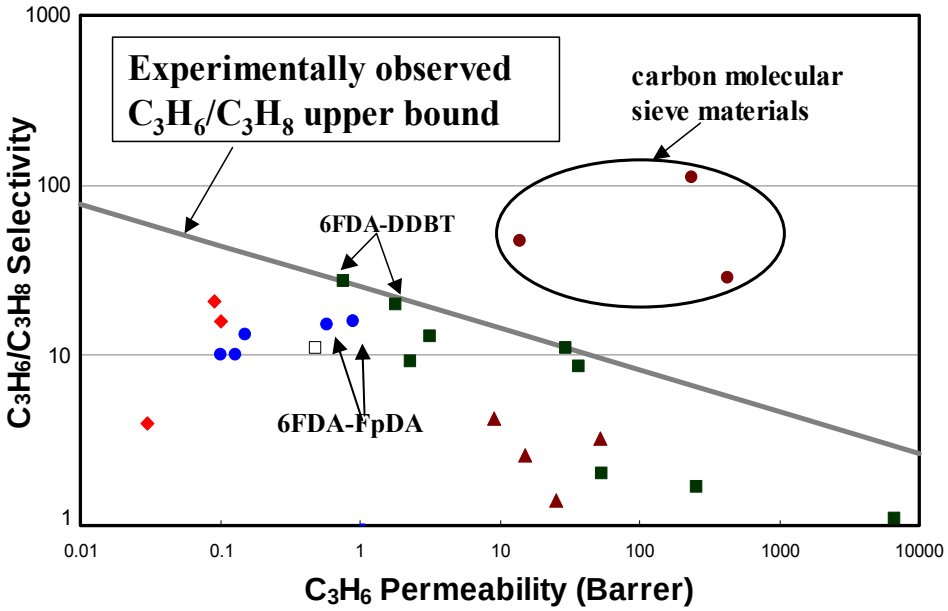

Figure-4.1: C_3H_6/C_3H_8 experimental upper bound based on pure gas permeation data over the range 1 – 4 atm feed pressure.□ = 100°C, ■ = 50°C, ● = 35°C, ▲= 30°C, ♦ = 26°C. [1]

Considerable research has been done on glassy polyimides, and polyimide-co-polypyrrolones [1]. Among all of these, polyimides based on 4,4'(hexafluorisopropylidene) dipthalic anhydride (6FDA) have exhibited the best performance (6FDA structure is shown in Chapter-3). The upper bound is currently defined by the 6FDA-based polymers prepared from the TrMPD (DAM) and DDBT. Ideal selectivities of these polymers are 11, 20, and 27 respectively at 50˚C with permeabilities of 30 and 1.8, 0.76 Barrer respectively. A value of 0.76 Barrer (propylene permeability) and 27 (selectivity) was later reported as the test result from an aged film

(with initial permeability of 1.8 Barrer and selectivity of 20) [3, 4]. Hence, the current upper bound is defined by two data points.

4.2.1. 6FDA-DDBT Structural Dependence and Impurity

Initially, research was pursued with 6FDA-DDBT by Burns [1]; however, the work indicated that this material is not the preferred matrix material. Two potential reasons were identified for this result. DDBT monomer used by Tanaka et. al [3] is dimethyl-3, 7-diaminodiphenylthiophene-5, 5-dioxide. This monomer is a mixture of 63% 2, 8 and 33% 2, 6 and 4% 4, 6 positions of two methyl groups obtained from Ube industries. On the other hand, DDBT used in our laboratory by Burns was a mixture of 70-75% 2, 8 and rest 4, 8 methyl isomers (source: Sigma-Aldrich). It is believed that the presence of methyl groups in 4, 8 position instead of 2, 6 and 4, 6 positions will change the polymer spacing which might change the polymer properties. Moreover, DDBT for this synthesis was 98% pure and could not be purified by sublimation due to very high sublimation temperature (~350^0C). Recrystalizing the monomer in water, a technique commonly used for monomer purification process was attempted, but resulted in essentially zero yield. Synthesis of 6FDA-DDBT was then done without purifying DDBT monomer. It was assumed that the monomer is 98% pure in order to match the dianhydride and diamine stoichiometric ratio. 6FDA-DDBT synthesized in our laboratory had a very low molecular weight and was too brittle to be casted as films. As described in the next section, monomer impurity is one of the main concerns for low M_w polymers. At this point, it was then decided to look into 6FDA-6FpDA polymer material.

4.2.2. Selection Of 6FDA-6FpDA Polyimide For C_3H_6/C_3H_8 Separation

6FDA-6FpDA is another polyimide for this particular gas pair with very high permeability and selectivity. As shown in Table-2.1, the permeability of propylene with 6FDA-6FpDA this polymer is 0.89 at 3.8 atm. The selectivity is 16 in this case. It should be noted here that propylene pressure reported is 3.8 atm, instead of 2 atm like other cases mentioned above. Due to dual mode pressure dependence, permeability at 2 atm should be higher than 0.89 Barrer. Moreover, the permeation test for 6FDA-6FpDA was done at 35^0C, instead of 50^0C like other cases. As mentioned in Chapter 2, high test temperature also increases the permeability while the selectivity reduces. So effectively, 6FDA-6FpDA is one of the highest performing polymers for $C_3H_6/C_3/H_8$ separations.

Following the difficulties with the DDBT monomer, 6FDA-6FpDA polymer was selected for the current research work. Another advantage of 6FDA-6FpDA polyimide is the excellent permeability matching with AlPO-14. As shown later in Chapter-6, polymer and molecular sieve matching is very important for mixed matrix material success. A very highly permeable molecular sieve can reduce the overall permeability of the mixed matrix membrane. This has been demonstrated and discussed in details in Chapter-6.

Although 6FDA-DAM is one of the highest performing polymers for this particular separation, it is too permeable with respect to AlPO-14 propylene permeability. Thus using 6FDA-DAM as polymer matrix would have essentially reduced the permeability of mixed matrix materials. This will be discussed in more details in Chapter-6 with mixed matrix material results.

4.2.2.1. Initial synthesis of 6FDA-6FpDA polyimide

Figure-4.2 shows the structure of 6FDA-6FpDA. Two batches of this polymer were synthesized by the thermal imidization process described in Chapter-3. Both batches had low M_w (highest molecular weight observed was ~50k with a PI >5.0) determined by GPC. A detailed study identified three major areas of difficulty during synthesis process. First, our 6FDA monomer was 99% pure, whereas 6FpDA was 98% pure creating a stoichiometric discrepancy in the molar weight ratio. High M_w weight can be achieved with desired end-group controlled by Carother's Equation [6] which depends strictly on the stoichiometric ratio.

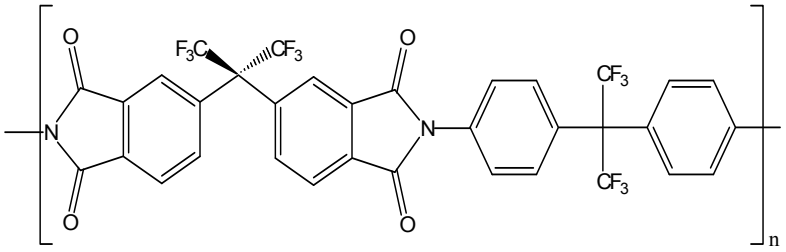

Figure-4.2: Structure of 6FDA-6FpDA polyimide

In the case of impure monomers, even if the monomers are added in a 1:1 stoichiometric ratio, impurities disturb the stoichiometric ratio, which is one of the most important parameters for high M_w and low PI. When the ratio is not actually 1:1, two possible reactions can take place during the polyamic acid formation step. First, the excess monomer can form di-mers or tri-mers and stop growing in length. These

relatively small molecules then contribute to the formation of a much broader polydispersity, thereby resulting in a much higher PI [7]. Second, if there are slow reacting impurities in the solution, there will be a competitive reaction between the impurities and monomers where impurities can end the chain growth in a polycondensation reaction. In this case, low molecular weight oligomers [7] will form instead of high M_w polymer. In all of these cases, a low molecular weight polyamic acid solution results in a low M_w polyimide.

Another important problem in the synthesis process is the presence of moisture. Since 6FDA is an anhydride, which attracts atmospheric moisture even at room temperature forming carboxylic acids. For the same reason, the number of available sites for diamine addition for a given amount of anhydride decreases the probability of creating the desirable repeat unit. This again results in a low molecular weight polymer. Lastly, one important parameter during synthesis is the local hot zone formation during 6FDA addition. 6FDA is added in a diamine solution (in NMP). As soon as the dianhydride is added, the polycondensation reaction starts. This reaction is exothermic and increases the temperature locally. Consecutively, the reaction stops in that particular region. It is desirable to have an ice bath during polyamic formation step of synthesis thus reducing the reaction temperature.

4.3. Synthesis Of High Molecular Weight 6FDA-6FpDA

The following changes in the polyamic formation process were made to ensure high molecular weight and low PI polyimide.

- Before monomer sublimation, both monomers were dried in a vacuum oven for overnight, around 20^0C below its sublimation point. (To increase the sublimation yield)
- Each monomer was sublimed twice to achieve required purity. (Yield increased – from 40% to 90%).
- Before the synthesis experiment, sublimed monomers were again dried in the vacuum oven overnight to eliminate residual water. (To remove any ambient moisture)
- During synthesis, measures were taken to add monomers rigorously in their stoichiometric ratios. (High M_w)
- NMP was needle-transferred to the reaction flask after being dehydrated by molecular sieves.
- An exact amount of diamine was added, while stirring the reaction flask continuously.
- An ice bath/cooling system is kept to maintain the solution temperature below room temperature (RT) after diamine addition.
- Once diamine dissolved in the solution completely, a pre-calculated amount of dianhydride was added portion wise (3-4 equal portion).

- The reaction was carried out first at low temperature and then at RT, with constant temperature monitoring.

Moreover, the thermal imidization process described in Chapter-3 was used instead of chemical imidization process. It is believed that in the chemical imidization process the ring closure is not always complete, whereas in the thermal imidization the ring closure is complete. Two batches of 6FDA-6FpDA were synthesized by following the above procedure strictly. *Ortho*-dichloro-benzene (ODCB) was used as the dehydrating agent. The M_w of the synthesized batches were 198k and 157k Daltons with PI around 2.5 and 3.0.

4.3.1. Role Of Monomer Impurities In Synthesis

To further understand the role of impurities and how it affects the molecular weight of 6FDA-6FpDA polymer, an extensive synthesis study was performed. M_w and PI was calculated by GPC. THF was used as the GPC solvent. Table-4.2 summarizes the synthesis condition with respective M_w and PI. To avoid additional variable, strict measures were taken to avoid moisture contact, especially with 6FDA. All the monomers were stored in desiccators. Sublimed monomers were used as soon as possible to maintain the purity achieved via sublimation.

For the first case in Table-4.2, pure 6FDA and pure 6FpDA were used. Both the monomers were sublimed at around 10^0C below their sublimation temperatures.

Monomers were added in 1:1 ratio to maintain the stoichiometry. As expected a very high molecular weight and narrow PI polymer was formed. In case 2, 6FpDA monomer was not sublimed while 6FDA monomer was sublimed as before. In general 6FpDA is received from Sigma-Aldrich as >99% pure and 6FDA is received as ~97% pure. So it was expected that an unsublimed 6FDA will have more inclination to form oligomers than the unsublimed 6FpDA. In this case our measured M_w was ~86k Daltons. The PI was 3.2, higher than the normal 2.0, but still in the acceptable range. Next synthesis was performed with pure 6FpDA and as received 6FDA (case-3). M_w in this case was ~50k and again with a PI of 3.3. Finally, 6FDA-6FpDA was synthesized with as received monomers (both 6FDA and 6FpDA, case 4). In this case the M_w was 73k and the PI was 3.7. It can be clearly seen that monomer purification does play an important role in the formation of these polyimides.

Table-4.2: Relation between molecular weight and monomer purity

No.	***Polymer Name***	***M_w*** ***(Daltons)***	***PI*** ***(M_W/M_N)***	***Monomer Purification***	***6FDA: 6FpDA***
1	6FDA-6FpDA	198k	3.0	Both monomers were sublimed	1:1
2	6FDA-6FpDA	86k	3.2	6FDA sublimed, 6FpDA impure	1:1
3	6FDA-6FpDA	50k	3.3	6FDA impure, 6FpDA sublimed	1:1
4	6FDA:6FpDA	73k	3.7	Both were unsublimed	1:1
5	6FDA-6FpDA	57k	3.9	Both were unsublimed	1.015:1

Sometimes dianhydrides are added in excess (typically 1.5 wt% excess). This excess addition then takes care of two unwanted side reactions during polyamic acid formation. One batch of such polymer was synthesized. But this case (case-5) also resulted in a low molecular weight and high PI polyimides. This can be again explained by the same "early-chain termination" theory [7] mentioned before, where the impurities/excess monomers stop the polymeric chain growth during the polycondensation reaction. Moreover, if there is excess monomer in the reaction flask, it can shift the reaction in a reverse direction, bringing down the M_w of the polyamic acid [7].

At this point, a repeatable synthesis process was established with the thermal imidization process; however, a more serious problem was identified with 6FDA-6FpDA synthesis. The next section describes the problem and the solution in details.

4.3.2. Thermal Imidization of 6FDA-6FpDA

While successful synthesis of high molecular weight 6FDA-6FpDA was achieved with the thermal imidization technique, a major concern was the formation of precipitates in solutions of 6FDA-6FpDA (with and without nonsolvent); and 6FDA-DAM-DABA / 6FDA-DAM (with nonsolvents). The precipitate is hypothesized to be high molecular weight polymer chains and/or "crystallosolvates" that drop out of solution over time. From preliminary spinning results, it is believed that precipitates decrease the spinnability of the spin dope.

One observation that seems to shed some light is the absence of these precipitates in chemically imidized 6FDA-6FpDA (with and without nonsolvent). This preliminary result indicated that there might be a difference in the polyimide chain structure produced by the thermal versus the chemical imidization processes, which leads to precipitate formation in 6FDA based thermally imidized polymer (Figure - 4.3 and Figure-4.4).

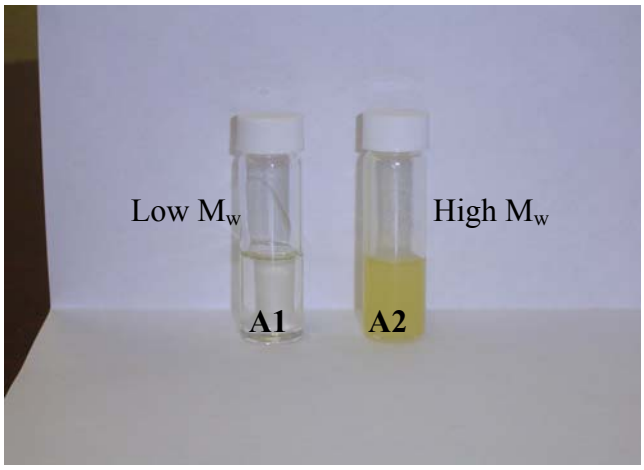

Figure-4.3: 6FDA-6FpDA polymer compositions
A1 - 20 wt% polymer, 15 wt% ethanol, and 65 wt% NMP (Chemically imidized)
A2 - 26 wt% polymer, 15 wt% ethanol, and 59 wt% NMP (Thermally imidized)

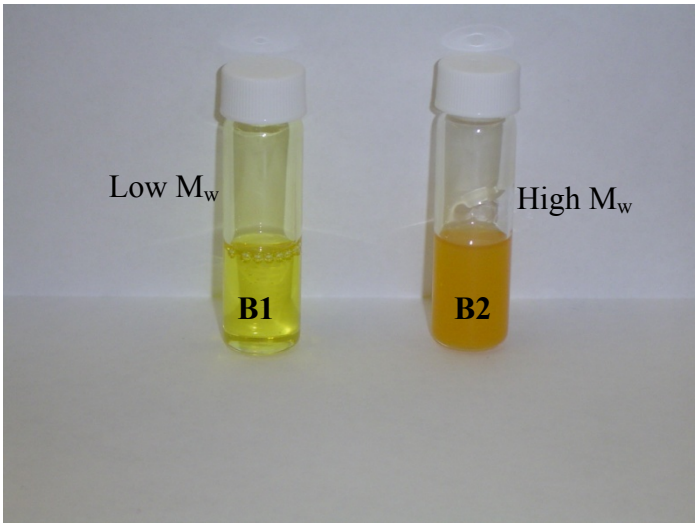

Figure-4.4:- 6FDA-DAM compositions

B1 - 20 wt% polymer, 20 wt% ethanol, and 60 wt% NMP (Chemically imidized)
B2 - 20 wt% polymer, 20 wt% ethanol, and 60 wt% NMP (Thermally imidized)

This was a point of concern because it is necessary to have a clear dope solution to be able to determine the phase separation point for spinning asymmetric hollow fiber

membranes. To solve this problem, the first step was to separate the white particles from the rest of the solution. The polymer solution as seen in Figure-4.3 was murky. A dilute polymer solution of Figure-4.3 (A2) was centrifuged (@10,000 rpm for 10 minutes) and the solid white particles were separated as precipitate. The solid particles were then dried under vacuum at room temperature for 30 minutes. The solid particles did not re-dissolve in any organic/inorganic solvents or strong acid.

The glass transition temperatures (Tg) of the solid particles were determined by DSC. The Tg for 6FDA-6FpDA pure polymer was measured to be ~317^{0}C whereas the Tg of this white solid was around ~316^{0}C. This finding indicated that the inherent structure of these two components (the solid particle and the original 6FDA-6FpDA polymer) might be essentially the same. FT-IR was performed on thermally imidized and chemically imidized 6FDA-6FpDA films to observe any structural difference between the two batches of polymers. All films were casted out of a dichloromethane solution.

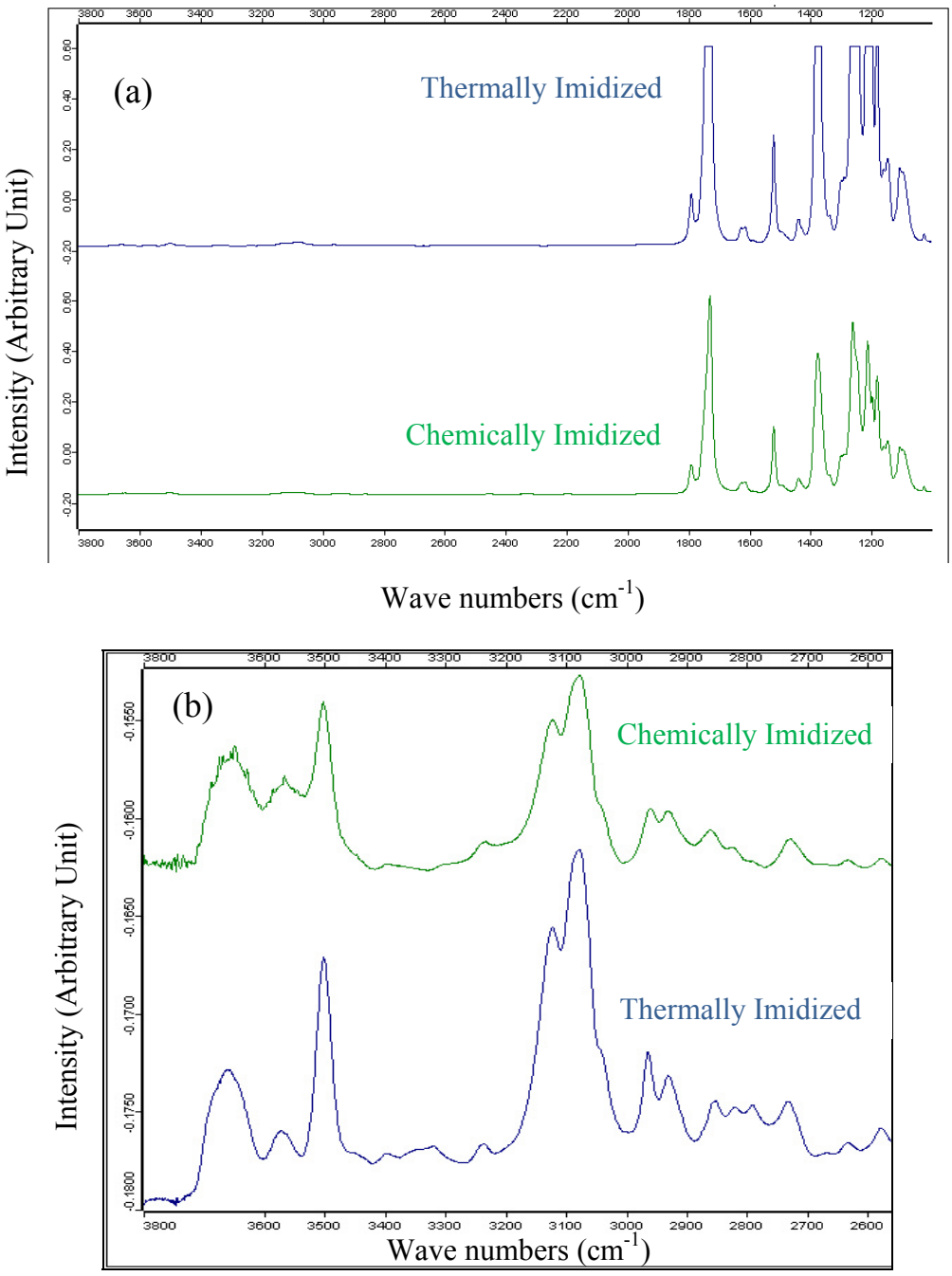

Figure-4.5: FT-IR of chemically and thermally imidized 6FDA-6FpDA (a) overall spectra (b) a close up (from 3800 – 3600 cm^{-1} wave numbers)

FT-IR measurements did not show any significant differences in these two films (Figure-4.5 (a) and (b)). Here it must be noted that the white precipitate is present at very low concentration , so it might be difficult to detect any difference via FT-IR. At this stage two possible hypotheses were formed.

1. The product is crystalline
2. There is some amount of crosslinking present in the polymer

In the first case, if there is some amount of crystallinity, the glass transition temperature will shift from the pure 6FDA-6FpDA polymer, which is not crystalline in nature. The glass transition temperatures reported in the previous sections were very similar. Moreover, XRD measurements revealed amorphous nature of the solid white powder. It was then concluded that the white precipitate might have formed due to undesired crosslinking during the thermal imidization/synthesis process. Since FT-IR did not show any differences between thermal and chemical imidization processes, proton solution NMR was used to characterize any differences between these two methods.

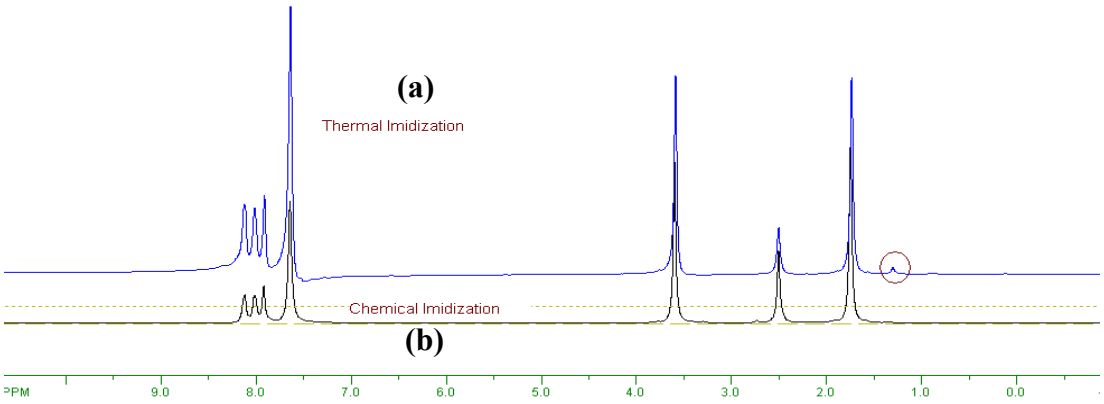

Figure-4.6: (a) Proton solution NMR of thermally imidized 6FDA-6FpDA in deuterated THF. (b) Proton NMR of chemically imidized 6FDA-6FpDA in deuterated THF solution

Figure-4.6 shows the solution NMR results of the two samples. A dilute solution of 6FDA-6FpDA was prepared in deuterated THF for solution NMR. The NMR spectra revealed a small additional for the thermal imidization. This extra peak was hypothesized to be the cause of white solid precipitate in the polyimides. To further investigate the effect of heat during imidization process, a batch of 6FDA-6FpDA polyamic acid was synthesized, and the polyamic acid was collected and precipitated in DI (de-ionized) water. The precipitated acid was then collected and dried under vacuum at 180^0C for 20 hours *to mimic* the heat treatment during the thermal imidization process. The final product was then collected and GPC was performed to see the PI and M_w. Our M_w was around 90,000 with a PI of 3.0 showing that we had the ring closure reaction due to heat treatment. Proton solution NMR was then performed on 6FDA-6FpDA sample in deuterated THF solution (Figure-4.7). Surprisingly, in this case no extra peak was

observed. The resulting polymer solution is clear and soluble in organic solvents (THF, DMSO) indicating a lack of crosslinking.

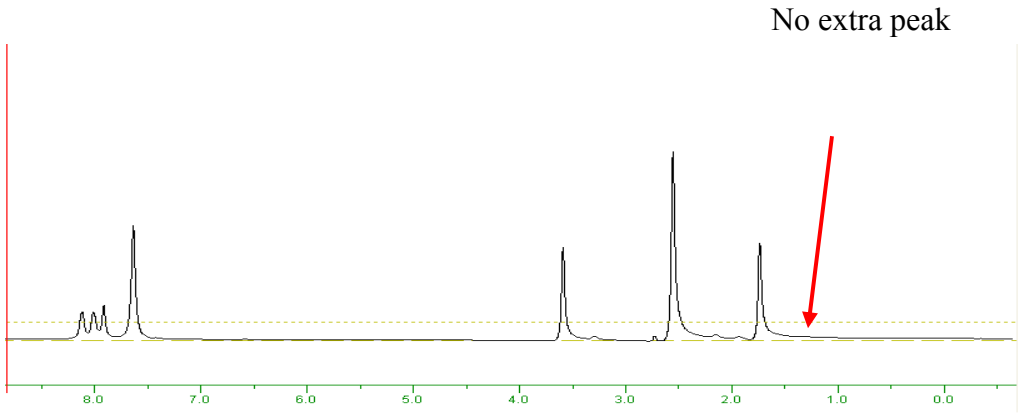

Figure-4.7: 6FDA-6FpDA NMR in deuterated THF. Polyamic acid was precipitated and then dried in vacuum oven. No extra peak was observed

The immediate conclusion from this result was: *heating the polyamic acid is not the sole cause of crosslinking*. To further investigate the effect of heating it was decided to heat the polyamic acid solution in NMP without precipitating in water (this is the normal path for the thermal imidization process). Moreover, it was decided to compare the effect of heating in thermal imidization with dehydrating agents used for chemical imidization (AcAn, tri-ethyl amine (TEA)/beta-picoline). The result then would clarify whether the thermal imidization agent (ODCB) is the cause of this extra peak.

At this stage, a large batch of polyamic acid in NMP was synthesized. This batch was divided in two parts (a) and (b). Part (a) was heated without any catalyst/reagent to 180^{o}C for 20 hours. Part (b) was heated at 180^{0}C for 20 hours after adding proportional

amount of *beta-picoline* and AcAn as described before (chemical imidization reagents). After 20 hours both parts were quenched with methanol and dried at 200^0C for 12 hours to conclude the ring closure. Proton solution NMR was performed on the two batches of polyimides. Two dilute solutions of polymer were prepared in dichloromethane to observe the solubility. Part (a) produced a clear solution and part (b) produced a murky solution (as seen in Figure-4.4). NMR spectra of the two batches are shown in Figure-4.8. Part (b) in Figure-4.8 shows the extra peak whereas part (a) doesn't.

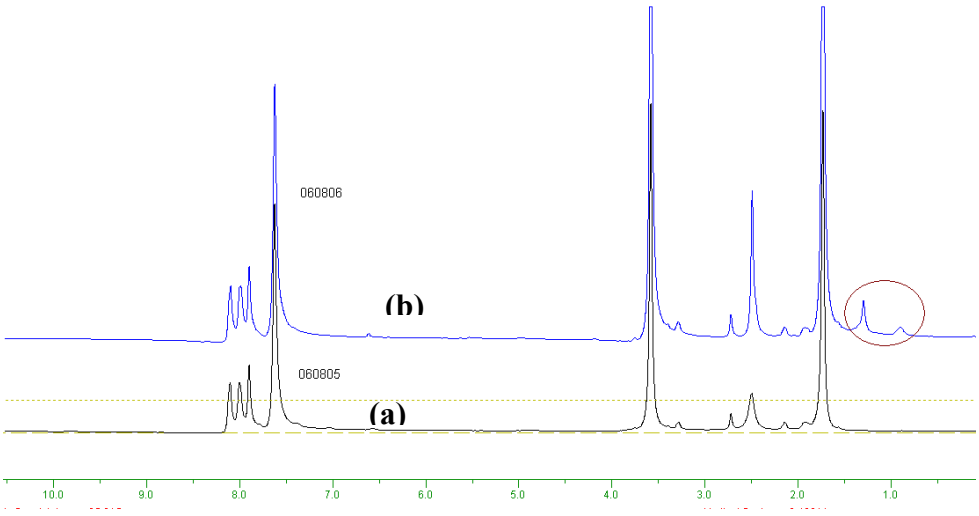

Figure-4.8: (a) 6FDA-6FpDA polyamic acid heated at 180^0C for 20 hours (b) 6FDA-6FpDA polyamic acid heated with *beta-picoline* and AcAn at 180^0C for 20 hours.

The only difference between part (a) and part (b) was the dehydrating agents. From this experiment it was concluded that any dehydrating agent added during thermal imidization, be it AcAn (originally used for chemical imidization) or ODCB (used for thermal imidization), is driving the short chain oligomers to crosslink amongst

themselves. We are particularly mentioning oligomers because according to our experience, small amount of white particles are generated during the thermal process. At this point, we believe that the oligomers, which are present after the polyamic acid reaction step, are activated in the presence of heat and dehydrating agents. This activation step is removing water molecules to form crosslinked oligomers.

4.4. Improved Chemical Imidization Of 6FDA-6FpDA

From the previous section it is obvious that for the synthesis of 6FDA-6FpDA polymer, heating of polyamic acid solution creates a murky solution not ideal for spinning process. On the other hand, previous researchers in our laboratory had very little success in achieving high M_w with the chemical imidization process. As mentioned in Chapter-3, the thermal imidization process is known to complete the ring closer process more completely than the chemical imidization process. The chemical imidization process previously used in our laboratory used an amine catalyst tri-ethyl-amine with acetic anhydride as the dehydrating agent. One drawback of this imidization process in our laboratory was the low molecular weight of the polymer (50k – M_w). In this research it was then decided to be able to successfully use chemical imidization process to achieve high molecular weight and narrow PI polymer. For the chemical imidization method, a dehydrating agent (like acetic anhydride) is added to the polyamic acid solution in presence of an amine based catalyst. Generally in presence of an acidic amine, a byproduct (isoimide) might form thus hindering the molecular weight distribution hence PI [7]. A basic catalyst is thus preferred for chemical imidization to perform complete

chain closure. To obtain high molecular weight polymer beta-picoline/TEA is used as the basic catalyst. In this particular case *beta*-picoline was used as the catalyst. *Beta*-picoline was used in this research because previous synthesis with TEA resulted in low molecular weight 6FDA-6FpDA polymer batches. Chapter-3 describes some of the problems with TEA as solvent.

As mentioned above, during the chemical imidization process, it is often hard to achieve complete ring closure. Moreover, there might be some isoimides present in the polyamic acid solution. For these reasons, a post treatment heating step is often performed after chemical imidization. In this method, after the polymer is precipitated out in pure methanol, it is dried under vacuum at an elevated temperature to complete the ring closure. Generally, a very high temperature helps. In this research, the polymers were dried between 200^0C – 250^0C for 12-16 hours. GPC tests were performed on the dried polymers with THF as the solvent. The molecular weight recorded was 227k Daltons with a PI of 2.0. Table-4.3 compares thermal and chemical imidization results.

Table-4.3: Comparison between thermal and chemical imidization process

No.	***Polymer Name***	***M_w*** ***(Daltons)***	***PI*** *(M_W/M_N)*	***Imidization Method***	***6FDA: 6FpDA***
1	6FDA-6FpDA	198k	3.0	Thermal	1:1
2	6FDA-6FpDA	203k	2.1	Chemical (*beta-picoline, AcAn*)	1:1
3	6FDA-6FpDA	227k	2.0	Chemical (*beta-picoline, AcAn*)	1:1

Figure-4.9 shows the dilute solutions from each imidization process. It is evident that the modified imidization process produces a clear solution with very high M_w and PI.

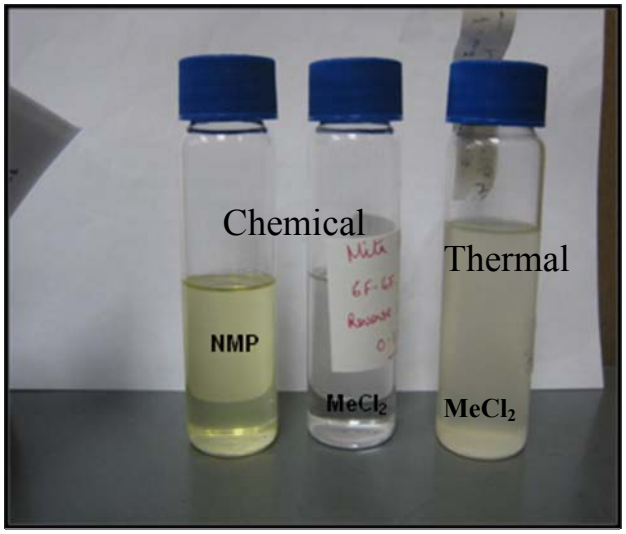

Figure-4.9: NMP and dichloromethane solution of 6FDA-6FpDA polymer from different imidization methods

Figure-4.9 clearly shows that we have successfully synthesized the desired 6FDA-6FpDA polymer. The results were reproducible as well (Table-4.3). Another significance of this synthesis was that the chemical imidization process is less complicated than the thermal imidization process (chemical imidization doesn't require a heating set up with continuous heat monitoring and condensation trap) and hence being less costly and more easily processable than thermal imidization process of 6FDA-6FpDA synthesis. Some further findings on the white "crystallosolvates" are discussed in the next section as well.

4.5. Conclusion

Once the cause and the source of the white solid were identified successfully, closer analyses of the NMR data were then performed to determine the elements responsible for the extraneous peak. A closer look at Figures 4.5, 4.6 and 4.8 revealed that the extra peak is due to the aliphatic carbon or N-H group present in the polyamic acid solution. A simple way to detect the presence of N-H/O-H is to run the sample NMR with Solvent + D_2O. If the peak is due to the presence of N-H group, then the peak will disappear when tested for proton NMR. The result of proton solution NMR in presence of D_2O is shown in Figure-4.10.

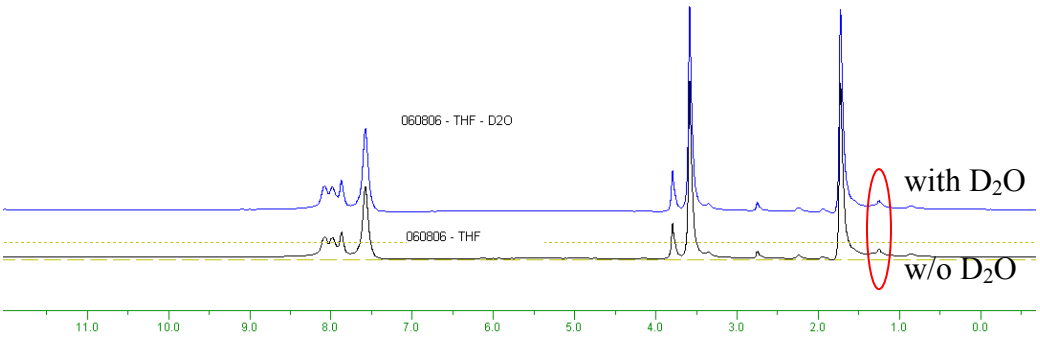

Figure-4.10: Proton solution NMR of 6FDA-6FpDA in THF (with and without D_2O)

It can be clearly concluded from the NMR results that there is unlikely any N-H groups present in the polymer. To further investigate the fact that the extra peak is due to the presence of aliphatic groups, solid state C-13 NMR was performed on the thermally imidized polymer. The sample was prepared by precipitating the white solid particles in NMP via centrifugation followed by drying at room temperature under vacuum. C13 NMR confirmed the presence of aliphatic carbon. Figure-4.11 shows these results.

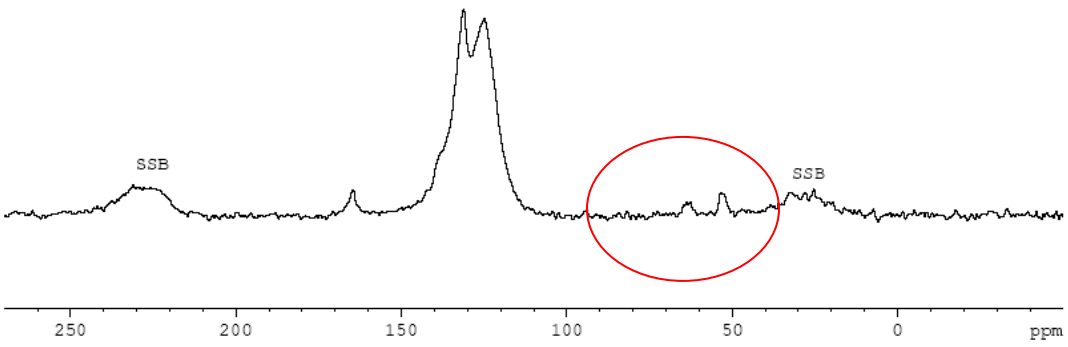

Figure-4.11: Solid white precipitate collected dried from 6FDA-6FpDA showing aliphatic peak

Here it is worth noting that there is no other aliphatic group in 6FDA-6FpDA other than methanol which is used to quench the polyimide before drying. This observation is interesting because methanol is known to have the ability to scission large

molecules. At this point we believe that the solid particles are the crosslinked oligomers formed due to the high heat in the presence of dehydrating agents. Once there was success with synthesis, the next step was to form membranes and characterize them via permeation and sorption experiments. The next chapter describes the permeation at different temperature with both pure and mixed gas with 6FDA-6FpDA polymer.

4.6. References

1. Burns R. L., Koros W.J., *Defining the challenges for C_3H_6/C_3H_8 separation using polymeric membranes*. JMS, 2003. **211**: p. 299-309.

2. Staudt-Bickel C, Koros W.J., *Olefin/paraffin gas separation with 6FDA-based polyimide membranes*. JMS, 2000. **170**: p. 205-214.

3. Tanaka K, A.T., Jianqiang Hao, H. Kita, K. Okamoto, *Permeation and separation properties of polyimide membranes to olefins and paraffins.* JMS 1996. **121**: p. 1997-207.

4. Okamoto, K., Jinaquiang Hao, K Tanaka, H Kita, *Permeation and separation properties of polyimide membranes to 1,3-butadiene and n-butane*. JMS, 1997. **134**: p. 171-179.

5. Yashino et al., *Olefin/paraffin separation performance as asymmetric hollow fiber membrane of 6FDA/BPDA-DDBT copolyimide*. JMS, 2003, **212**: p-13-27

6. Christopher J. Cornelius, *Physical and Gas permeation properties on a series of Novel hybrid inorganic-organic composites based on a synthesized fluorinated polymer.* PhD -Virginia Tech **2000**

7. Ohya et al, *Polyimide Membranes:Applications, Fabrications, and Properties*, Gordon Breach & Publishers, **1996**

CHAPTER 5

PERFORMANCE OF 6FDA-6FPDA FOR PROPYLENE/PROPANE SEPARATIONS

5.1. Abstract

The first part of this chapter describes the challenges faced by previous researchers with 6FDA-6FpDA polyimide for propylene/propane separations due to plasticization. A study on pure film annealing temperature has been shown here to optimize and standardize further test conditions to avoid any anomalies. Plasticization suppression was achieved by performing high temperature permeation on properly annealed dense films made with high molecular weight polymer. A detailed analysis of pure gas and mixed gas results using different permeability models has been shown in this chapter. The annealing effects in terms of plasticization suppression, permeability and selectivity have been discussed in detail. According to our best knowledge, this is for the first time plasticization suppression for propylene/propane has been reported with any polyimide dense film membrane. Results of pure gas sorption experiments using a pressure decay method with un-annealed and annealed films have been discussed. These sorption experiments have been used to analyze the permeation data using the dual-mode model. Mixed gas permeation results also have been explained with dual mode and bulk flow transport models.

5.2. Review of Plasticization Behavior of 6FDA-6FpDA

Propylene and propane tend to plasticize 6FDA-6FpDA at moderate test pressure and temperature (p>3 atm, T=35^{0}C). As discussed in Chapter-2, plasticization occurs as a result of swelling in the polymer and therefore an upswing in the propylene and propane permeability occurs, thereby suppressing the selectivity. An upturn in the permeability values with a sharp decrease in selectivity characterizes the onset of plasticization for a particular gas. Figure-5.1 shows the plasticization behavior of 6FDA-6FpDA (6F-6F) with propylene [1] observed by Staudt-Bickel and Koros. They reported an upturn in permeability values around 3 atm propylene upstream pressure onwards. Permeation tests were performed with pure gases in Figure-5.1.

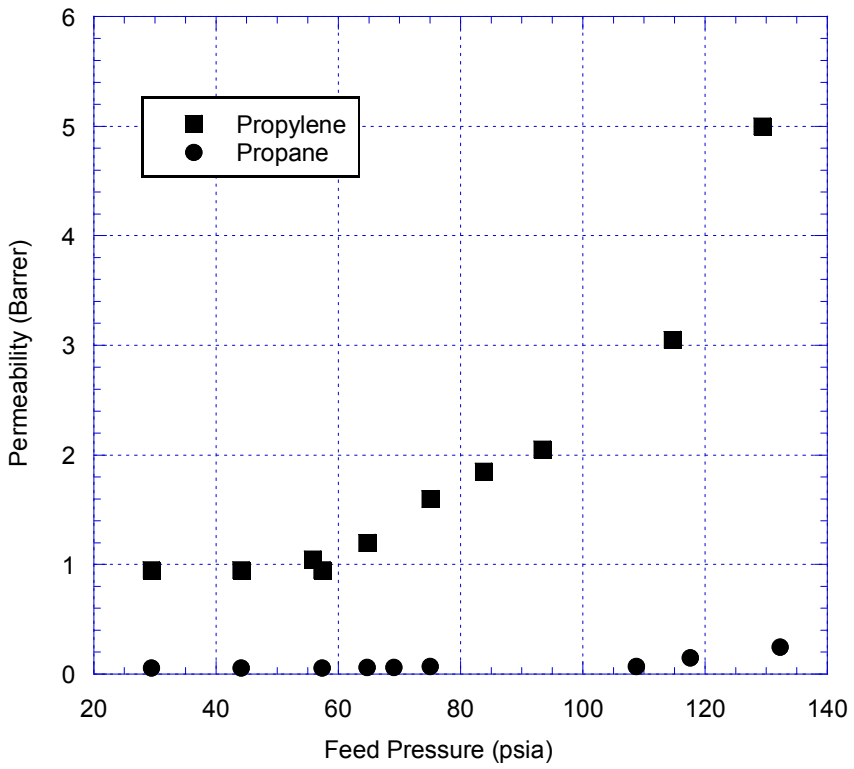

Figure-5.1: 6FDA-6FpDA plasticization behavior with pure gas. Tested at 35^0C [1]. ■ – Propylene permeability, ● - Propane permeability.

This behavior is unacceptable in a realistic process stream as a swelled membrane will have very low selectivity when tested under mixed gas compositions.

Figure-5.2 demonstrates this effect with a mixed gas propylene/propane permeation test. Permeation tests were done with a 50:50 propylene/propane gas mixture [1]. The mixed gas selectivity in this case drops down to 7 from an originally starting value of 13 (around 50% decrease in selectivity). Table-5.1 summarizes pure gas and mixed gas values observed by Staudt-Bickel et.al with 6F-6F polymer.

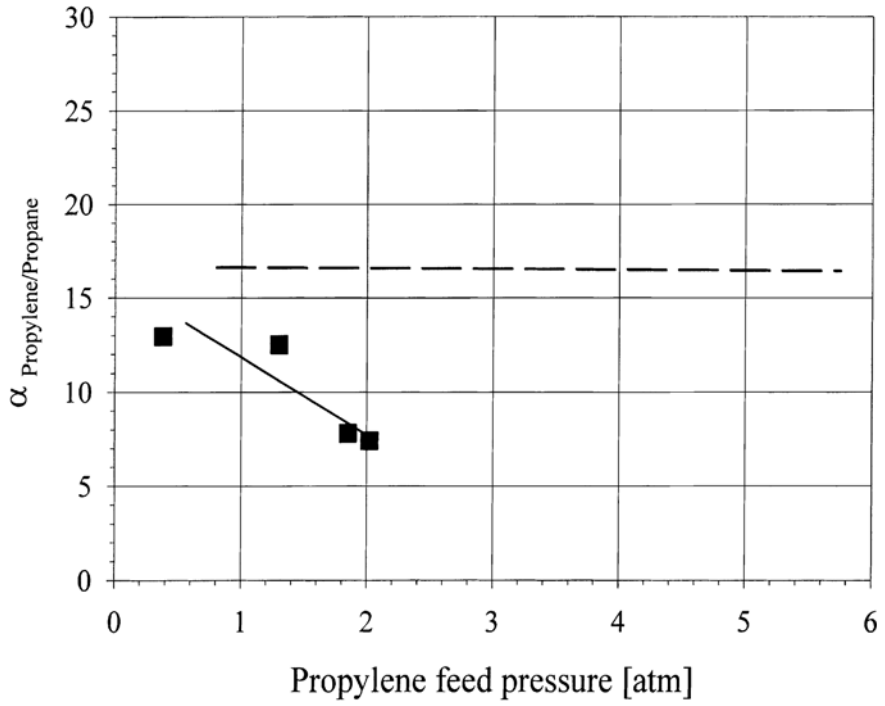

Figure-5.2: 6FDA-6FpDA plasticization behavior with mixed gas (50:50). Tested at 35^0C [1]. ■ – Experimental mixed gas selectivity, ---- - Ideal propylene/propane selectivity.

Table-5.1: Pure gas and mixed gas (50:50) permeabilities and selectivities of 6FDA-6FpDA propylene/propane separations at 35^0C. As reported by Staudt-Bickel et. al [1]

Condition	Propylene feed pressure (psia)	P_{C3H6} (Barrer)	C_3H_6/C_3H_8
Pure gas	29.4	0.89	16
Mixed Gas	19.1	0.48	13
	29.7	0.677	7

Since the ultimate applications of membranes are in the presence of mixed gas streams, it is important to achieve a high selectivity for propylene/propane mixed gas dense film experiments to demonstrate commercial viability. In a typical propylene/propane separation plant, elevated temperature operating conditions would be attractive to increase diffusion coefficients and to suppress sorption-induced swelling for a given feed pressure. Three approaches to solve this problem were proposed and executed. First, high temperature permeations were performed (70^0C). Second, systematic annealing of the samples was explored to optimize the annealing temperature, since preliminary work suggested that such a post membrane formation process leads to plasticization resistance. A third approach was to produce high molecular weight and low PDI polymer consistently. High molecular weight polymer is required for hollow fiber membrane production. Since this work is fundamental for future hollow fiber research, it is necessary to test dense film samples with similar properties (high M_w and low PI). Synthesis of high molecular weight and low PI polymer has already been discussed in Chapter-4. The next section describes the applications of first two above mentioned approaches for successful plasticization suppression.

5.3. Plasticization Suppression

5.3.1. High Test Temperature Effect On 6FDA-6FpDA

6FDA-6FpDA films were solution casted with dichloromethane as the solvent and dried at 110^0C in a vacuum oven for ~20 hours. Initial permeation tests were done at 35^0C and around 2 atm to compare our results with previous works. Pure gas permeation test results are shown in Table-5.2 with some of the previous results. The results in Table-5.2 are in good agreement with that seen by Burns and Koros and Sejour and Koros [2, 3].

Table-5.2: Pure gas permeation results for propylene/propane with 100^0C film drying temperature. Permeation tests were done at 35^0C and 2 atm.

	Pressure (psia)	Temperature (^{0}C)	P_{C3H6} (Barrer)	C_3H_6/C_3H_8
This Study	29.4	35	0.85±0.05	17±0.5
Sejour and Koros [3]	29.4	35	0.92	16.4
Burns and Koros [2]	29.4	35	0.89	16.0

In this case a small decrease in permeability with an increased selectivity was observed. Polymer permeabilities and selectivities are known to vary with the polymer synthesis and post drying conditions. Since the results mentioned in this research are obtained with a modified imidization approach, it was expected that the results might be little different than seen by others. This difference in the permeability and selectivity is perfectly within the acceptable range and were reproducible. To test the reproducibility,

at least three permeation tests were performed with each gas at a particular pressure. If the results were within 5-8% error range, it was considered to be reproducible. Oxygen and nitrogen permeabilities were also measured as benchmark gases. Table-5.3 shows these results at 35^0C.

Table-5.3: Pure gas permeation results for oxygen/nitrogen with 100^0C film drying temperature. Permeation tests were done at 35^0C and 2 atm.

Condition	Pressure (psia)	Temperature (^{0}C)	P_{O2} (Barrer)	O_2/N_2
Pure gas	29.4	35	17.0±0.6	4.2±0.4

High test temperature permeation tests were performed after successfully reproducing propylene/propane results at 35^0C. As noted earlier, at this point, it was hypothesized that permeation at elevated temperature (in this case 70^0C) will delay the effect of plasticization. Figure-5.3 shows the propylene isotherm obtained with 70^0C permeation test temperature. At high temperatures the solubility coefficient decreases, thereby decreasing the permeability and hence suppressing plasticization, so it was expected that performing permeation at a higher temperature would suppress the plasticization to a higher pressure.

Figure-5.3 clearly indicates that there is plasticization with propylene even at 70^0C. This result was unexpected under these test conditions. Moreover in this case, the onset of plasticization is earlier than 3 atm (2.5 atm) as reported by Staudt-Bickel [1]. One of the main differences between these two experiments was the casted film drying

temperature. While in Staudt-Bickel's cast films were annealed above 200°C for several hours, in this study the films were dried at 110°C for several hours.

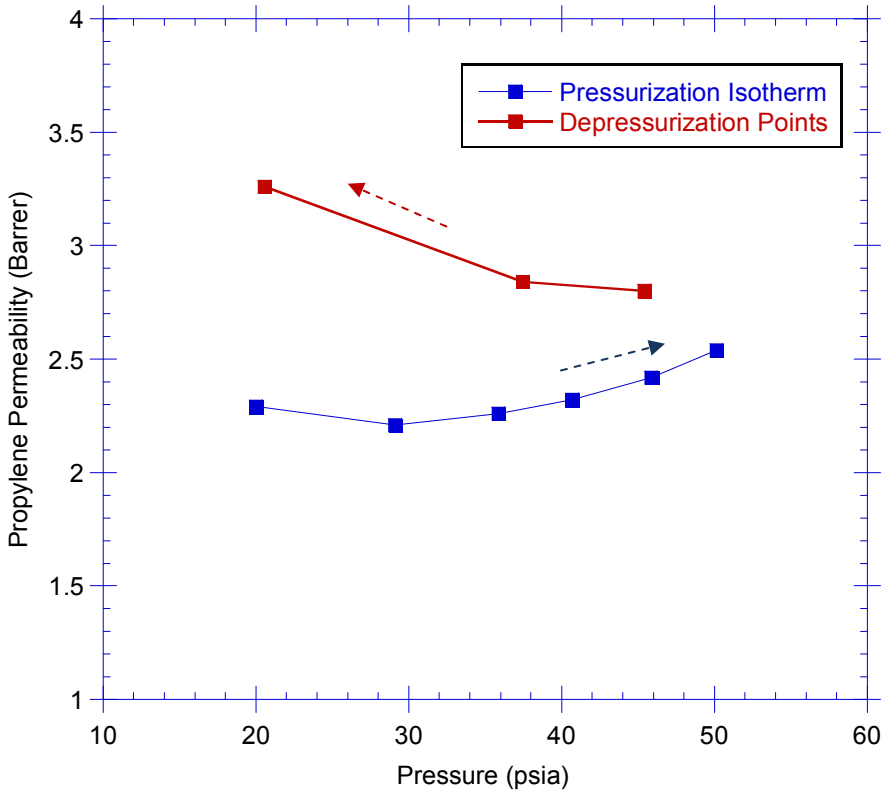

Figure-5.3: Propylene permeability isotherm at 70^0C. ■ – propylene pressurization, ■ – propylene de-pressurization

To probe more into these results, a detailed study of the post treatment conditions was conducted. Annealing studies were performed in which exposure to > 200^0C for 24 hr. was compared to 110^0C and 150^0C for roughly an equivalent period.

5.3.2. Annealing Effect On Pure Gas Permeation

Table-4 shows the result of this annealing effect on oxygen/nitrogen. The annealing effect is prominent with oxygen/nitrogen data in Table-5.4. Permeability of oxygen decreased with increasing annealing temperature, whereas the selectivity of oxygen/nitrogen increased.

Table-5.4: Pure gas permeation results for oxygen/nitrogen with different film drying temperatures. Permeation tests were done at 35^0C and 2 atm.

Annealing Condition	Pressure (atm)	Temperature (^{0}C)	P_{O2} (Barrer)	O_2/N_2
110^0C	29.4	35	17.0±1.0	4.2±0.4
150^0C	29.4	35	16.5±0.8	4.5±0.2
210^0C	29.4	35	16.2±0.4	4.7±0.4
220^0C	29.4	35	16.0±0.5	4.8±0.2

This phenomenon is typical for the annealing effect by which polymer chains become more relaxed and hence more densified as we increase the annealing treatment temperature. Based on these results, it was decided to follow annealing temperature of 210^0C for 18-20 hours for all experiments onwards to maintain consistency. From this point, any film dried at 110^0C will be referred to as "un-annealed", and films dried at 210^0C as "annealed". Table-5.5 summarizes the propylene/propane annealing results with different permeation test temperatures. In the case of propylene/propane separations also we saw a decrease in permeability and increase in selectivity after annealing.

Table-5.5: Pure gas permeation results for propylene/propane with different film drying and test temperatures. Permeation tests were done at 2 atm.

Drying Condition	Test Temperature (^{0}C)	Pressure (psi)	P_{C3H6} (Barrer)	C_3H_6/C_3H_8
110^{0}C	35^{0}C	29.4	1.0 ± 0.05	17±0.8
210^{0}C	35^{0}C	29.4	0.7 ±0.05	19±1.0
110^{0}C	70^{0}C	29.4	2.21± 0.1	12.0
210^{0}C	70^{0}C	29.4	0.96 ±0.08	13.0±0.5

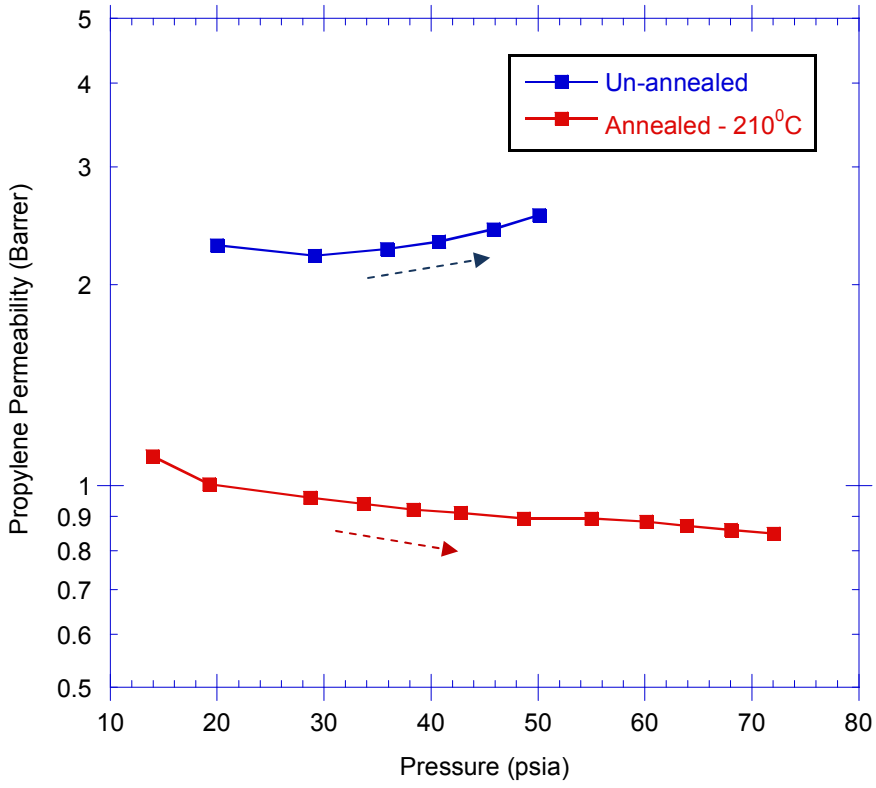

Figure-5.4: Propylene permeability isotherm with 6FDA-6FpDA at 70^{0}C, ■ – un-annealed at 110^{0}C, ■ – annealed at 210^{0}C.

Figure-5.4 shows the successful plasticization suppression results with annealed 6FDA-6FpDA films at the 70^0C test temperature. At least three films from different casted films were tested for each pressure point. The results were within 5% error range. After each pressurization isotherm, depressurization points were also noted and compared with the corresponding points. Unlike un-annealed films, annealed films did not show any plasticization effect up to 70 psi upstream pressure. Figure-5.5 shows the pressurization and depressurization behavior of both propylene and propane at 70^0C test temperature.

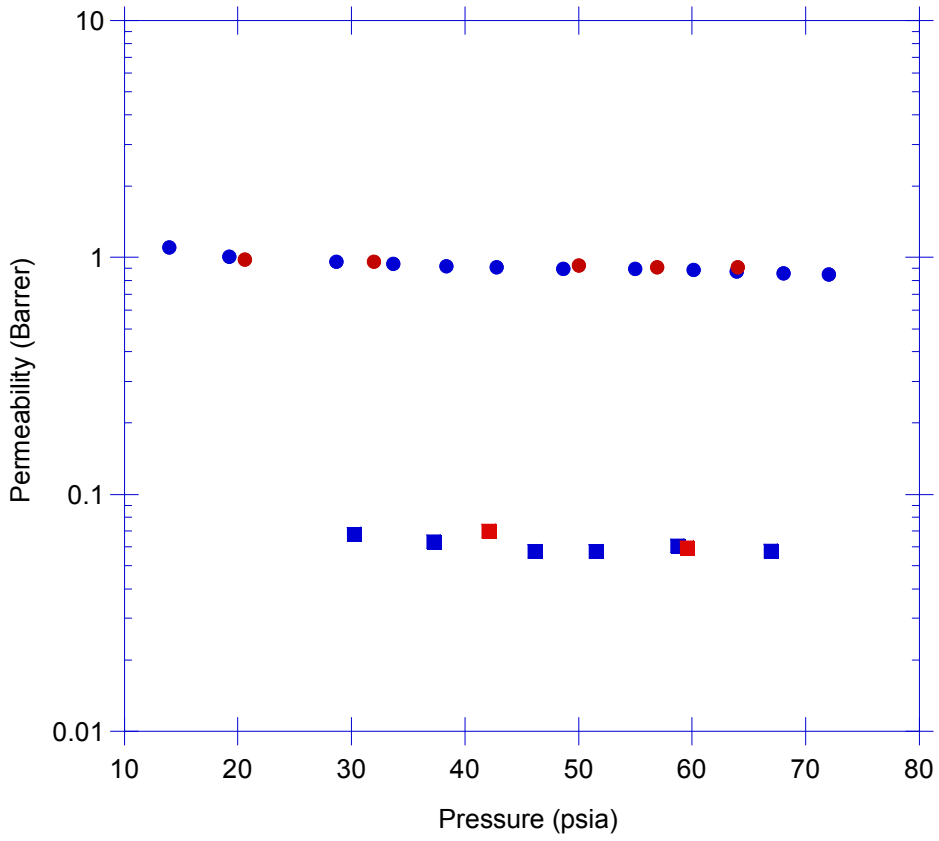

Figure-5.5: Plasticization suppression behavior. 6FDA-6FpDA propylene/propane. ●- propylene pressurization isotherm, ●- propylene depressurization point, ■ – propane isotherm, ■ – propane depressurization points. All tests were performed at 70^0C

Similar trends were observed with propane permeation as well. 6FDA-6FpDA did not plasticize up to 70 psi upstream pressure. The depressurization isotherm also suggested no indication of plasticization effect. This result suggests that suppression of plasticization was indeed achieved by annealing the films and performing permeation experiments at 70^0C. While this is for the first time we observed plasticization suppression of propylene with 6FDA-6FpDA up to 70 psi upstream pressure, as mentioned earlier, mixed gas composition experiments are the real tests for plasticization suppression. The next section describes the results from mixed gas experiments.

5.3.3. Mixed Gas Permeation Results

Mixed gas results were obtained for 50:50 mol% propylene/propane gas mixtures. Mixed gas experiments were conducted at 35^0C and 70^0C test temperatures to compare with our previous pure gas experiments. In both cases, no plasticization behavior was observed within the tested pressure range. We were able to eliminate early onset of plasticization for propylene in 6FDA-6FpDA even at 35^0C. As mentioned earlier, Staudt-Bickel observed very low mixed gas selectivity around 1.8 atm (26.5 psia). In our case, no plasticization behavior was observed up to 42 psia at 35^0C.

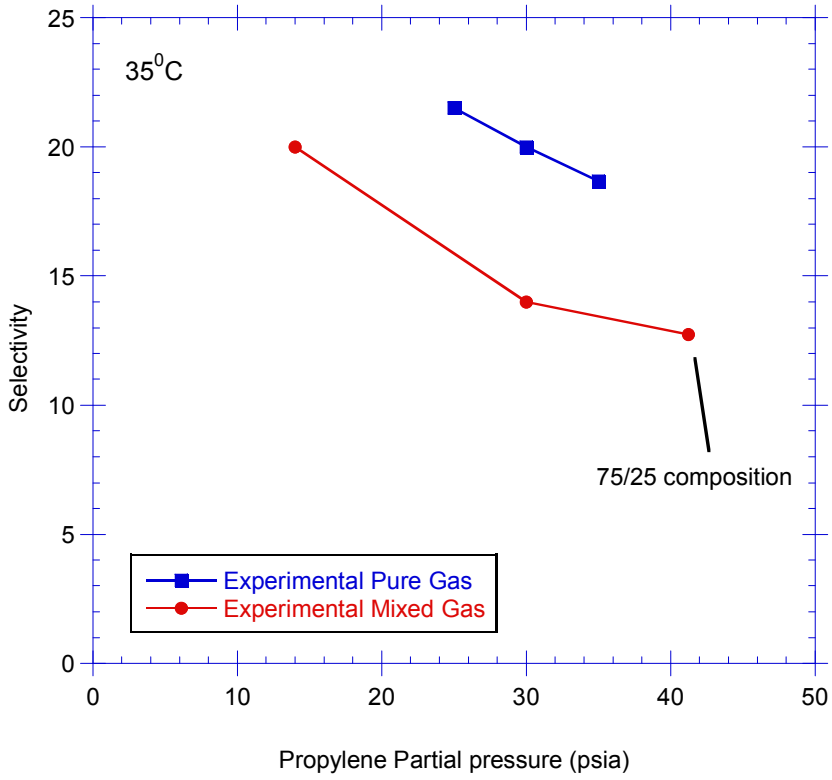

Figure-5.6: Pure gas and mixed gas results of propylene/propane separations with 6FDA-6FpDA. 50/50 mixed gas composition at 35^0C

A similar trend was observed with 70^0C permeation results as well. Figure-5.6 and Figure-5.7 represent 50:50 mixed gas results with propylene/propane at 35^0C and 70^0C respectively. Moreover, we noticed that the selectivity of mixed propylene/propane decreases more than previously observed for the pure propylene/propane case. This trend is similar to Staudt-Bickel's propylene/propane mixed gas observation (Figure-5.2) and is explained in the later section in terms of the dual mode transport model. According to the dual mode sorption and transport model, both propylene and propane permeability decreases in mixed gas environment.

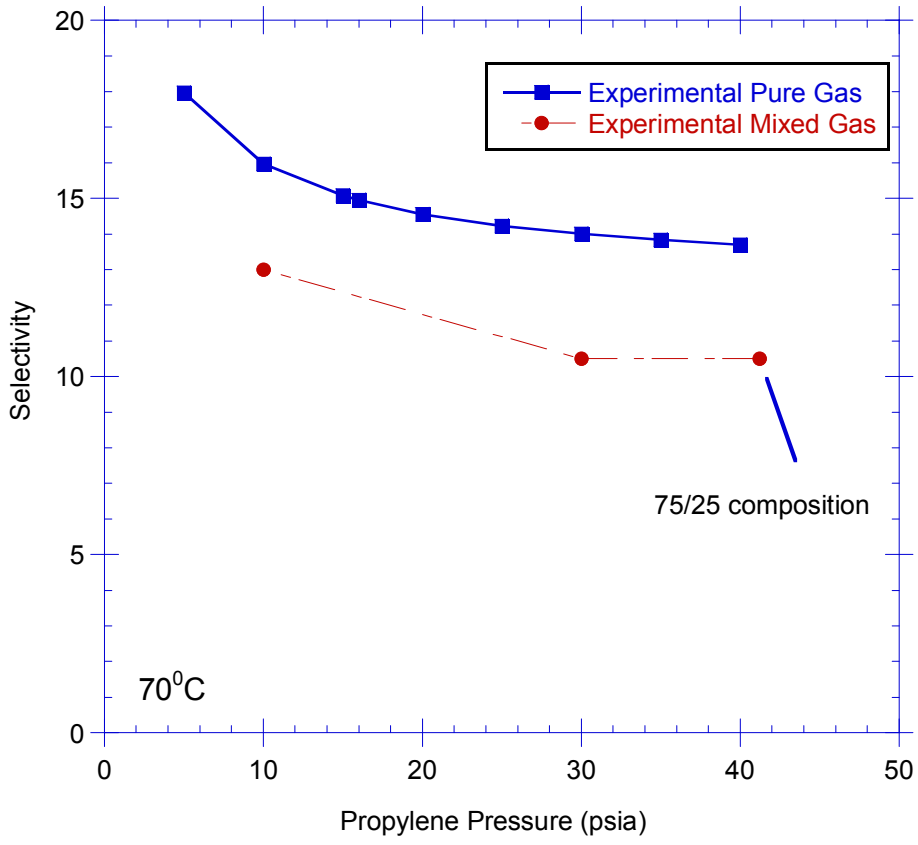

Figure-5.7: Pure gas and mixed gas results of propylene/propane separations with 6FDA-6FpDA. 50/50 mixed gas composition at 70^0C

To explain the mixed gas selectivity behavior in greater detail, a series of sorption experiments were done to determine (a) sorption behaviors of propylene and propane individually, (b) predicted mixed gas selectivity and permeability from sorption and permeation data and (c) bulk flow contribution to mixed gas selectivity and permeability for propylene/propane separations at 35^0C and 70^0C. The following sections describe all three of the above observations respectively.

5.3.3.1. Sorption experiments of 6FDA-6FpDA

Sorption experiments with propylene and propane were done at 35^0C and 70^0C. To maintain consistency with dense film permeability results, all the films were annealed around 210^0C for 18-20 hours. As mentioned in Chapter-2, the variation of gas permeability with pressure in glassy polymers is represented by a dual mode model. The model accounts for the differences in gas sorption properties in idealized Henry's law and Langmuir domain of a glassy polymer. The Langmuir concentration C'_{HA}, for gas A, describes sorption in the "microvoids" or "holes" throughout the matrix, which are the packing defects in the non-equilibrium glassy matrix. The sorption in glassy polymers is given by;

$$C_A = k_{DA} p_A + \frac{C'_{HA} b_A p_A}{1 + b_A p_A} \qquad [5.1]$$

Where k_{DA} is the Henry's law constant, C'_{HA} is the Langmuir capacity constant, and b_A is the Langmuir affinity constant. The sorption coefficient S_A is then given by;

$$S_A = \frac{C_A}{p_A} = k_{DA} + \frac{C'_{HA} b_A}{1 + b_A p_A} \qquad [5.2]$$

From the sorption experiments, k_d, C'_H, and b values were determined by Kaleidagraph model fit software.

Figure-5.8 depicts the sorption behavior of propylene and propane at 35^0C test temperature with 6FDA-6FpDA. As noted in Table-6, the sorption value S (in cc stp/cc.cm Hg) is around 1.6 times higher in the case of propylene than propane. This confirms the fact that the separation is mainly diffusion controlled in the case of this particular gas pair.

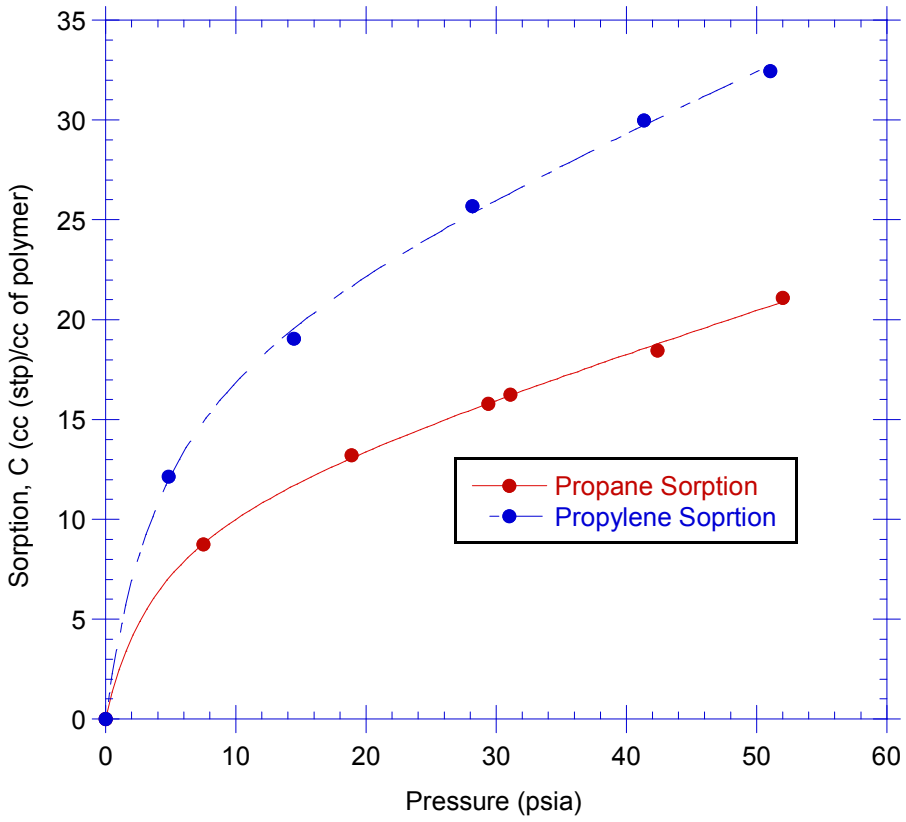

Figure-5.8: Pure gas propylene propane sorption results with 6FDA-6FpDA at 35^0C

Table-5.6 also shows the k_d and C'_H values of both the gases. As expected, the Langmuir sorption capacity parameter is lower for propane, since propylene is a more compact and condensable gas. The k_d values for both the gases were very similar at 35^0C.

Table-5.6: Pure gas propylene propane sorption results with 6FDA-6FpDA at 35^0C

Pure 6F-6F Annealed	*k_d (cc (stp)/(cc pol. psia)*	*C_H' cc (stp)/cc pol.*	*b $psia^{-1}$*	*S, (cc (stp)/cc pol.cm Hg) @ 29.4 psia*
Propylene	0.26 ± 0.03	20.3 ± 1.78	0.24 ± 0.05	0.169± 0.04
Propane	0.20 ± 0.016	11.35 ± 0.96	0.22 ±0.058	0.104± 0.02

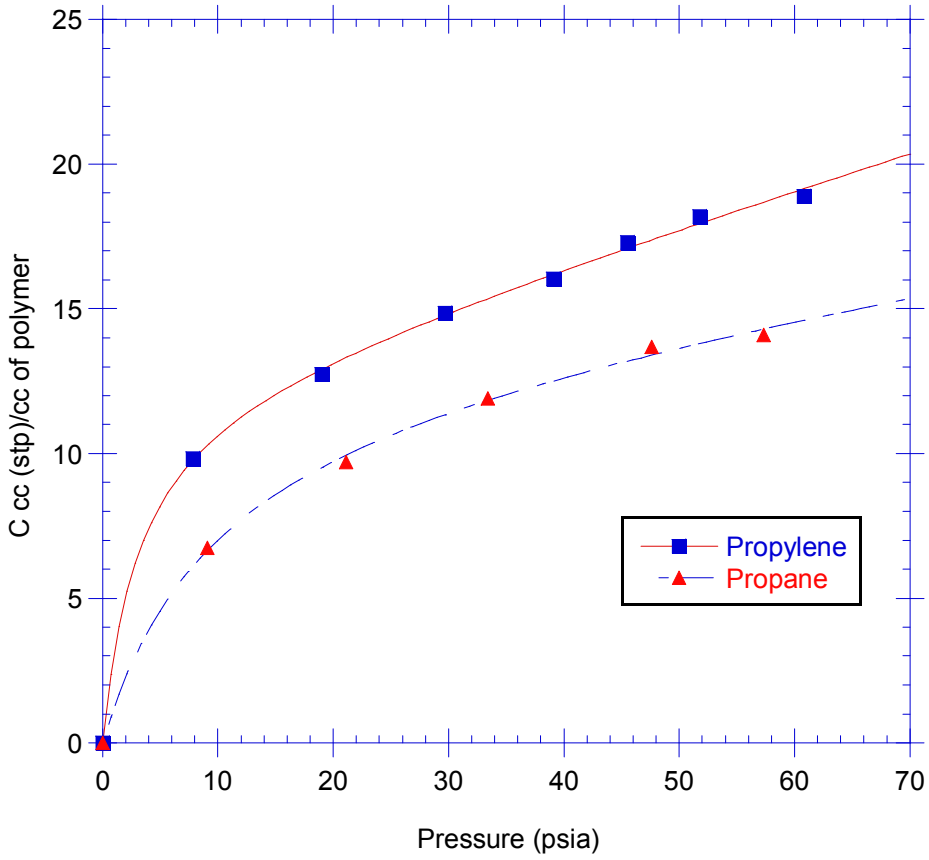

Figure-5.9: Pure gas propylene propane sorption results with 6FDA-6FpDA at 70^0C

Table-5.7: Pure gas propylene propane sorption results with 6FDA-6FpDA at 70^0C

Pure 6F-6F Annealed	k_d *(cc (stp)/(cc pol. psia)*	C_H' *cc (stp)/cc pol.*	*b* $psia^{-1}$	*S, (cc (stp)/cc pol.cm Hg) @ 29.4 psia*
Propylene	0.12 ± 0.01	12.3 ± 0.72	0.32 ± 0.07	0.097± 0.02
Propane	0.10 ± 0.012	9.87 ± 0.80	0.15 ±0.03	0.074± 0.015

A very similar trend with 70^0C sorption experiments was also observed (Figure-5.9 and Table-5.7). In this case k_d values were again similar for propylene and propane. Whereas, the Langmuir sorption site value (C'_H) was higher in the case of propylene than in propane. Sorption parameter values are also given in Table-5.7. Table-5.6 and Table-5.7 compare the solubility values of propylene and propane at different test temperatures and as expected, the solubility of both the gases decreased with increasing permeation test temperature.

5.3.3.2. Application of dual mode parameters in mixed gas permeability-selectivity prediction

In glassy polymers, the mixed gas sorption can be described as:

$$C_A = k_{DA} p_A + \frac{C'_{HA} b_A p_A}{1 + b_A p_A + b_B p_B} \qquad [5.3]$$

Where, A and B are two different gases (e.g. propane and propylene). In this case we can predict the permeability of gas A in a gas mixture.

Mixed gas sorption values were predicted with the dual mode sorption parameters for propylene and propane at 35^0C and 70^0C test temperatures according to Equation-5.3.

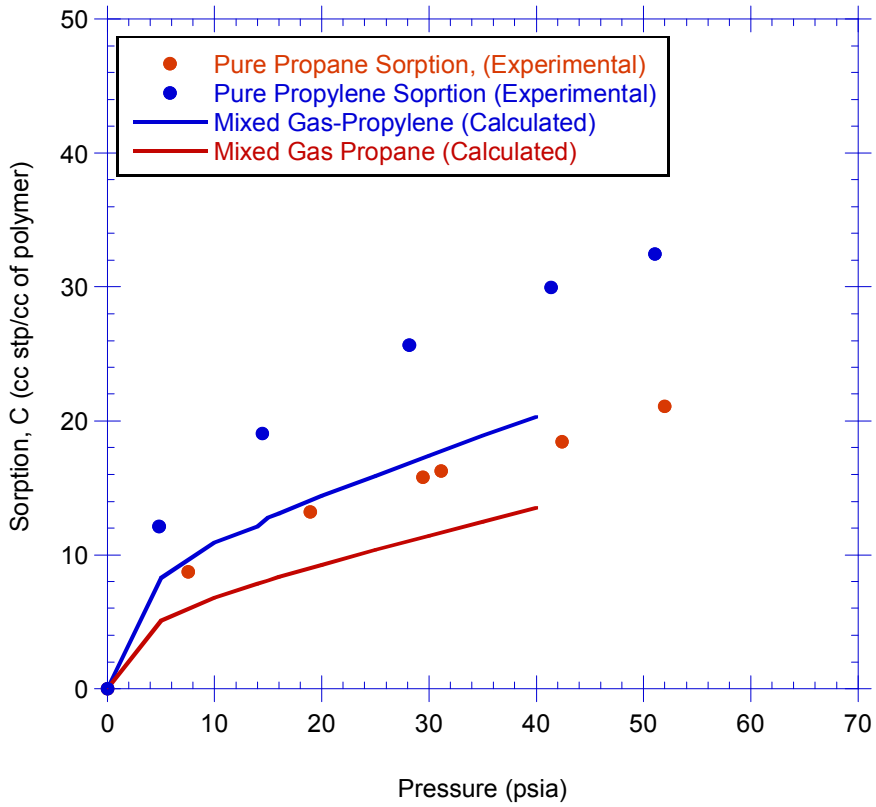

Figure-5.10: Pure gas propylene propane sorption results with mixed gas prediction in 6FDA-6FpDA at 35^0C

Figure-5.10 shows this predicted mixed gas sorption values for propylene and propane at 35^0C test temperature with a 50/50 propylene/propane mixture. Both propylene and propane are predicted to show a decrease in solubility in the mixture. A closer look at Figure-5.10 reveals that the decrease in propylene solubility is more than the decrease in propane solubility in a 50/50 gas mixture. In other words, at a given pressure, both propylene and propane permeabilities decrease more than their respective pure gas permeabilities, but in case of propylene, this decrease is more than in case of propane. Thus with a 50/50 mixture, it is expected that the selectivity of

propylene/propane will decrease from pure gas selectivity on the basis of solubility factors, even in the absence of mobility factors.

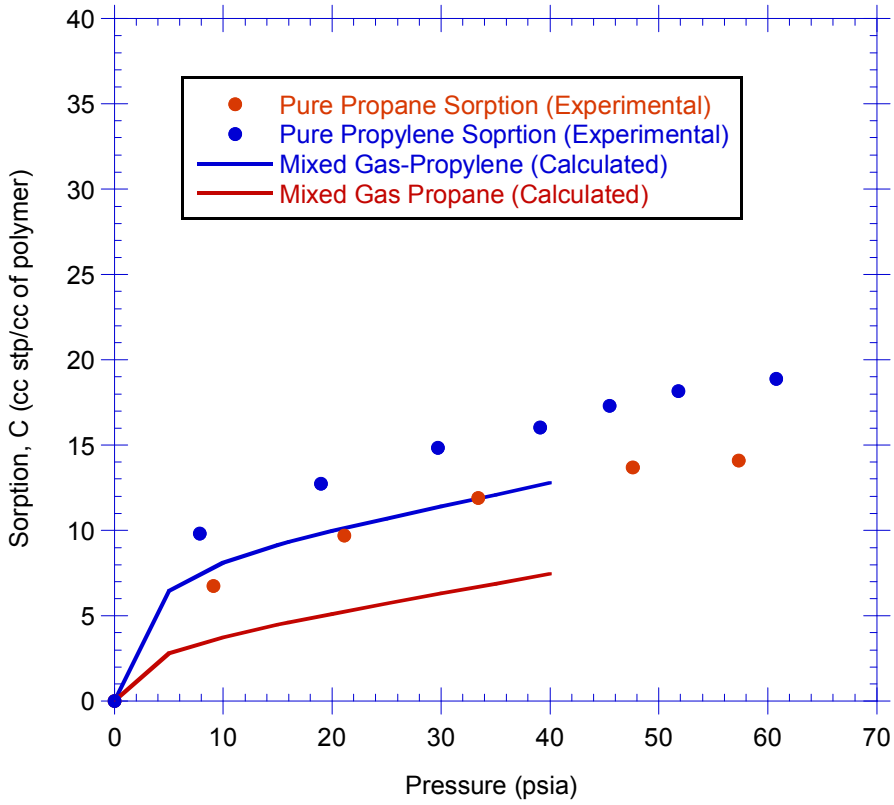

Figure-5.11: Pure gas propylene propane sorption results with mixed gas prediction in 6FDA-6FpDA at 70^0C

Similarly, Figure-5.11 shows the predicted mixed gas sorption for propylene and propane at 70^0C test temperature. In this case, we also see a decrease in both propylene and propane permeability. Unlike the previous case, here both propylene and propane permeabilities decreased the same order of magnitude, suggesting that on the basis of solubility effects, the mixed gas selectivity will be similar to the pure gas selectivity at 70^0C test temperature in the absence of plasticization. Although our experimental results (Figure-5.7) suggest that the mixed gas solubility selectivity decreases more than pure

gas selectivity, this change could be coming from so-called "competition" effects or a bulk flow contribution (described in the next section).

It is possible to fit the dual mode parameter for permeability versus pressure data with sorption parameters. As mentioned in Chapter-2, D_{DA} is the diffusion coefficient of *A* through the Henry's law environments, and D_{HA} is the diffusion coefficient of *A* through the Langmuir environments. The permeability equation for the case of a vacuum downstream is then given by:

$$P_A = k_{DA} D_{DA} \left(1 + \frac{F_A K_A}{1 + b_A p_A + b_B p_B} \right) \qquad [5.4]$$

$$F_A = \frac{D_{HA}}{D_{DA}} \qquad [5.5]$$

In Equation-5.4, K is the defined as the equilibrium coefficient between the Henry's region and the Langmuir region, and is mathematically described as: $C'_{HA}b/k_{D.}$ For single gas permeation Equation-5.4 can be re-written as:

$$P_A = k_{DA} D_{DA} \left(1 + \frac{F_A K_A}{1 + b_A p_A} \right) \qquad [5.6]$$

This permeability expression includes not only the sorption effects discussed in the context of Equation 5.1-5.3, but also diffusion coefficients effects. The Henry's law and Langmuir mode diffusion coefficient values, D_D and D_H, respectively, can be obtained by plotting P_A versus 1/(1+*b.p*) and taking the slope and intercept according to Equation-5.6. For this study, several permeability measurements at different pressure points were noted and then D_D and D_H values were calculated using the sorption values mentioned earlier. Figure-5.12 shows an example of such a plot (propylene permeation at 70^0C). Table-5.8 summarizes these values for propylene and propane at different test temperatures.

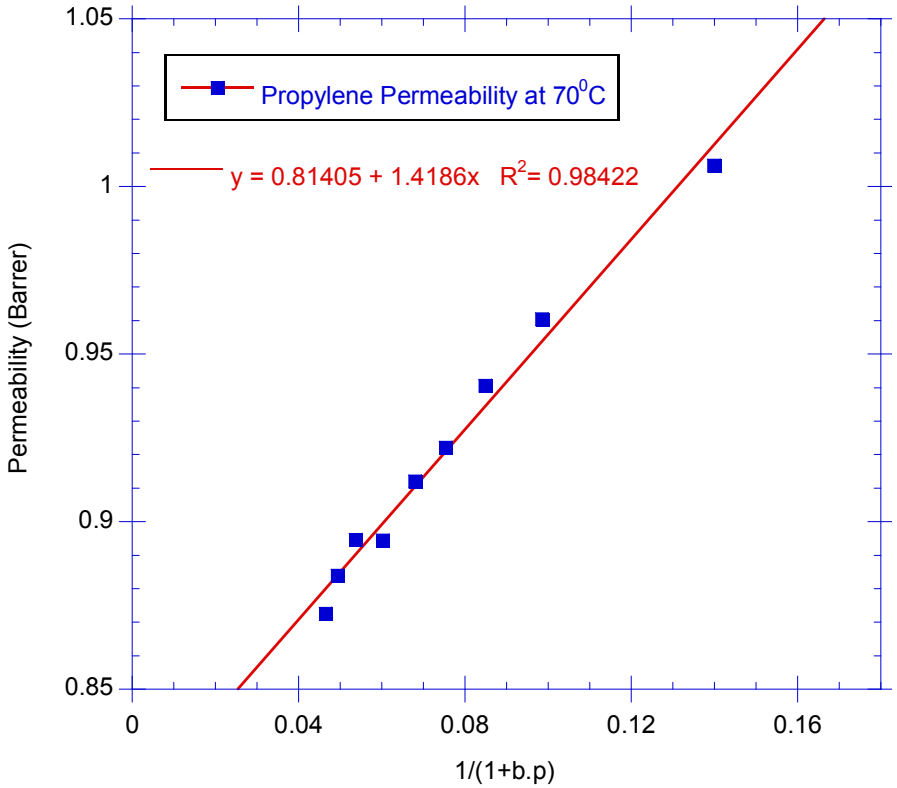

Figure-5.12: Permeability versus 1/ (1+bp) plot to determine D_D and D_H values. Propylene permeation experiments at 70^0C. Solid line is the curve fit.

Table-5.8: Dual mode permeability parameter values for propylene and propane.

Gas	*Test Temperature (^0C)*	*D_D (1×10^{10}) Cm^2/s*	*D_H (1×10^{10}) Cm^2/s*	*F*
Propylene	35	5.96	3.92	0.66
Propane	35	0.84	0.085	0.10
Propylene	70	34.49	1.86	0.054
Propane	70	3.11	0.03	0.01

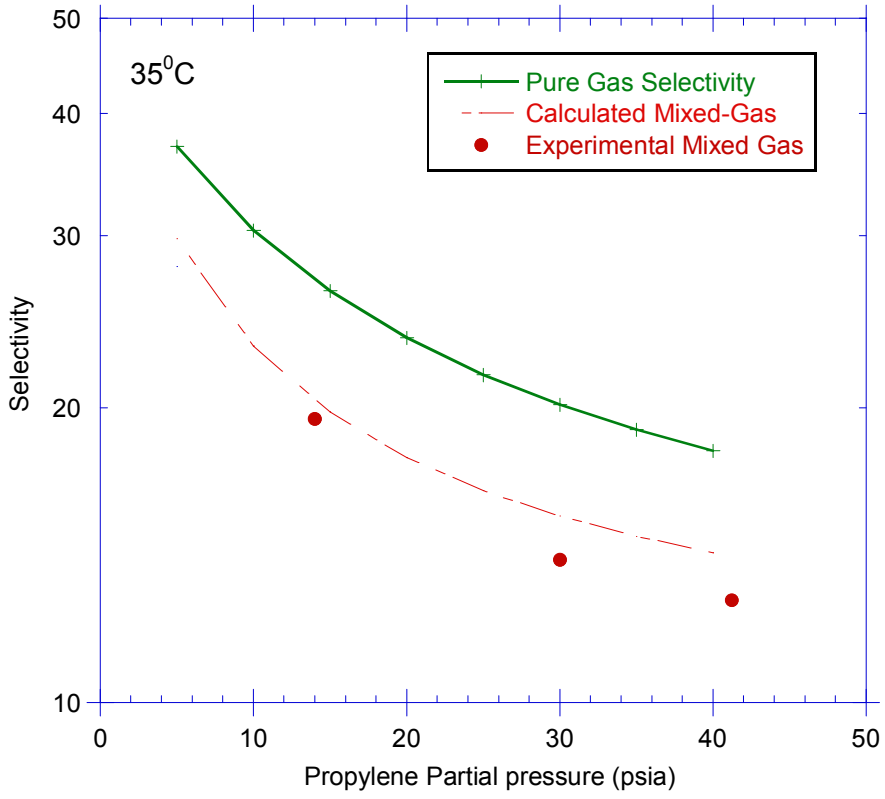

Figure-5.13: Dual mode parameter calculated mixed gas and experimental mixed gas results at 35^0C.

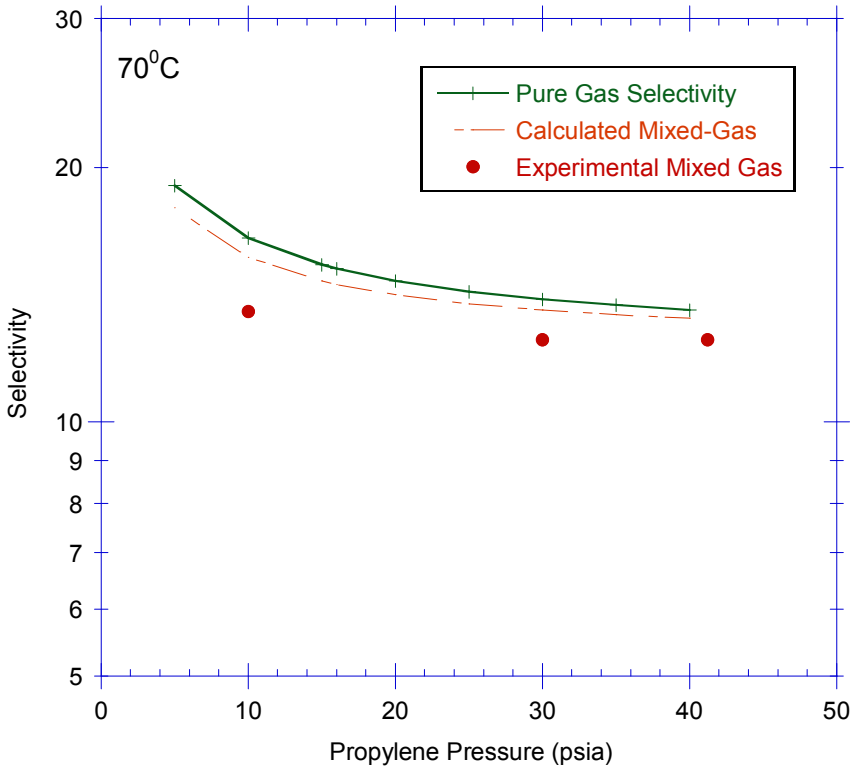

Figure-5.14: Dual mode parameter calculated mixed gas and experimental mixed gas results at 70^{0}C.

To further understand the effect of mixed gas permeation, frame of reference calculations [7] were performed for both the gases at 35^{0}C and 70^{0}C test temperatures. The next section describes the method and results in details.

5.3.3.3. Calculation of frame of reference model/bulk flow model contribution

The frame of reference treatment describes the behavior when one gas in the presence of another in a mixed gas experiment, provides a significant convective

movement of the center of mass of the system. Equations 5.7-5.13 [7] were used iteratively to solve each pressure point for propylene and propane.

$$P_A = \frac{22400.n_A}{M_A.\Delta p_A} \qquad [5.7]$$

$$r = \frac{n_A}{n_B} \qquad [5.8]$$

$$n_A = \rho.D_{DA}.\frac{\ln\left[\dfrac{1}{1-w_A.\left(1+\dfrac{1}{r)}\right.}\right]}{\left(1+\dfrac{1}{r}\right)} \qquad [5.9]$$

$$n_B = \rho.D_{DB}.\frac{\ln\left[1-w_B(1+r)\right]}{(1+r)} \qquad [5.10]$$

$$\prod_A = \frac{w_A(1+1/r)}{\ln\left[\dfrac{1}{(1-w_A(1+1/r)}\right]} \qquad [5.11]$$

$$\prod_B = \frac{w_B(1+r)}{\ln\left[1-w_B(1+r)\right]} \qquad [5.12]$$

$$P_A^* = (1 - \Pi_A).P_A \qquad [5.13]$$

Initial guesses of n_A and n_B were made from Equation-7 to begin with the iteration process. Final n_A, n_B and r values were determined by using Equations 5.8-5.10 iteratively. Once the satisfying convergence was achieved, Equations 5.11 and 5.12 were used to calculate the bulk flow contribution. Finally, P_A was calculated from Equation-5.13. P^*_A is the permeability calculated by dual mode transport model (Equation-5.4). The mass fractions (*w*) were calculated from the respective sorption data and taken to be the "mobile fraction" as defined by Kamaruddin and Koros [7]. Chapter-2 describes the details of this calculation.

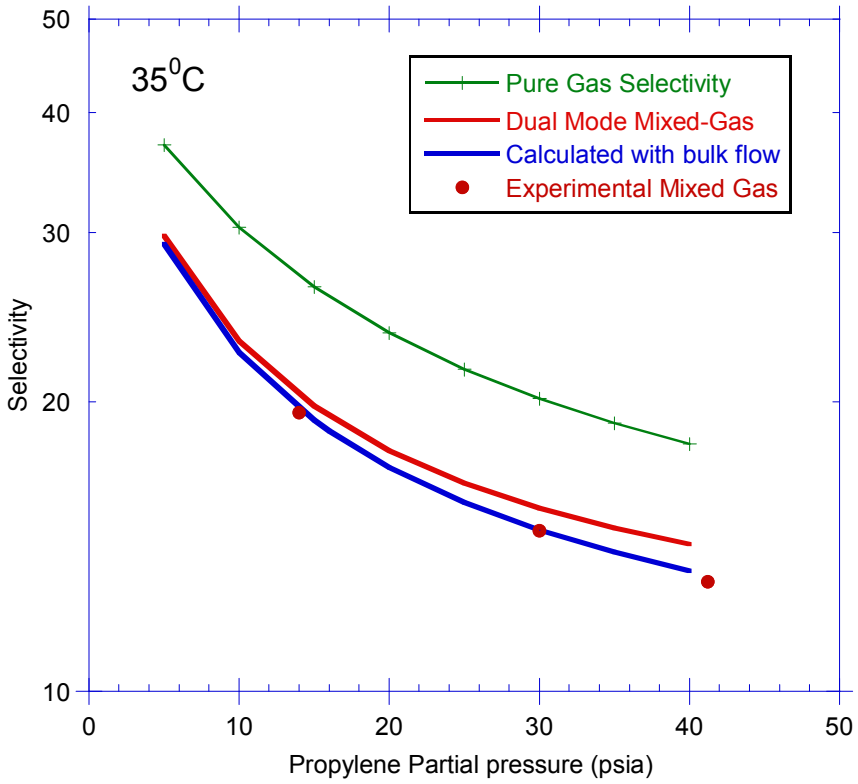

Figure-5.15: Propylene/propane 50/50 selectivity calculated with bulk flow model and compared with dual mode model at 35^{0}C.

Figure-5.15 shows the effect of including frame of reference/bulk flow calculations in selectivity prediction at 35^{0}C. As shown, predicted selectivities were in good agreement with the observed experimental mixed gas experiments. Another interesting observation from Figure-5.15 is that the major drop in selectivity still resulted from the dual mode mixed gas model rather than the bulk flow contribution. Figure-5.16 shows the same calculations in case of 70^{0}C permeation test temperature. The bulk flow model exactly predicts the mixed gas selectivities at different propylene upstream pressure. Although unlike 35^{0}C, the drop in selectivity is due to the equally combined effect of bulk flow and dual mode transport model prediction.

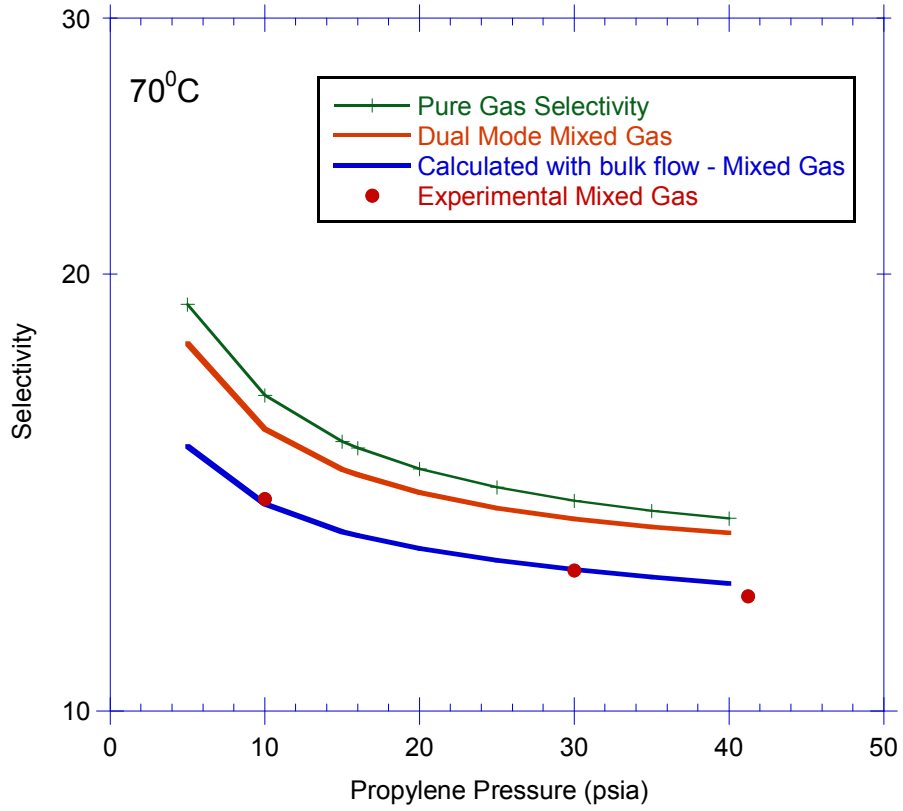

Figure-5.16: Propylene/propane 50/50 selectivity calculated with bulk flow model and compared with dual mode model at 70^{0}C.

It was shown in the above section that plasticization suppression was successfully achieved with both pure and mixed gas experiments. The drop in selectivities during mixed gas experiments were explained with the help of dual mode and bulk flow theories. This is for the first time plasticization suppression was achieved by adopting the high test temperature and systematic annealing approach, according to our best knowledge. Even at a lower test temperature (35^{0}C), no plasticization was observed even up to 42 psi propylene upstream pressure. This result was surprising and to probe more into this, we performed a more detailed study with our sorption and permeation. At this

point, it was hypothesized that since we are starting with a high molecular weight and more rigid material (our polymer has an average molecular of ~200K, with PI of around 2.0), may be the onset of swelling/plasticization is pushed towards higher upstream pressures. Following sections describe the related sorption results and the final conclusion on this result. The annealing effect on sorptions was also investigated in order to address the differences in permeabilities and selectivities seen in un-annealed and annealed films.

5.3.4. Annealing Effect On Sorption

It has been shown earlier that the plasticization effect for 6FDA-6FpDA pure film can be controlled by annealing the films at a higher temperature (in this case 210^0C) and performing the permeation test at a higher temperature (70^0C). When we annealed the film at a higher temperature a sharp decrease of permeability was seen relative to the un-annealed films (Figure-5.4). Table-5.9 summarizes the permeabilities of 6FDA-6FpDA pure films at different temperature and conditions. From Table-5.9 we can see that at a 70^0C test temperature, propylene permeability went down by 56%. To further understand the annealing effect, we performed propylene sorption experiment on both un-annealed and annealed films at 70^0C. Although after annealing we see a decrease in permeability, permeance in an asymmetric membrane (even with a relatively thick selective layer e.g. 0.2 micron) would still be 4.8 GPU. We believe that this permeance is in an acceptable range.

Table-5.9: Comparison of un-annealed and annealed 6FDA-6FpDA permeation properties

Drying Condition	*Test Temperature (^0C)*	*Pressure (psi)*	*P_{C3H6} (Barrer)*	*C_3H_6/C_3H_8*
110^0C	70^0C	29.4	2.21± 0.1	12.0
210^0C	70^0C	29.4	0.96 ±0.08	13.0±0.5

Figure-5.17 shows the comparison between un-annealed and annealed film propylene sorption at 70^0C. As the figure suggests, we see a decrease in the sorption capacity from un-annealed to annealed films. The sorption dual mode parameters as calculated from Figure-5.17 are given in Table-5.10.

Table-5.10: Sorption dual mode parameters for propylene – un-annealed and annealed. Tested at 70^0C

Pure Films	*k_d (cc (stp)/(cc pol. psia)*	*C_H' cc (stp)/cc pol.*	*b $psia^{-1}$*	*S @ 29.4 psia (cc stp)/cc.cmHg)*	*D x 10^9 (cm^2/s)*
Un-annealed	0.17 ± 0.01	15.2 ± 0.44	0.36 ± 0.04	0.124	1.78
Annealed	0.12 ± 0.012	12.31 ± 0.72	0.32 ± 0.07	0.097	1.0

As shown in Table-5.10, the solubility constant (S) has decreased by 22% after annealing, The diffusivity constant was calculated from the available permeability and solubility values (P=D.S), and also were checked with the diffusivity calculated from the time-lag method. Both values were in agreement within calculation uncertainties. The diffusivity

constant has decreased by ~44%. This explains the decrease in permeability around 56% (Table-5.9) at 70^0C (e.g. (1-0.22)*(1-0.44) = 0.44= (1- 0.56)).

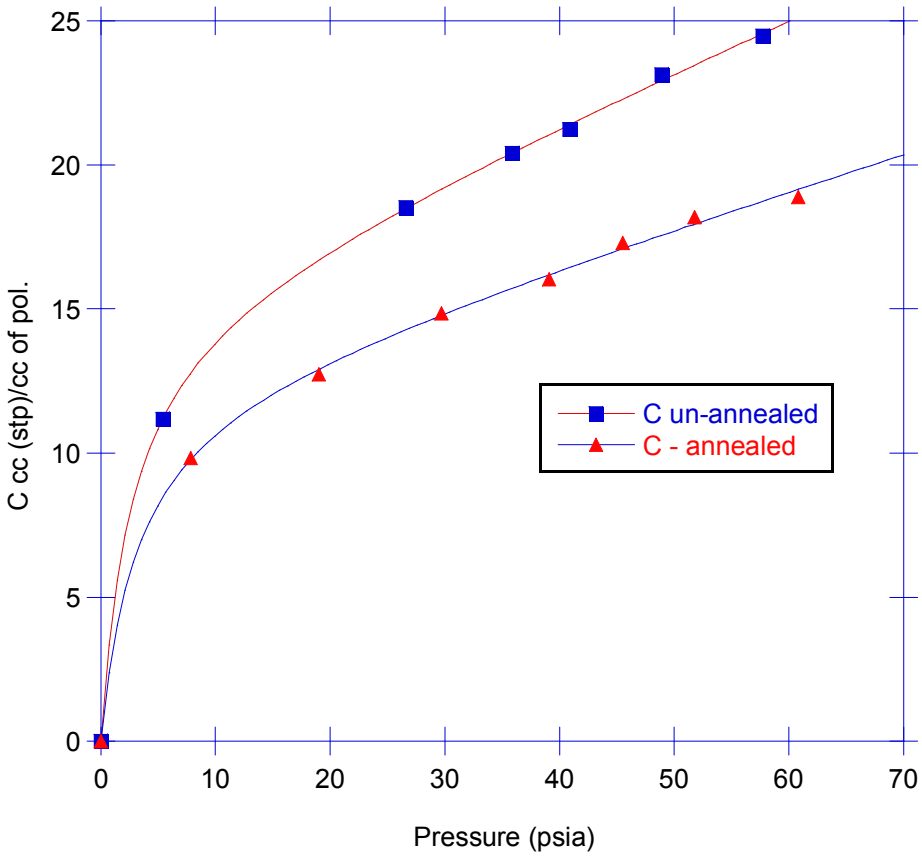

Figure-5.17: Propylene sorption isotherm at 70^0C. Solid lines are sorption dual mode model fit.

Annealing a film at an elevated temperature (in this case 210^0C) reduces the number of Langmuir sorption sites as the polymer chains relax and reorganize. Moreover, idealized Henry's regions may rigidify and thus decreasing the k_d value. In our experiments, we observed a decrease in Langmuir sorption site capacity and k_d values. Annealed films behave as more densified (lower free volume) materials than un-annealed

films. This phenomenon was reflected by the observed decrease in the diffusivity constant. Ideally, the affinity constant should not be affected by annealing temperature. However, in our case, we observed a small decrease in the affinity constant, which is considered within experimental error limits.

5.3.5. High Molecular Weight Effect

It is useful to compare the effects of annealing for the sorption and transport properties at low (35^0C) temperature for work done earlier by Staudt-Bickel [1]. Moreover, since we are performing our mixed matrix mixed gas work at 35^0C, it is important to characterize and benchmark pure film work at 35^0C. Propylene sorption was done with annealed films (annealed at 210^0C) at 35^0C.

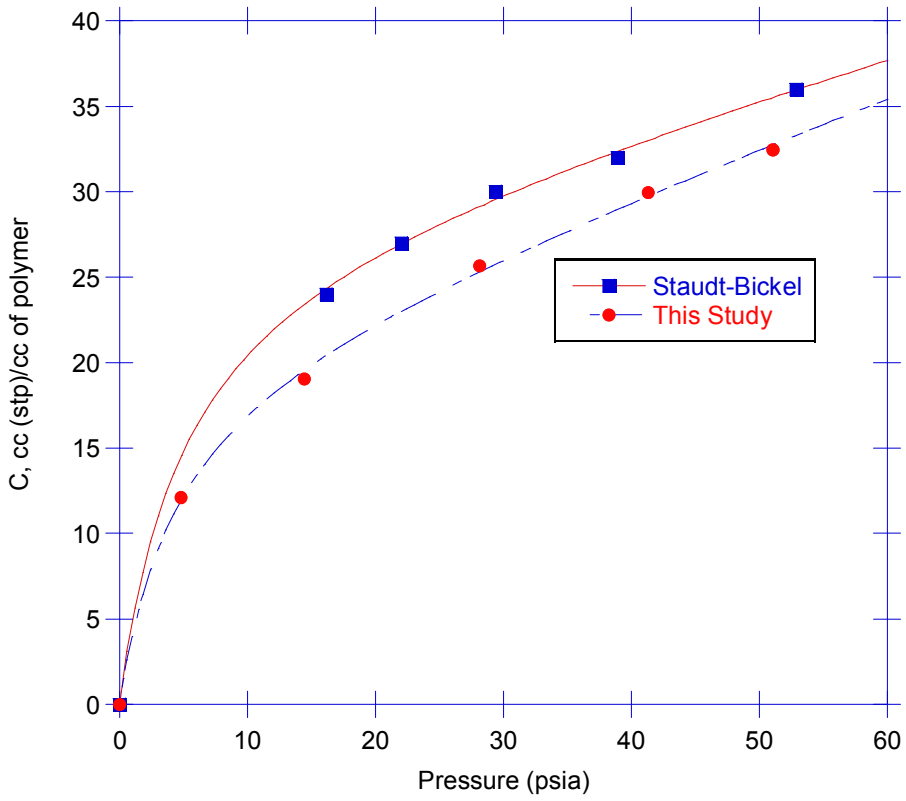

Figure-5.18: Propylene sorption isotherm at 35^{0}C. Solid lines are sorption dual mode model fit.

The experimental results were then fit with the dual mode sorption model. Comparisons of Staudt-Bickel's result and this research study are shown in Figure-5.18 and Tables- 5.11, 5.12.

Table-5.11: Comparison of sorption dual mode parameters with propylene annealed at 210^{0}C

Pure 6F-6F Annealed	k_d *(cc (stp)/(cc pol. psia)*	C_H' *cc (stp)/cc pol.*	*b psia*$^{-1}$
Staudt-Bickel	0.20 ± 0.05	27.5 ± 4.03	0.20 ±0.1
This-Study	0.26 ± 0.03	20.3 ± 1.78	0.24 ± 0.05

Table-5.12: Comparison of P, D and S – propylene at 35^0C

Pure film Annealed	*Drying Condition*	*Propylene Permeability (Barrer)*	*Mw*	*S (C/p) @ 29.4 psia cc (stp)/cc.cmHg*	*α*	*D x 10^{-10} (cm2/s)*
Staudt-Bickel	>200^0C	0.9 ± 0.05	Low	0.193	16.0	4.73
This-Study	210^0C	0.7 ±0.05	High	0.168	19.0±1.0	4.16

If we compare permeabilities in these two cases, we can clearly see that in this study we have a reduced permeability (P decreased by 22%). Our calculated D and S values allowed us to see the percentage decrease in D and S. As shown in Table-5.12, we see that both diffusivity and solubility play equal roles in decreasing the permeability. The only real difference between Staudt-Bickel's film and these films is the molecular weight difference of the polymer. Since we now have an improved method to synthesize the polymer, we can consistently produce high M_w and low PI polymer. Due to this high molecular weight, there are less chain ends and hence free volume in the material is lower. While it is surprising that this subtle difference in polymer properties translates to the significant permeability and even selectivity properties, it is well known that the synthesis and the drying processes play an important role in the permeability and selectivity of a particular gas pair. Moreover, the quenching technique after annealing the film at a higher temperature (cooling down the film under vacuum versus exposing the film to atmosphere right after annealing) might play a role in the C_H' values and hence in the overall sorption values which is also reflected in a lower C_H' in this study. Also,

depending on the casting technique during the dense film development, the initial C_H' values might be different for different films.

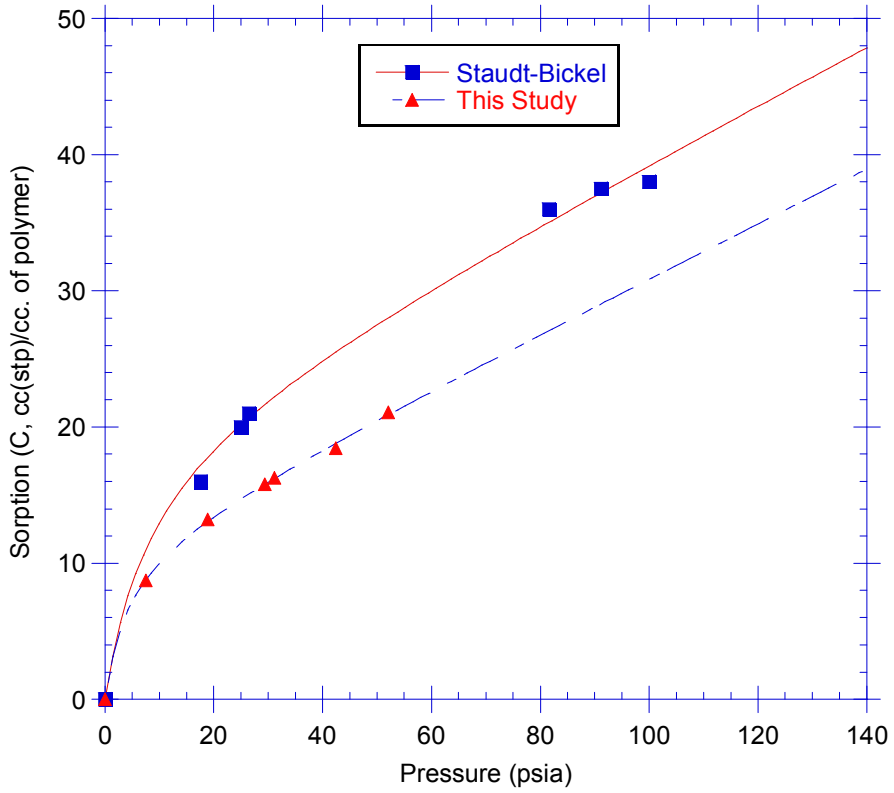

Figure-5.19: Propane sorption isotherm at 35^{0}C. □ – annealed Staudt-Bickel (dried at >200^{0}C), Δ – annealed-This study (dried at 210^{0}C). Solid lines are sorption dual mode model fit.

Table-5.13: Comparison of sorption dual mode parameters with propane annealed at 210^{0}C

Pure 6F-6F Annealed	*k_d (cc (stp)/(cc pol. psia)*	*C_H' cc (stp)/cc pol.*	*b psia^{-1}*
Staudt-Bickel	0.20 ± 0.07	20.0 ± 9.27	0.12 ±0.16
This-Study	0.20 ± 0.016	11.35 ± 0.96	0.22 ±0.06

Sorption of propane was also performed at 35^0C and the results are presented in Figure-5.19 and Table-5.13 and Table-5.14.

Table-5.14: Comparison of P, D and S – propane at 35^0C

Pure film Annealed	*Drying Condition*	*Propylene Permeability (Barrer)*	*Mw*	*S (C/p) @ 29.4 psia cc (stp)/cc.cmHg*	*α*	*D x 10^{-10} (cm2/s)*
Staudt-Bickel	>200^0C	0.0563	Low	0.141	16.0	0.40
This-Study	210^0C	0.037±0.005	High	0.104	19.0±1.0	0.35

Figure-5.19 shows the sorption data for Staudt-Bickel and this study. We observed a decrease in propane permeability relative to Staudt-Bickel (decreased by 34%). Similar Tables were constructed as before, and as seen, sorption values decreased by 26% between Staudt-Bickel and this study. Diffusivity decreased by 12.5%. In this case, sorption values were affected more than the diffusivity values. The main reason might be again coming from the annealing process and the molecular weight effect. At this point further study is needed to firmly conclude the causes for this effect. As mentioned earlier, dense film properties depend on casting, drying and annealing techniques besides high molecular weight. Based on the above preliminary results it was concluded that the combined effect of high molecular weight and film drying techniques played a significant role in suppressing plasticization even at a lower test temperature.

An in depth control study is required to determine the reason of this behavior but it is unfortunately outside of the scope of this research. Once we established the successful plasticization suppression at high temperature and benchmarked our work at 35^0C, the next objective was to successfully incorporate the molecular sieve material in a mixed membrane environment. Chapter-6 describes the development and successes of this mixed matrix membrane.

5.4. References

1. C. Staudt-Bickel, W.J.Koros, *Olefin/paraffin gas separation with 6FDA-based polyimide membranes*. JMS, 2000. **170**: p. 205-214.

2. R. L. Burns, W.J. Koros, *Defining the challenges for C_3H_6/C_3H_8 separation using polymeric membranes*. JMS, 2003. **211**: p. 299-309.

3. H. Sejour, *Investigation of dithiolenes for propylene/propane membrane separation,* 2007, Georgia Institute of Technology, GA. p. 54

4. M. Yashino et al., *Olefin/paraffin separation performance as asymmetric hollow fiber membrane of 6FDA/BPDA-DDBT copolyimide*. JMS, 2003, **212**: p-13-27

5. Christopher J. Cornelius, *Physical and Gas permeation properties on a series of Novel hybrid inorganic-organic composites based on a synthesized fluorinated polymer.* PhD -Virginia Tech 2000

6. H Ohya et al, *Polyimide Membranes: Applications, Fabrications and Properties*, Gordon and Breach Publishers, **1996**

7. Kamaruddin, H.D. and W.J. Koros, *Some observations about the application of Fick's first law for membrane separation of multicomponent mixtures*. JMS, 1997. 135: p. 147-159.

CHAPTER 6

MIXED MATRIX MEMBRANES WITH 6FDA-6F$_P$DA AND ALPO-14

6.1. Abstract

This chapter describes the efficacy of mixed matrix membranes for increasing the permeability-selectivity tradeoff performance of mixed matrix material beyond the existing pure polymer upper bound performance.

The first part of this chapter describes the importance of polymer-molecular sieve matching required for a successful mixed matrix membrane. A brief review of the use of AlPO-14 to separate propylene/propane via pressure swing adsorption by UOP has been described. The later part of this chapter describes the success of this research in incorporating AlPO-14 into 6FDA-6FpDA polymer to enhance the selectivity and permeability. Characterization of pure sieve properties at 35^0C has been discussed in detail. Both pure and mixed gas results have been discussed. Mixed gas results were measured at two different temperatures (35^0C and 70^0C). Results from Chapter-5 have been used as pure film properties for model prediction. Experimental results have been compared with Maxwell and a modified Cussler models.

6.2. Separation With Mixed Matrix Membranes

As described in Chapter-2, the propylene/propane upper bound curve shows that the performances of pure polymer membranes are on or below the upper bound line (Figure-6.1) [1]. On the other hand, inorganic materials have excellent membrane separation properties. Hybrid or "Mixed Matrix" materials comprising a mixture of inorganic domains in a traditional organic polymer are excellent candidates to overcome the "upper-bound" constraint associated with pure polymers.

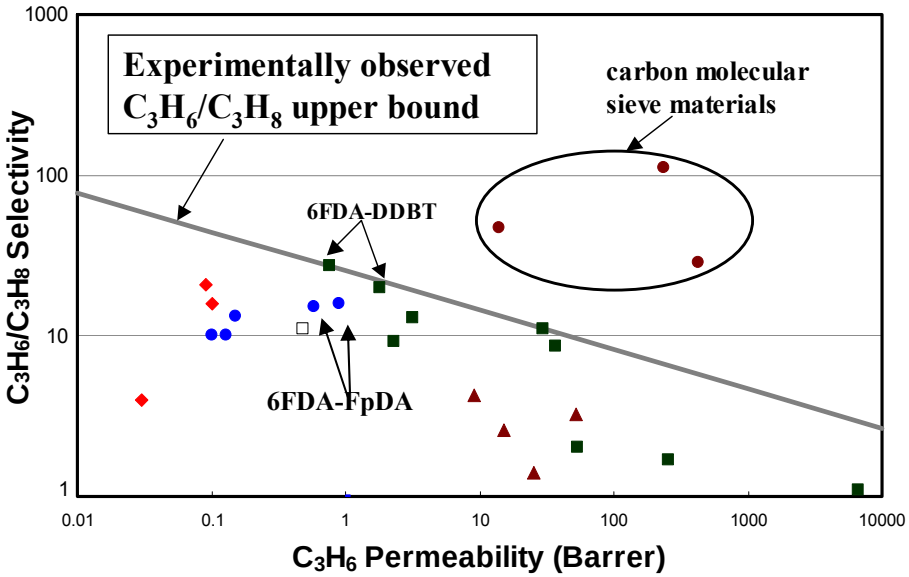

Figure-6.1: C_3H_6/C_3H_8 experimental upper bound based on pure gas permeation data over the range 1 – 4 atm feed pressure. □ = 100°C, ■ = 50°C, ● = 35°C, ▲= 30°C, ♦ = 26°C.

The most common description of the performance of such materials is given by the so-called "Maxwell Model" (Equation-6.1), viz.

$$P_{MM} = P_M \left(\frac{P_D + 2P_M - 2\Phi_D(P_M - P_D)}{P_D + 2P_M + \Phi_D(P_M - P_D)} \right) \qquad [6.1]$$

Where P is permeability, Φ_D is the volume fraction of the dispersed phase, the MM subscript refers to the mixed matrix membrane, the M subscript refers to the continuous matrix, and the D subscript refers to the dispersed phase present at a volume fraction of Φ_D. The selectivity of the hybrid for component A vs. B is simply the ratio of the composite permeability of component A vs. B, e.g. P_{CA}/P_{CB}, determined using P_{CA} and P_{CB} from Equation. Research conducted to date on mixed matrix membranes has focused on combination of a solid molecular sieving phase, such as zeolites or carbon molecular sieves, with a processable bulk polymer matrix. For optimum results, the sieving phase in solid/polymer mixed matrix media should have a selectivity that is significantly larger than the pure polymer. Addition of a small volume fraction of sieves to the polymer matrix, therefore, increases the overall separation efficiency significantly. The concept of mixed matrix membranes has been demonstrated at UOP [2] in the mid 1980's using silicalite/cellulose acetate mixed matrix membranes for CO_2/H_2 separation.

Zeolites have been the most commonly used solid fillers in mixed matrix work. The ideal mixed matrix membrane will exhibit both an increase in selectivity and permeability as the solid phase volume fraction is increased, and the Maxwell model can be used to estimate these separation properties [3]. This is illustrated in Figure-6.2. For

example, starting with pure 6FDA-6FpDA polymer which is under the upper-bound curve, the mixed matrix permeability and selectivity will follow the Maxwell model as shown (for 20, 30 and 40 wt% loading). Different starting permeabilities for molecular sieves (propylene/propane selectivity was 100 in all cases) were considered and are shown by different sets of colors. The index in Figure-6.2 shows the starting permeabilities in Barrer for each color. For example red represents mixed matrix with starting molecular sieve permeability of 1 Barrer. Similarly, green points represent molecular sieves with 2 Barrer permeability and 100 selectivity. The values of permeabilities and selectivities were calculated by Maxwell model using Equation-6.1.

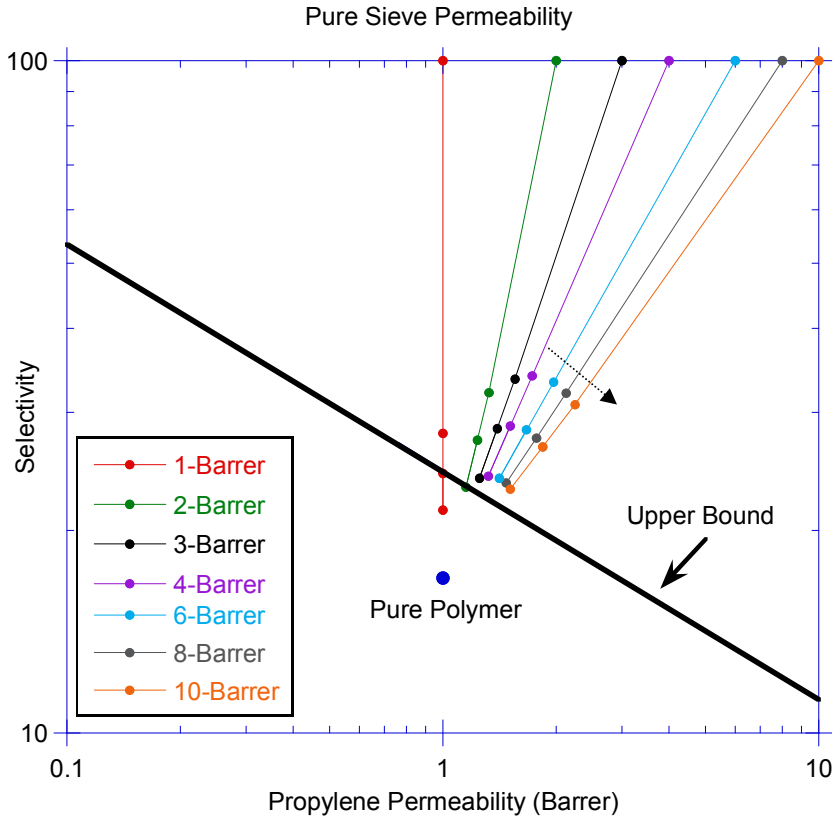

Figure-6.2: A graphical representation of mixed matrix membrane transport properties for propylene/propane separations. Selectivity = 100 for every case with pure sieve permeabilities 1-10 Barrer cases illustrated for Maxwell model.

This example demonstrates the importance of the intrinsic molecular sieve properties for any particular gas pair separation. A closer look at Figure-6.2 reveals that there is a maxima of selectivity achieved via mixed matrix membranes at a given loading (Φ_D). In this particular example a maxima was noticed around ~4 Barrer sieve permeability (magenta points). As the permeability via molecular sieve increases, gases prefer to permeate through the molecular sieves instead of the polymer matrix ultimately turning the matrix as plugged surface. In other words, from Equation-1, $P_{MM} \rightarrow 0$, at all Φ_D values for $P_M/P_D \rightarrow 0$.

Characterization of AlPO-14 at 35^0C was done to depict the mixed matrix behavior. These characterization values were used to fit with Maxwell and Cussler model to predict the enhancement. The next section describes some of the characteristics and properties of AlPO-14.

6.3. Characterization of AlPO-14

6.3.1. AlPO-14 For Propylene/Propane Separations

As described in Chapter-2, AlPO-14 has been successfully used for propylene propane separations via pressure and vacuum swing adsorption experiments by UOP [3, 5]. Padin et al demonstrated that propylene/propane separation is favorable with equilibrium isotherm since almost no amount of propane was sorbed by AlPO-14 [6]. Following the success of AlPO-14 in commercial PSA applications, characterization of

AlPO-14 was done at 35^0C to determine the compatibility with 6FDA-6FpDA as polymer matrix.

The frameworks for AlPO-14 are mainly composed of both tetrahedral AlO_4 and PO_4 units. It is an 8-member ring zeolite with the chemical composition of $Al_8P_8O_{32}$. One interesting characteristic of AlPO-14 is that it has four crystallographic orientations. Figure-6.3 shows the diffusion paths for AlPO-14 molecular sieve. As we can see, there are four possible directions of diffusion through AlPO-14. The most important feature of AlPO-14 molecular sieves is the pore size opening. Table-6.1 shows the pore size window openings at the above mentioned four different crystallographic directions [7]. Propane and propylene molecular diameters are shown in Figure-6.4 [8]. Due to the double bond in propylene, there is a "nose" like structure that facilitates propylene diffusion via a pore opening that is around 3.4 Å.

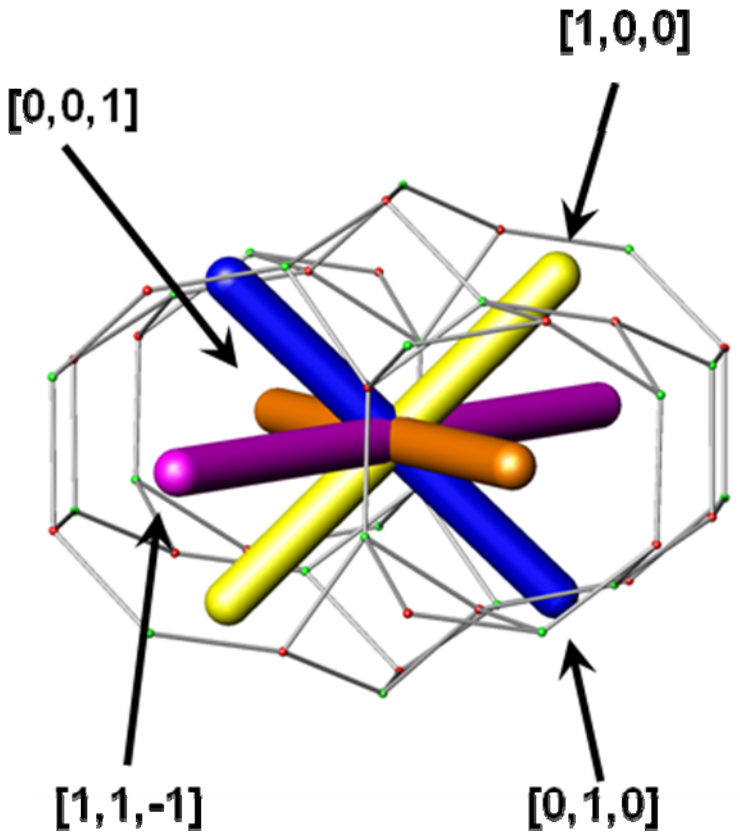

Figure-6.3: AlPO-14 diffusion paths. Single cage bounded by eight 8-rings, consisting of 4 pairs oriented along the four shown crystallographic directions [7]

Table-6.1: AlPO-14 Structure Data [7]

Channel direction	Color (Figure-2)	8-ring pore dimensions
[1,1,-1]	**Magenta**	**3.4 x 3.5**
[0,0,1]	**Gold**	**2.8 x 4.1**
[0,1,0]	**Blue**	**2.1 x 4.9**
[1,0,0]	**Yellow**	**1.9 x 4.9**

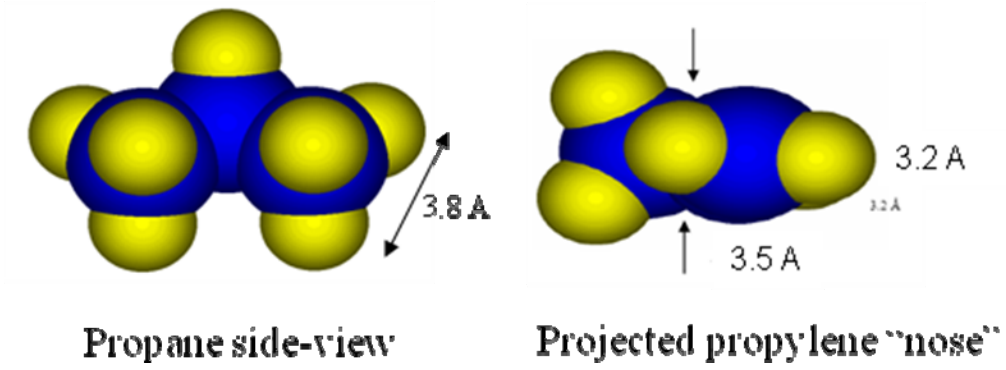

Figure-6.4: Propylene and propane molecules [8].

From Table-6.1 and Figure-6.4 it is clear that there is only one pore window aperture feasible for propylene selective diffusion. The channel direction is in [1, 1-1] trajectory direction, indicated by magenta color in Figure-6.3. All the pore window apertures essentially exclude propane from entering the AlPO-14 framework. Thus AlPO-14 is the ideal molecular sieve for propylene/propane separations. Figure-6.3 shows the unit cell structure of AlPO-14. Once the pore window apertures were determined, the energy barriers at each pore openings were then examined to determine the separation performance of AlPO-14 for propylene/propane separation. Figure-6.5 (a) – (d) shows the relative energy barrier for propylene and propane for the above mentioned four channel directions [7].

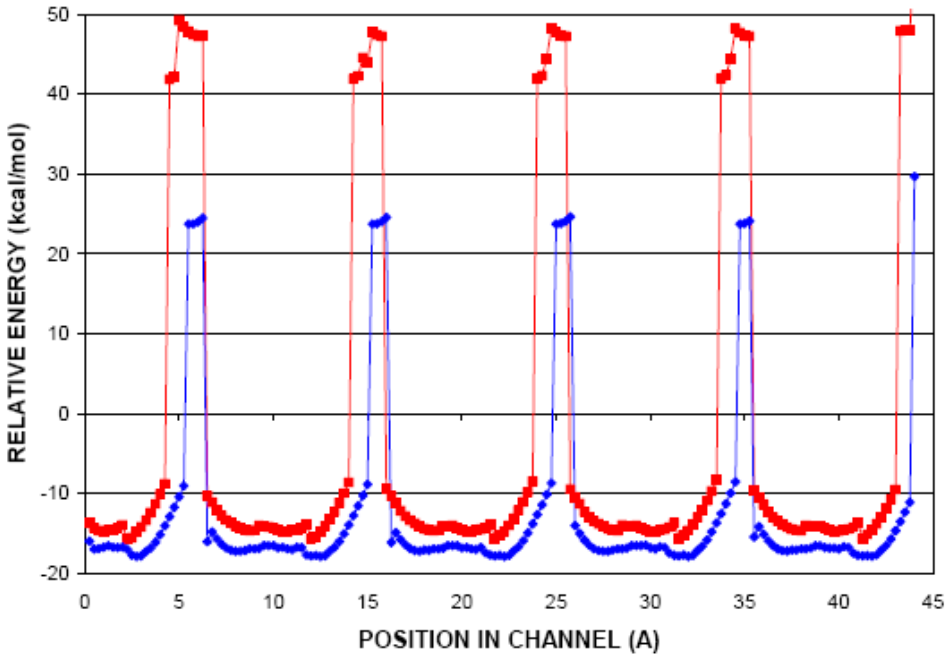
RELATIVE ENERGY (kcal/mol)
50
40
30
20
10
0
-10
-20
0
5
10
15
20
25
30
35
40
45
POSITION IN CHANNEL (A)

(a)

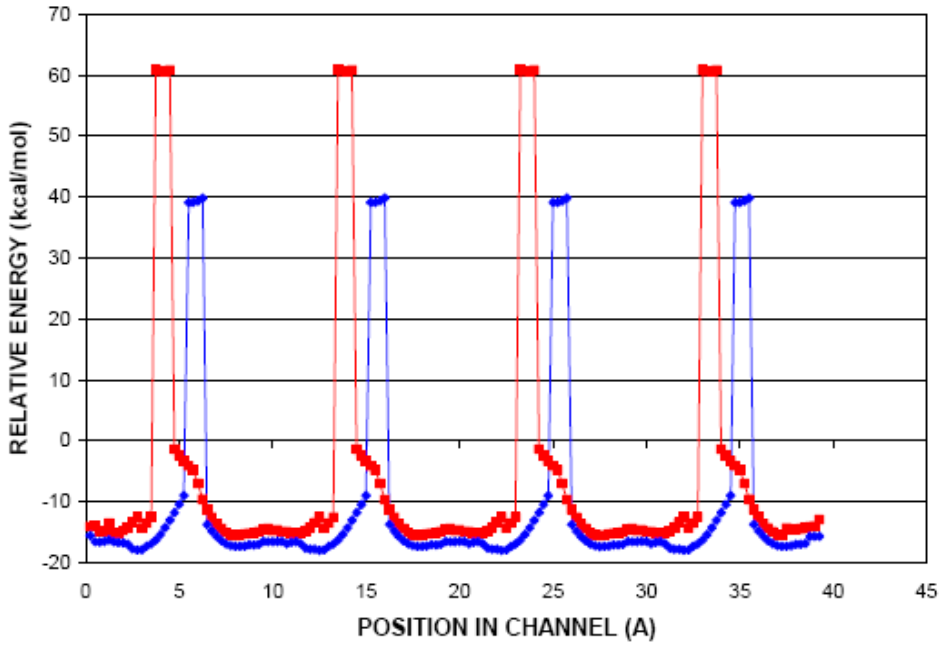
RELATIVE ENERGY (kcal/mol)
70
60
50
40
30
20
10
0
-10
-20
0
5
10
15
20
25
30
35
40
45
POSITION IN CHANNEL (A)

(b)

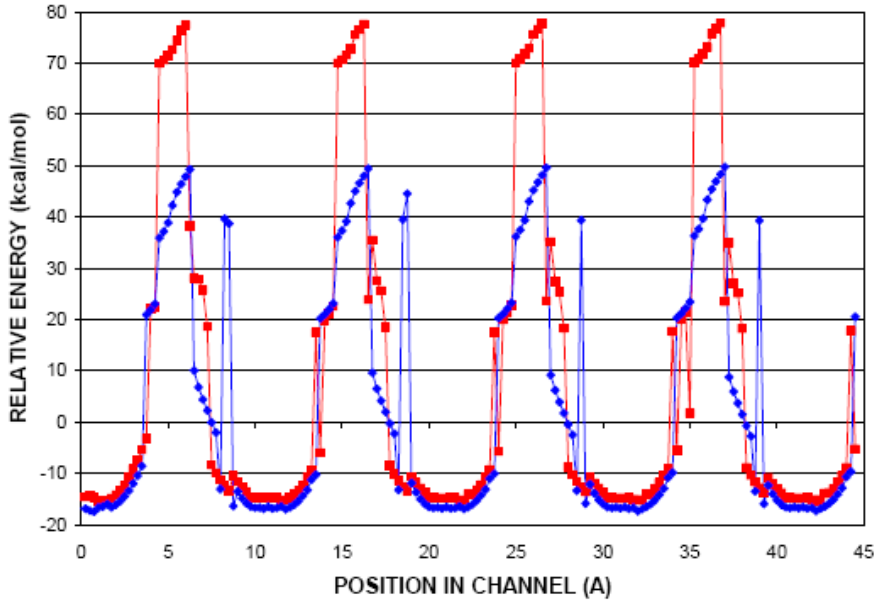

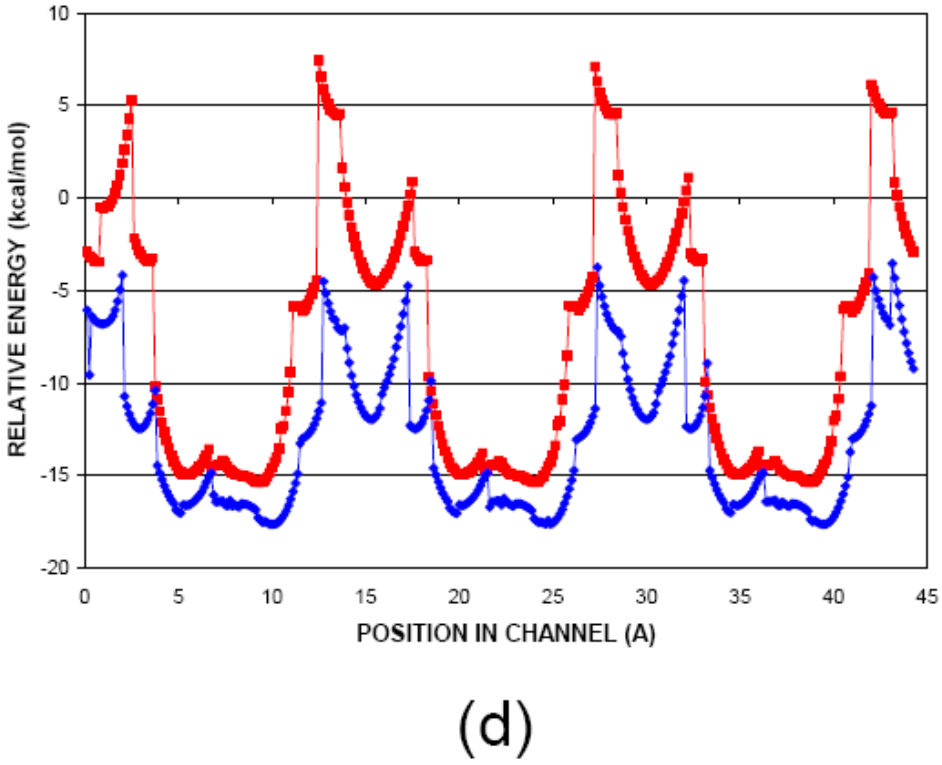

Figure-6.5: Energy profiles through the four difference 8-ring pore openings in AlPO-14 determined by molecular mechanics [7]. Trajectories were along (a) <100> (b) <010> (c) <001> (d) <11-1>. ■ propylene, ■ propane

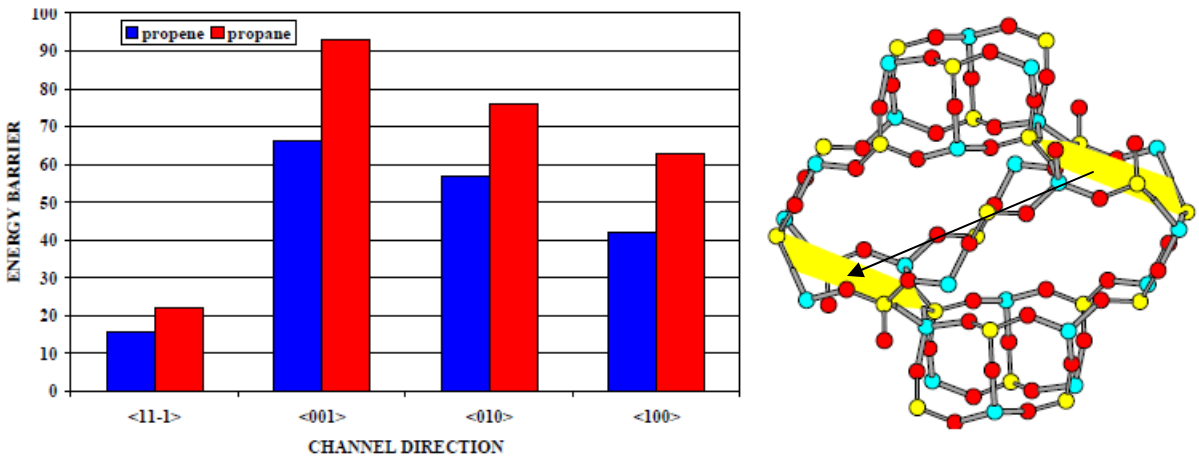

Figure-6.6: Left: Summary of diffusion energy barriers for propylene and propane in four different directions. Right: pore openings along the only favorable diffusion paths are shown by yellow areas [9].

For determining the propylene/propane selectivity, we referred to the activation energy data. From Figure-6.5 and Figure-6.6, it is clear that the propylene/propane separation is possible via only one pore (<1, 1,-1>). Selectivity was calculated as follows from the differences in energy barriers (propylene = 15 kcal/mol and propane = 22 kcal/mol from Figure-5);

$$\alpha = \exp\left[{}^{7000}\!/_{R.T}\right] = 92779 \qquad [6.2]$$

Energetically, propylene diffusion "jumps" are much more favorable than propane. The above calculated selectivity value was used for mixed matrix membrane separation performance via Cussler and Maxwell model predictions. In Figure-5, the unit cell of AlPO-14 can grow in "x-y" plane to add more unit cells faster than it can grow in z direction. Hence, to model AlPO-14 with Maxwell and Cussler models, a

plate of thickness “L” was created (Figure – 6.7 (b)). The effective minimum path for propylene diffusion is in the direction shown in 6.7 (b) by arrows (defined as L’). Since this direction is not perpendicular to the “x-y” plane, Figure-6.7 (c) was drawn to show the “effective” path length as perpendicular to the diffusion plane.

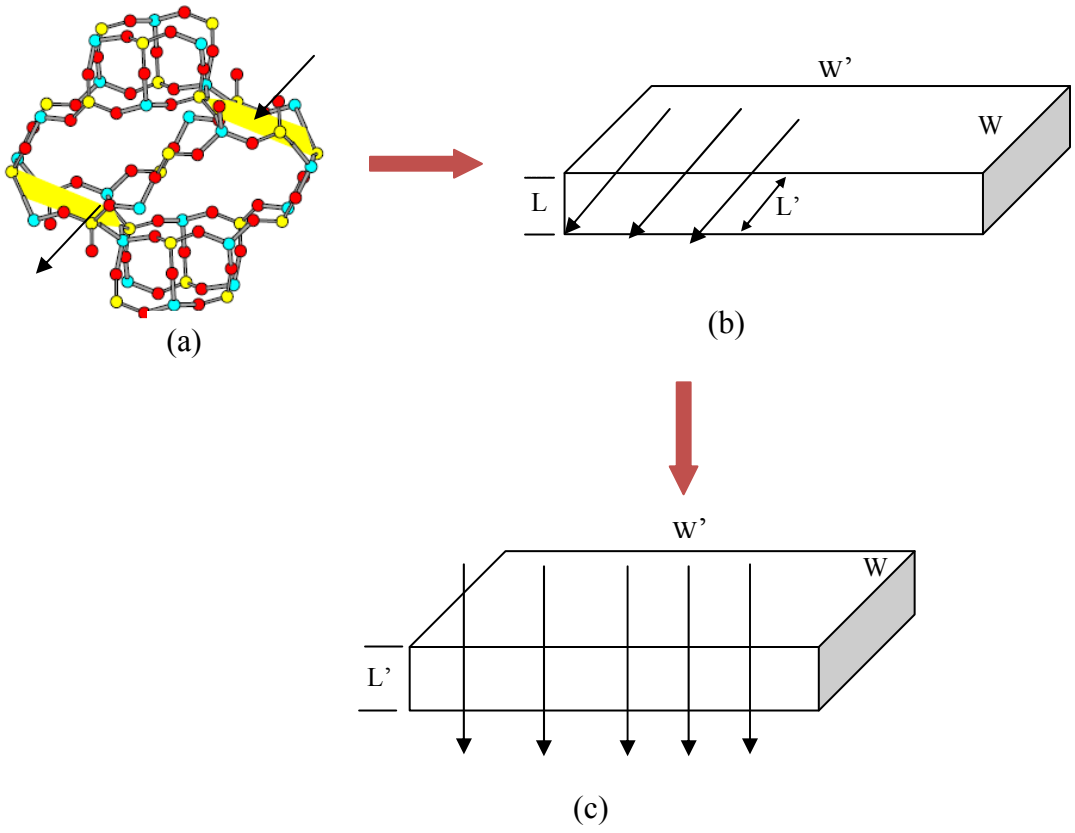

Figure-6.7: (a) Only favorable diffusion paths of propylene are shown by yellow areas [9]. (b) An equivalent parallelepiped of thickness “L”. (c) Representation of the same parallelepiped with “effective” thickness L’

Once the characteristic length was determined by the above method, sorption experiments were then performed with AlPO-14 molecular sieves. These experiments were then used to determine diffusivity and solubility performance of propylene and propane with AlPO-14 at 35^0C. The next section describes these results.

6.3.2. Equilibrium And Kinetic Sorption Experiments

AlPO-14 samples were supplied by UOP for this research. Figure-6.8 shows the SEM images of the samples used for this work. A pressure decay sorption method was used for the sorption measurements. Both kinetics data and the sorption isotherms were measured on the same sample at 35^0C. As mentioned earlier, there is only 1-dimensional diffusion possible for AlPO-14 with propylene and if at all with propane (in <1, 1, -1> direction. One micron long characteristic dimension was considered based on the inspection of SEM images (following Figure-6.7 (c)) of samples of the AlPO-14 we used.

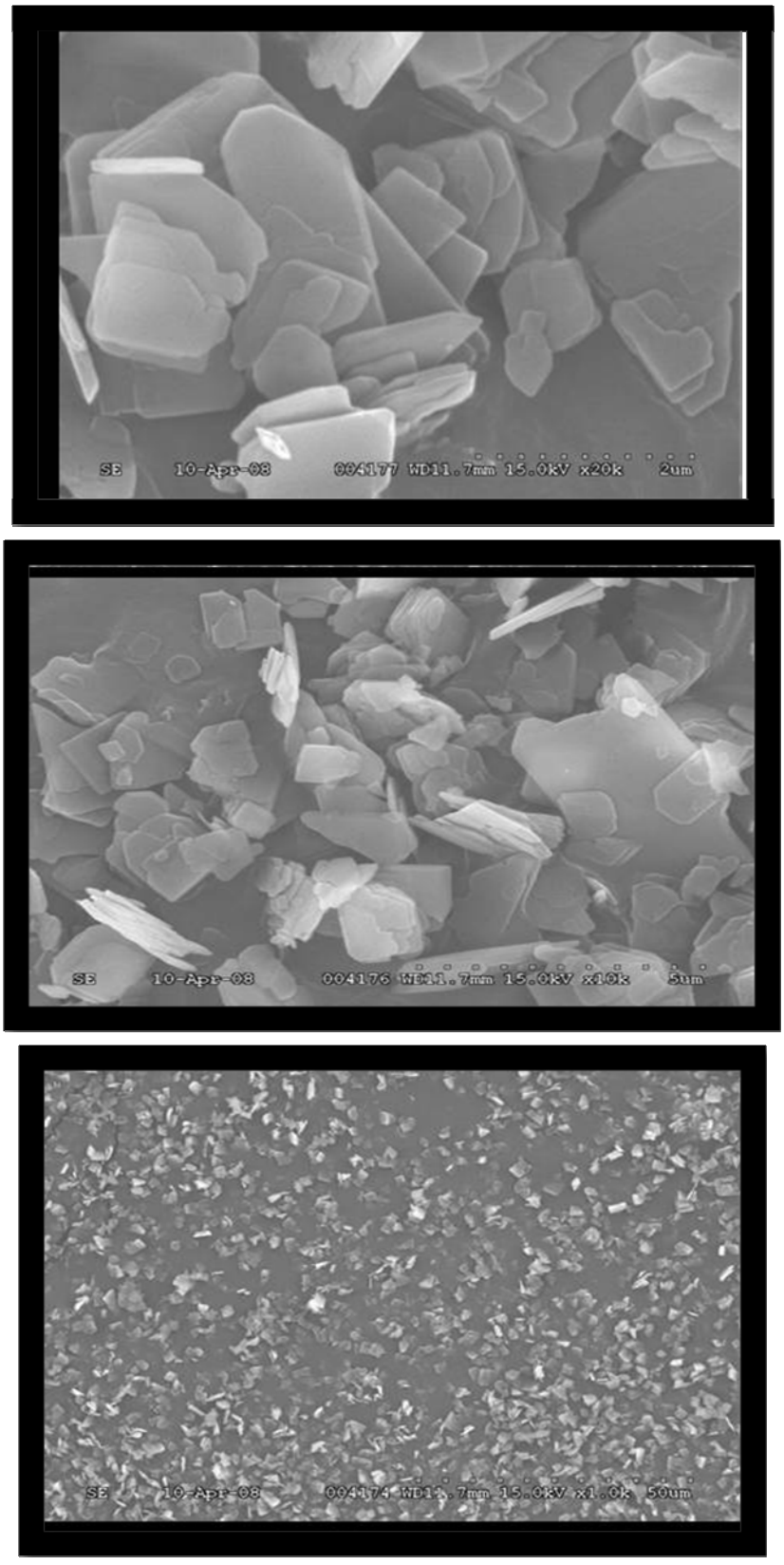

Figure-6.8: SEM images of AlPO-14 used for this research.

Figure-6.9 shows the sorption isotherm of AlPO-14 at 35^0C test temperature. Prior to loading in the sorption cell, the molecular sieves were dried at 150^0C in a vacuum oven overnight to remove any moisture from the sieve particles. In the case of molecular sieve materials, there is no Henry's densified region. The sorption in this case only takes place via Langmuir region and can be described by Equation-6.3;

$$C_A = \frac{C'_{HA} b_A p_A}{1 + b_A p_A} \qquad [6.3]$$

Where C'_{HA} is the Langmuir capacity constant and b_A is the Langmuir affinity constant.

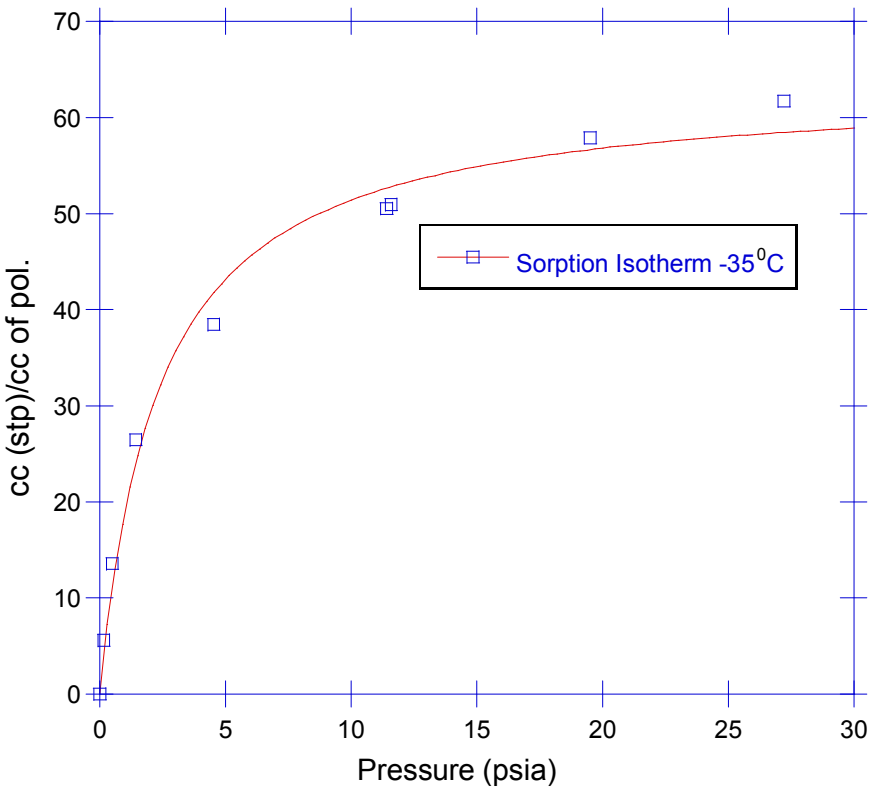

Figure-6.9: Propylene sorption isotherm with AlPO-14 at 35^0C. □ – experimental values, —— Curve fit

The propylene isotherm was then modeled with Equation-6.3. Table-6.2 shows the sorption parameters for this case.

Table-6.2: Sorption isotherm parameters for AlPO-14 with Propylene at 35^0C

AlPO-14 35^0C	C_H' *cc (stp)/cc pol.*	*b* $psia^{-1}$	*S (C/p) @ 29.4 psia* *cc (stp)/cc.cmHg*
AlPO-14	63.51 ± 2.16	0.43± 0.06	0.387± 0.04

To estimate the diffusivity of the AlPO-14 molecular sieves, kinetic data was collected through data acquisition. To determine propylene diffusivity, a plot of M_t/M_∞ with square root of time was constructed. Figure-6.10 shows this plot. We then determined the exact time when $M_t/M_\infty = 0.5$. Since AlPO-14 is a high aspect ratio particle, it was then considered to be as a slab and $D_{propylene}$ (cm^2/sec) was calculated. In case of a 1-dimensional diffusion into an object with characteristic thickness dimension of l, the equation for diffusion constant is: $\sqrt{\frac{D.t}{l^2}} = 0.43$ [10].

If we consider that our half-time is 5s (Figure-6.10), our calculated D is 3.87 x 10^{-10} cm^2/s (considering one micron long characteristic dimension. As demonstrated in Figure-6.7 (c), L' = 1 micron).

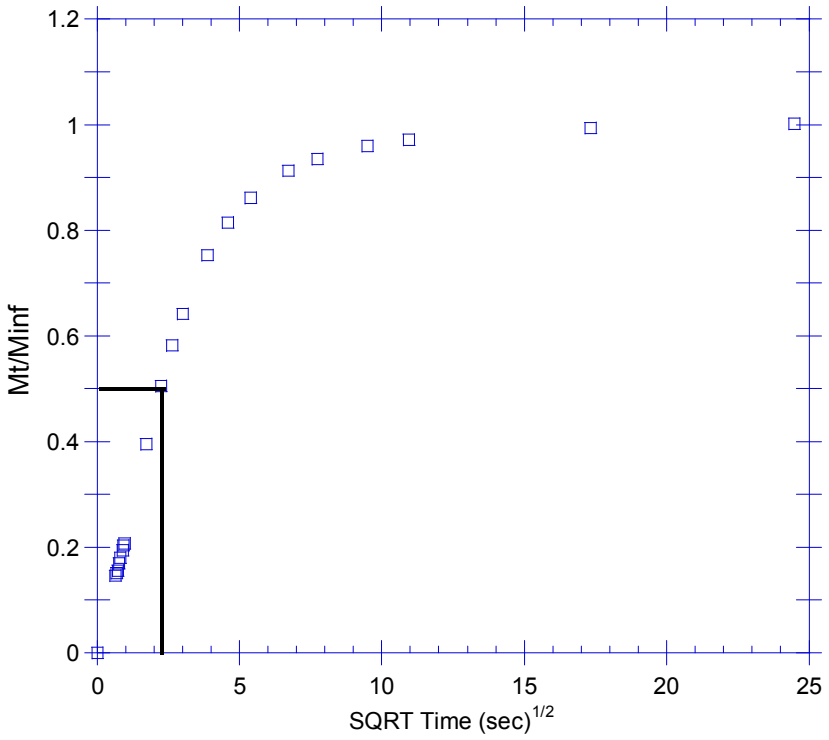

Figure-6.10: Propylene kinetic sorption at 35^0C.

A comparison of P, D and S values between pure polymer and molecular sieve is shown in Table-6.3. An excellent polymer-sieve matching can be observed in this particular case. Propylene is more soluble in AlPO-14 than in 6FDA-6FpDA pure polymer, although it has a lower diffusion coefficient. Permeability of propylene in AlPO-14 is almost double that of pure polymer, due to its higher solubility. Similar sorption experiments were performed with propane, but no significant change in mass was observed for more than seven days. Hence it was concluded, propane cannot enter AlPO-14 sieves. Previous discussion on AlPO-14 structure also supports this observation.

Table-6.3: Calculated propylene permeability, diffusivity and solubility for Pure-6FDA-6FpDA and AlPO-14 at 29.4 psia and 35^0C

Material	*Propylene Permeability (Barrer)*	*S (C/p) @ 29.4 psia cc (stp)/cc.cmHg*	*D (cm^2/s)*
Pure-6F-6F	0.7 ± 0.05	0.168	4.2×10^{-10}
AlPO-14	1.42	0.387	3.69×10^{-10}

After successfully characterizing AlPO-14, mixed matrix membranes were prepared and tested with pure gas and mixed gas feeds for propylene/propane separation performances. The next section describes the pure gas mixed matrix membrane experimental and modeling results.

6.4. Mixed Matrix Membrane – Pure Gas Results at 35^0C

Mixed matrix membranes (MMMs) were prepared with ~ 15 wt% of AlPO-14 (one film was prepared with 13 wt%) in 6FDA-6FpDA polymer matrix. All the cast films were annealed at 210^0C around 18 hours to be consistent with the pure film work. Figure-6.11 shows the mixed matrix pure gas results. Three different films were tested for from three different cast films for repeatability of the mixed matrix membrane results. As shown in Figure-6.11, the MMM results were highly reproducible with very close permeability and selectivities. Enhancements in both permeability and selectivity were observed in this case. This was for the first time permeability and selectivity enhancement via mixed matrix membrane for propylene/propane separations has been reported according to our best knowledge.

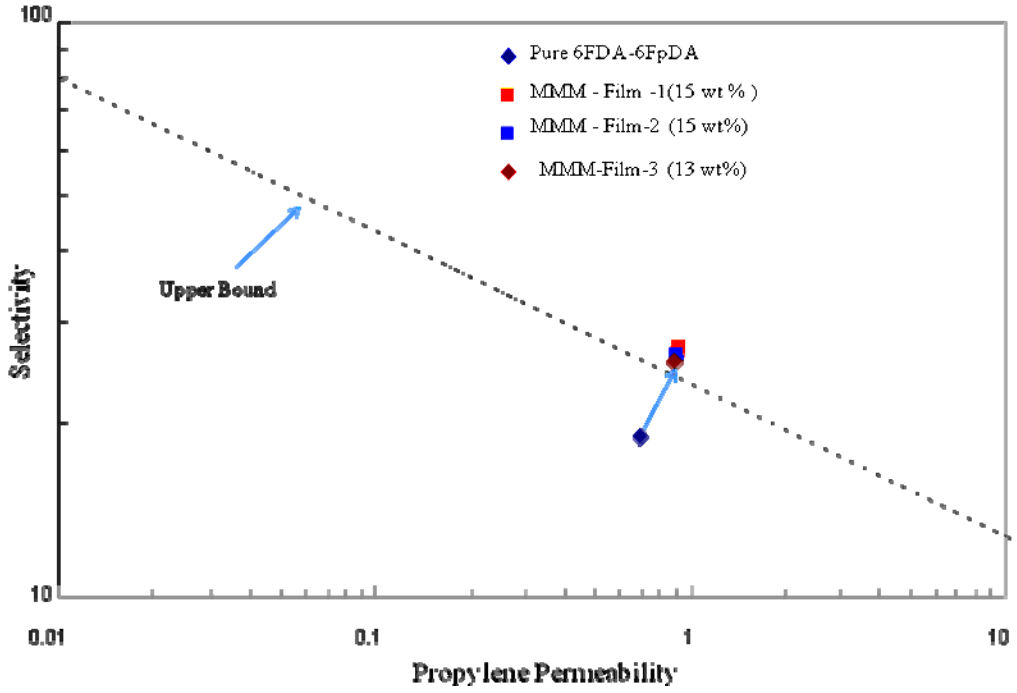

Figure-6.11: Pure gas mixed matrix results. Permeation tests were performed at 2 atm upstream pressure and 35^0C temperature

Table-6.4 shows pure gas permeation results and the comparison between pure film and mixed matrix results. In case of mixed matrix membranes, diffusivity coefficient (D) was calculated from the the time-lag recorded during permeation test, therefore there might be some small error associated with this calculation; especially with the slower gas propane. The tested films were around 3.2 mils in thickness. At this film thickness, the propane flux was very low, making it hard to pin-point the time-lag. Hence, the calculated diffusivity of propane via time-lag method is more erroneous than propylene diffusivity.

Table-6.4: Pure gas permeability, selectivity, diffusivity and solubility values for pure film and mixed matrix membranes (29.4 psia, 35^0C)

Material	*Propylene Permeability (Barrer)*	*Propylene/Propane Selectivity*	*D (cm^2/s)*	*S (cc.(stp)/cc.cm Hg)*
Mixed Matrix	0.97±0.01	27±1.0	4.11×10^{-10}	0.233±0.02
Pure Film	0.70 ± 0.05	19±1.0	4.20×10^{-10}	0.168±0.04

As shown in Table-6.4, the main enhancement in propylene permeability comes via enhanced sorption capacity of mixed matrix membrane with respect to the pure film. This agrees with previous observation in Table-6.3 that AlPO-14 molecular sieve has a much higher sorption coefficient value than the pure film propylene. Table-6.5 shows mixed matrix membrane values calculated from permeability and diffusivity (P = D.S) for propylene and propane. Pure film data were taken from Chapter-5. Pure film data are shown in Table-6.6 for comparison.

Table-6.5: Mixed matrix membrane permeability, diffusivity and solubility for propylene and propane (Pure gas at 29.4 psia, 35^0C)

Gases	*Permeability (Barrer)*	*S (cc.(stp)/cc.cm Hg)*	*D (cm^2/s)*
Propylene	0.97±0.01	0.233±0.02	4.11×10^{-10}
Propane	0.036±0.005	0.095±0.05	3.7×10^{-11}

Table-6.6: Pure film permeability, diffusivity and solubility for propylene and propane (Pure gas at 29.4 psia, 35^0C)

Gases	*Permeability (Barrer)*	*S (cc.(stp)/cc.cm Hg)*	*D (cm^2/s)*
Propylene	0.7±0.05	0.168±0.04	4.20×10^{-10}
Propane	0.036±0.005	0.104±0.02	3.6×10^{-11}

As shown in Table-6.5 and Table-6.6, propylene sorption coefficient value increased from 0.168 cc. (stp)/cc.cm.Hg to 0.233 cc. (stp)/cc.cm.Hg in mixed matrix membrane, whereas the sorption coefficient value of propane decreased from 0.104 cc. (stp)/cc.cm.Hg to 0.095 cc. (stp)/cc.cm.Hg. These values again agree with previous observations with pure AlPO-14 sieve materials.

To explain the excellent enhancements in permeability and selectivity (Figure-6.11), pure AlPO-14 and pure 6FDA-6FpDA values were then used to fit in Maxwell and Cussler transport models. The next section describes model predictions and their interpretation for the current work.

6.4.1. Mixed Matrix Membrane Results – Maxwell and Cussler Models

As described earlier, the most common description of the performance of mixed matrix materials is given by the so-called "Maxwell model" (Equation-6.1). Table-6.7 shows the values used to calculate Maxwell model predictions. Figure-6.12 shows the Maxwell model predictions along with experimental results.

Table-6.7: Values used for model prediction

Gases	*Propylene Permeability (Barrer)*	*α (Selectivity)*	*Density (gm/cc)*
Pure polymer	0.7	19.0	1.466
Pure AlPO-14	1.42	92779	1.761

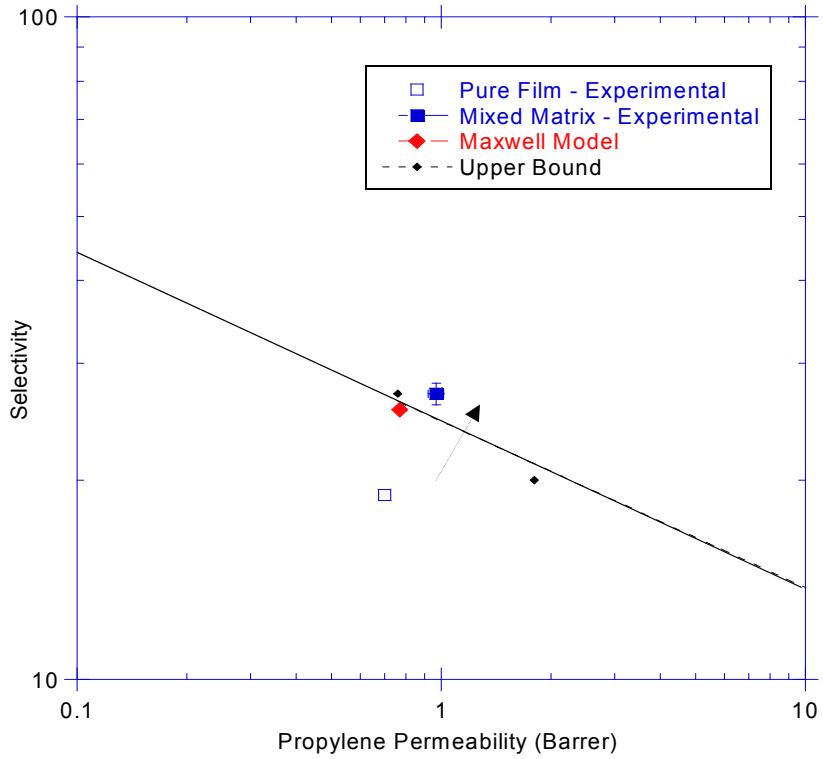

Figure-6.12: Comparison of Maxwell model and pure gas mixed matrix experimental results. Permeation tests were performed at 2 atm upstream pressure and 35^{0}C temperature

As seen in Figure-6.12, the Maxwell model underestimates the permeability and selectivity of 6FDA-AlPO-14 mixed matrix membrane performance. Both permeability

and selectivity are lower than what we observed with pure gas experimental results Maxwell Model is a good representation when the particle aspect ratio is equal to unity. As shown in the SEM images (Figure-6.8), AlPO-14 is a high aspect ratio molecular sieve. Therefore to correctly handle this geometry, we considered an alternative model. The Cussler model is more appropriate [11]. As described in Chapter-2, the Cussler model considers enhancements in diffusivity for permeable sieves and is expressed by, viz:

$$\frac{J_0}{J} = 1 - \phi + \left[\frac{1}{\frac{1}{\delta\phi} + \frac{4(1-\phi)}{A_R{}^2 \phi^2}} \right] \qquad [6.4]$$

where J_0 is pure polymer flux across the membrane, J is the flux across the mixed matrix membrane. Φ is the volume fraction of the sieve in the mixed matrix membrane, A_R is the sieve aspect ratio (defined as W'/L' from Figure-6.7 (c)) and δ is the ratio of diffusivity coefficient of polymer to sieve. Please note that in the original Cussler equation, a term α was used instead of A_R and was defined as $\alpha = A_R/2$. Throughout this work α has been used to describe the selectivity, hence the new term A_R was introduced to avoid any confusion. The above equation was then used to calculate the potential transport enhancements. As seen in Figure-6.8, it is hard to determine the original aspect ratio for this particular material, because the range of aspect ratio is broad in this case. Permeabilities were predicted using the Cussler model for A_R values of 2 to 20.

Figure-6.13 shows the Cussler model prediction from two approaches. First, it was assumed that the selectivity enhancements are as a result of the diffusivity differences in propylene and propane. In this case, the left side of Equation-6.4 was replaced by $P_0/P_{propylene}$ (P_0 = propylene permeability in pure polymer and $P_{Propylene}$ = calculated propylene permeability in the mixed matrix membrane). Since all the terms on the right hand sides of Equation-4 are known (for example, $\delta = 0.493$, $\Phi = 0.128$, $P_0 = 0.7$) $P_{Propylene}$ was then determined. This calculation was done for a range of A_R (A_R=2 to A_R=20). Similar calculations were then performed for propane using values from Table-6.6. Selectivity was calculated for a particular A_R simply by taking ratio of $P_{Propylene}$ and $P_{propane}$. In Figure-6.13, the red points are calculated propylene permeability and propylene/propane selectivity. The arrow shown is the increasing direction of A_R starting from 2 (the lowest red points) to 20 (the top most points).

One problem we observed with this standard Cussler model prediction was that the enhanced sorption capacity of AlPO-14 sieve was not considered as part of the model prediction. A second calculation was done with the enhanced sorption coefficients for propylene in AlPO-14. In this method, instead of $P_0/P_{Propylene,}$ we more correctly interpreted Equation-4 as the diffusion ratio $D_0/D_{Propylene}$. The value of D_0 is listed in Table-6.6. Once we had the predicted $D_{Propylene}$ in mixed matrix membrane from Equation-4, it was then multiplied by the enhanced sorption capacity ($S_{Propylene} = S_0(1-\Phi) + S_{AlPO-14}.\Phi$) for propylene. Table-6.3 and Table-6.6 values were used for this calculation. Similarly $D_{Propane}$ and $S_{Propane}$ were determined by Equation-6.4. Lastly, $P_{Propylene}/P_{Propane}$ were calculated by $(D_{Propylene}.S_{Propylene}) /(D_{Propane}.S_{Propane})$.

In Figure-6.13, the blue points are the permeability and selectivity calculated with the enhanced sorption coefficient factors included for $2 \leq A_R \leq 20$.

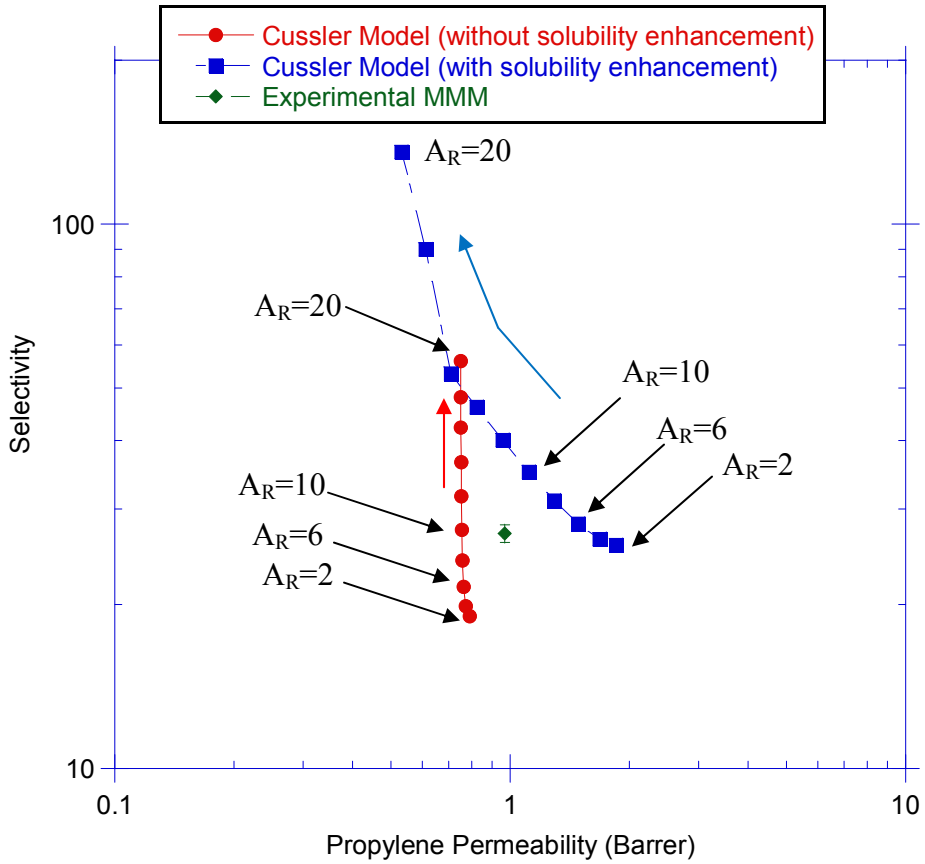

Figure-6.13: Cussler model predictions for A_R=2 to A_R=20. Red dots are the predictions without enhanced sorption coefficients. Blue dots are the predictions with enhanced sorption coefficients. Experimental result with pure gas is also shown. A_R increases from the bottom to the top.

As shown in Figure-6.13, the two different methods of calculating permeability predicted somewhat different results. The enhanced sorption capacity of the mixed matrix membrane is a key factor; therefore the second method of calculation is a better fit (the blue points with modified Cussler model) for this particular mixed matrix membrane separation. From the blue points the average aspect ratio of the molecular sieves was then

estimated for the current work. A closer look at Figure-6.13 reveals that the experimental selectivity matches with an A_R value of around 5-6. This seems within a reasonable range based on the SEM images of the dispersed AlPO-14 sieves (Figure-6.8). However, the observed experimental permeability is lower than predicted by the Cussler model. This observation will be addressed in the last section of this chapter. The next section describes the mixed gas permeation results for the same mixed matrix membranes.

6.5. Mixed Matrix Membrane – Mixed Gas Results at 35^0C

Following the success with pure gas tests on mixed matrix membrane, mixed gas (with 50/50 and 75/25 propylene/propane mixture) feeds were then used to test the permeability and the selectivity of the dense film mixed matrix membrane in a more realistic environment. These results were compared with pure film mixed gas results (described in Chapter-5). Mixed gas permeates were sent to a GC and the ratio of areas was used to determine the selectivity. Chapter-3 has the details of the GC set-up. Figure-6.14 shows the pure film and mixed matrix membrane results with propylene/propane mixed gas. We observed enhanced selectivity (selectivity increased by 30%). However, the observed mixed gas selectivity was lower than the pure gas mixed matrix selectivity (selectivity decreased from 27.0 to 18.5). This observation is in accordance with reported results in Chapter-5, where a decrease in selectivity from pure gas to mixed gas was observed (around 24% decrease was observed in the case of pure polymer film mixed gas permeation tests). This result is still very promising, and in our best knowledge this is the first time selectivity enhancement with mixed matrix membrane has been observed with

propylene/propane separations. Moreover, as discussed in Chapter-5, we again observed no onset of plasticization at 35^0C, even with propylene upstream pressure of 2 atm.

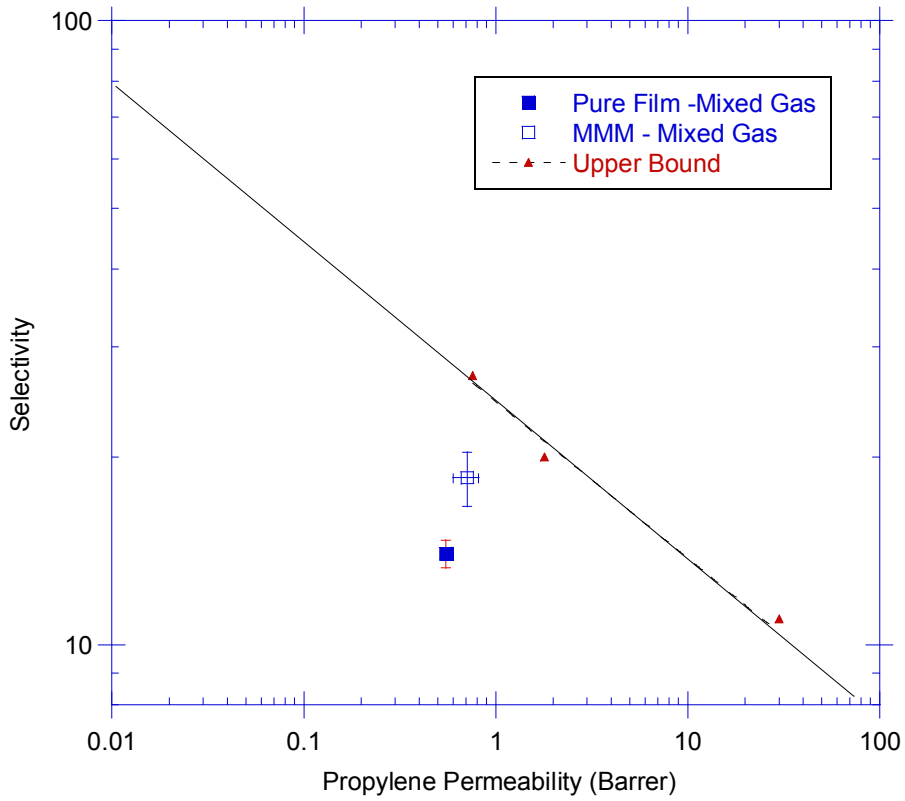

Figure-6.14: Mixed matrix membrane mixed gas experiment results (50/50 and 75/25 propylene/propane mixture). Experiments were done at 35^0C and around 2 atm propylene upstream pressure

Although in the case of mixed gas permeation (Figure-6.14) the experimental point is below the upper bound, it is worth pointing at that the upper bound curve was constructed with the pure gas permeation data and at 50^0C. It is well known that generally with 6FDA based polyimides, propylene/propane mixed gas selectivity is lower than the pure gas selectivity, so the upper bound of mixed gas experiments is much lower than the pure gas upper bound.

6.5.1. Mixed Matrix Membrane Mixed Gas Results – Cussler Model

Once we successfully demonstrated that the mixed matrix membrane has enhanced selectivity and permeability, even in the mixed gas environment, the Cussler model was then used to predict the expected mixed gas selectivity and permeability. In this case, a couple of approximations were adopted. Table-6.8 shows the values used for the model prediction. As shown in Table-6.8, propylene permeability and propylene/propane selectivity for pure polymer mixed gas experimental values were used for calculation. Unfortunately, we are currently not equipped to perform mixed matrix mixed gas sorption experiments. Hence, pure AlPO-14 permeability and selectivity values were used. Figure-14 shows the calculated selectivity and propylene permeability for mixed matrix mixed gas experiments. Moreover, we assumed that A_R=5. As described in the previous section, the blue solid point represents the selectivity with enhanced sorption coefficient. The red point represents the enhanced selectivity prediction where the flux expressions were directly replaced by the permeabilities. As shown in Figure-6.15, the experimental data point falls in between these two values. It is also noticeable that the permeability value is within 10-15% range of the two predicted permeabilities. In the case of selectivities, the Cussler model prediction with enhanced sorption coefficients has a higher predicted selectivity (25% higher value was predicted than the experimentally observed value).

Table-6.8: Values used for model prediction - mixed gas

Gases	*Propylene Permeability (Barrer)*	*α (Selectivity)*	*Density (gm/cc)*
Pure polymer	0.55	14.5	1.466
Pure AlPO-14	1.42	92779	1.761

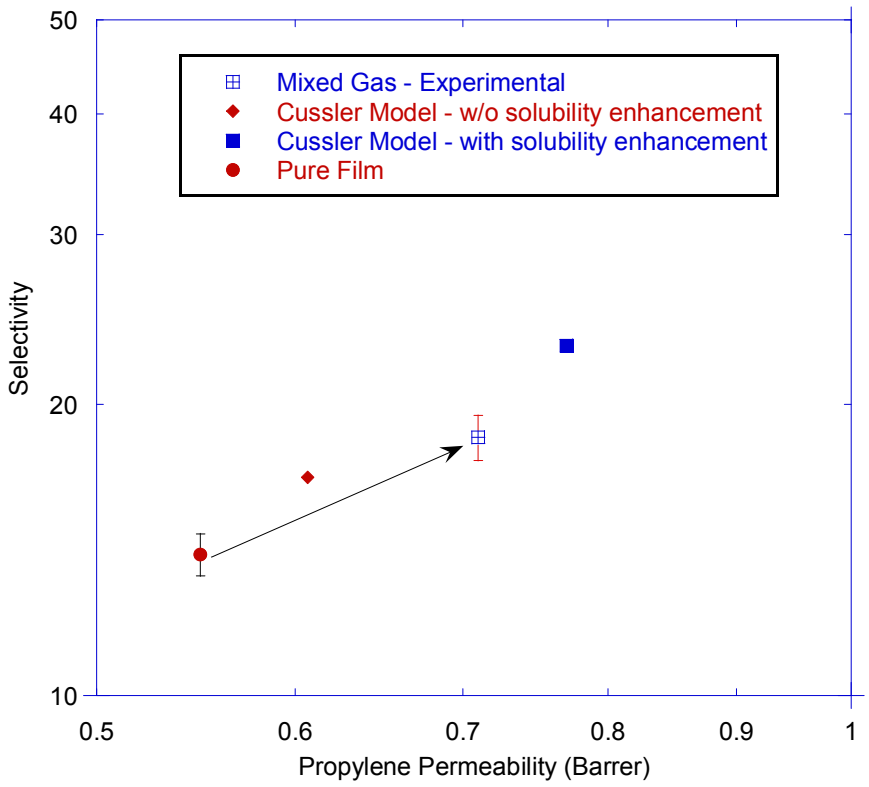

Figure-6.15: Mixed matrix membrane mixed gas experiment results (50/50 and 75/25 propylene/propane mixture) at 35^0C and 2 atm propylene upstream pressure. Cussler model predictions are shown in red and blue dots. Red dot is without enhanced sorption coefficient. Blue dot is the prediction with enhanced sorption coefficient. Experimental result with pure gas is also shown. A_R =5 was assumed in this case.

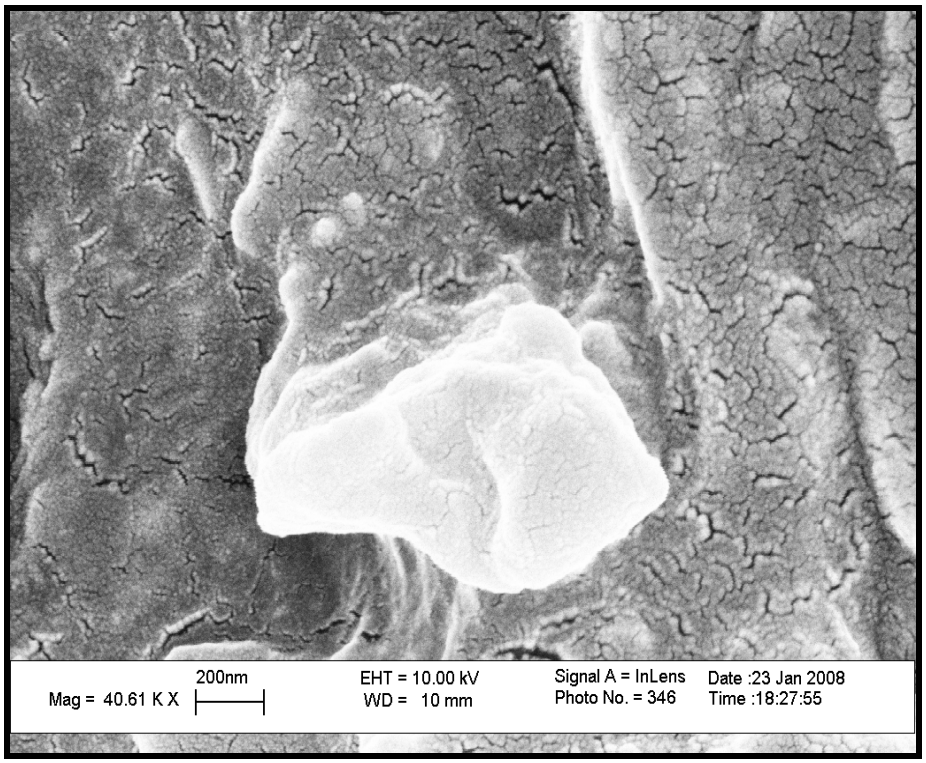

Figure-6.16: SEM image of 6FDA-6FpDA and AlPO-14 mixed matrix membrane.

Figure-6.16 shows the polymer-sieve adhesion observed under SEM. As seen from the figure, and especially from the permeation results, we were able to achieve good adhesion between the polymer and the AlPO-14 sieve without any surface modification. We believe that this good adhesion is due to the less hydrophilic and less acidic nature of AlPO-14 which helps in polymer-sieve interaction and hence success in mixed matrix membrane mixed gas experiments.

One of the main assumptions in the Cussler model is that the high aspect ratio molecular sieves are perfect platelets with permeation in the direction normal to the shortest axis. But in practical cases, it is hard to determine whether the sieves are in

perfectly parallel to each other or not. Although the casting process might have some influence on aligning the sieves in an ordered manner, nevertheless, it is "less-perfect" than as described in the Cussler model. In that case, it is not possible to achieve as high selectivity as predicted by the Cussler model (even accounting for an enhanced sorption coefficient). Moreover, the effect of high aspect ratio particle is most useful when the selective pathway for the fast gas is in the perpendicular direction ([0,0,1] trajectory direction). As shown in Figure-7 (a), (b) and (c), this particular molecular sieve is not selective in that direction. Instead, [1,1,-1] is the favored trajectory. As a result the fast gas also becomes relatively slower since it has to travel a longer pathway. These facts may explain our experimentally observed lower selectivity than predicted by the original model. More work is needed to be done to carefully include all the non ideal behaviors in a mixed matrix environment based on these very promising preliminary results. The next section describes the results obtained from 70^0C mixed matrix permeation tests. Only mixed gas experiments were performed and the findings are described below.

6.6. Mixed Matrix Membrane Results – Mixed Gas – 70^0C

In the previous section, successful enhancement of propylene/propane separation with mixed matrix membrane has been demonstrated. Moreover, like pure film results (Chapter-5) and mixed matrix membranes, no onset of plasticization with mixed matrix mixed gas experiments was observed. The same mixed matrix membranes were further tested at 70^0C with propylene/propane 75/25 mixture. To maintain consistency, we pulled

downstream vacuum on the mixed matrix membranes used for 35^0C experiments. We waited at least six times longer than the original propane time-lag before starting the high temperature permeation experiments. Two different films were tested with 75/25 propylene/propane mixture and the results are shown in Figure-6.17.

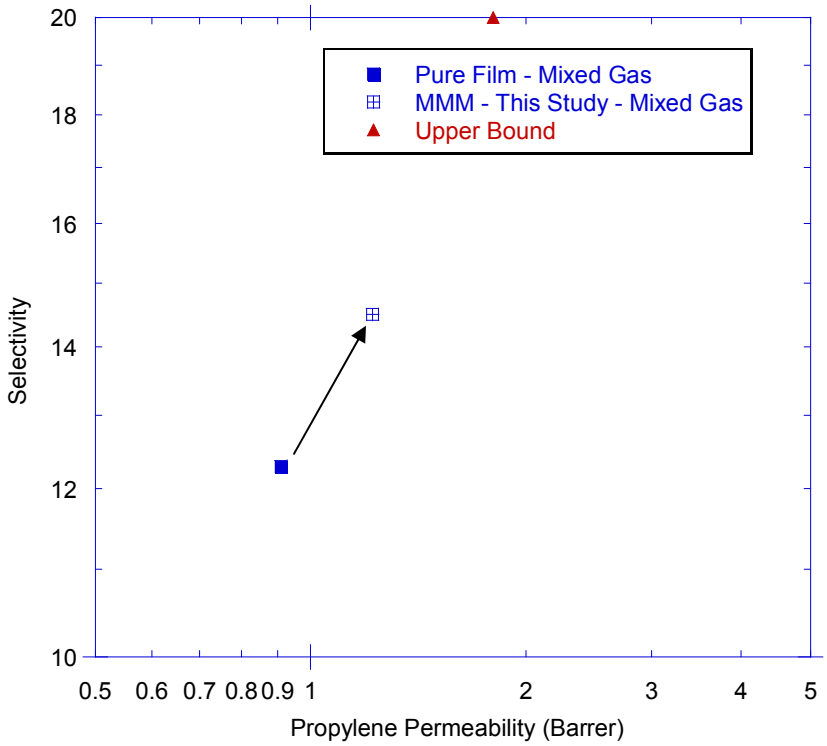

Figure-6.17: Mixed matrix membrane permeation tests at 70^0C. Pure gas and mixed gas (75/25) are shown. Experiments were performed around 2 atm propylene upstream pressure.

Again also permeability and selectivity enhancements were observed. Our observed selectivity increased by 18% and the propylene permeability increased by 34%. To further test any effect of high temperature permeation, the system was evacuated after each permeation test and then mixed gas experiments at 35^0C were repeated with 50/50

propylene/propane to note any anomaly. Successful reproduction of the previous results as described in the above section was observed.

6.7. Conclusions

In this chapter, mixed matrix membranes were formed with 6FDA-6FpDA as the polymer matrix and AlPO-14 as the molecular sieve material. AlPO-14 was chosen due to its success with PSA and VSA for propylene/propane separations. AlPO-14 is a unique molecular sieve which is one dimensional for propylene and almost excludes propane from entering the interior cage. Permeation results with pure and mixed gases at 35^0C showed very promising enhancements in both propylene permeability and propylene/propane selectivity. According to our best knowledge, this is the first time enhanced selectivity and permeability were achieved in a mixed gas environment for this gas pair using the mixed matrix hybrid material approach. The main observation we would like to highlight was the excellent polymer-sieve matching. A 6FDA-6FpDA-AlPO-14 combination holds a bright future for large scale propylene/propane separations.

6.8. References

1. R. L. Burns, W.J. Koros, *Defining the challenges for C_3H_6/C_3H_8 separation using polymeric membranes*. JMS, 2003. **211**: p. 299-309.

2. Kulprathipanja, S.; Neuzil, R. W.; Li, N. N. *Separation of fluids by means of mixed matrix membranes*. **US 4,740,219**, 1988.

3. Liu. C, Hillock A.M., Husain S., Koros, W. J. ,Kulprathipanja, S. *Review of Recent Progress in Mixed Matrix Membranes, Chapter in Advances in Membrane Science,* Wiley & Sons Publishers, N. L. Li Editor

4. Cheng L, Padin J, Rege S. U., Wilson S. T., Yang R T. *Process for purifying propylene*. **US 6,406,521**, 2002

5. Padin J, Rege S. U., Yang R. T., Cheng L. S., *Molecular sieve sorbents for kinetic separation of propane/propylene.* Chemical Engineering Science, **55**, 4525.

6. Cheng L, Wilson S.T., *Vacuum swing adsorption process for separating propylene from propane.* **US 6,296,688,** 2001

7. Data supplied by UOP

8. Steel Keisha, *Carbon membranes for challenging gas separations,* PhD Dissertation, The University of Texas at Austin, 2000.

9. Yang N., Greenlay N., Karapetrova J., Zschack P., Gatter M., Wilson S. T., Broach R. W., *In Situ Characterization of AlPO-14 Using Synchrotron Powder Diffraction*, SRMS-5 Conference , Chicago July 30- Aug.2, 2006.

10. Hines and Maddox, *Mass Transfer, Fundamentals and Applications*, 1985. Prentice Hall

11. Cussler E. L., *Membranes containing selective flakes,* JMS, 1990. **52:** p. 275-288

CHAPTER 7

SUMMARY AND RECOMMENDATIONS

7.1. Summary and Conclusions

As mentioned in the first chapter, the goal of this project was to *develop a mixed matrix membrane with enhanced properties for propylene/propane separations.* To start with the project, one of the high performance 6FDA based polyimides was identified as the polymer matrix for the rest of the project (objective-1). The chosen polymer (6FDA-6FpDA) was successfully synthesized in the laboratory.

During the synthesis process the key objectives for high molecular weight and low polydispersity index polymer were identified. High molecular weight 6FDA-6FpDA was synthesized via two different methods – chemical imidization and thermal imidization. The thermal imidization process was preferred initially since it produces high molecular polymer without any isoimide formation. unfortunately, with the thermal imidization process, a white precipitation was observed, which turned the polymer-solvent solution murky in nature, making it difficult to work with. This precipitation is believed to be the polymer/oligomer crosslinked due to the heat treatment during thermal imidization process [6].

At that point, chemical imidization with a different catalyst (a weaker base *beta*-picoline was used instead of TEA) was done with a post treatment of high temperature heating under vacuum. This modified method consistently produced high molecular weight, narrow PI polymer with a clear solution. Currently, this method is being implemented in our laboratory for other polyimides with excellent results. The results related to this objective have been described in Chapter-4.

After successful synthesis of the high performance polymer, pure polymer dense films were tested for transport properties. One problem identified with 6FDA-6FpDA polymer films for propylene/propane separations was plasticization. The aim of the second objective of this research was to develop a method for plasticization suppression. Initially, permeation and sorption tests on pure polymer dense films were done to benchmark the transport properties and observe the reproducibility. The results were quite satisfactory at par with previous researches.

A careful annealing control study was first performed to optimize the annealing temperature of a newly cast membrane. Oxygen and nitrogen permeabilities and selectivities were used as benchmark gases. Once the annealing temperature was optimized, propylene propane permeations with elevated temperature (70^0C) were performed which showed plasticization suppression until 70 psia for pure propylene gas and 42 psia (propylene upstream pressure) in the mixed gas environment. The annealing approach even worked at 35^0C test temperature, showing no sign of plasticization until 42 psia of propylene upstream pressure (Chapter-5).

To the best of our knowledge, this is for the first time plasticization suppression was achieved with pure polymeric membrane material for propylene/propane separations with pure and mixed gases. The observed mixed gas experimental selectivity was lower than the pure gas selectivity which was explained by the combination effect of dual mode and bulk flow effect.

The last objective of this project was to successfully incorporate molecular sieve materials to form a mixed matrix membrane hybrid material with enhanced transport properties (Chapter-6). First, an ideal molecular sieve for propylene/propane separation was identified and characterized. AlPO-14 was chosen for this research following its success with propylene/propane pressure swing adsorption.

AlPO-14 has a unique structure where it excludes propane via steric hindrance, while allowing propylene to diffuse through. Characterizations of AlPO-14 molecular sieve at 35^0C were done to estimate the transport properties with propylene and propane gases. Mixed matrix membranes were successfully produced and tested for enhanced transport properties. Both pure and mixed gas results showed promising results with enhanced propylene permeability and propylene/propane selectivity. The experimental results were modeled with the Cussler and Maxwell models. A modified Cussler model was presented in this work. This is the first time an enhancement in the transport properties with mixed matrix membrane for propylene/propane separations has been observed. This fundamental dense film work holds a bright future for the scale up of propylene/propane separations.

7.2. Recommendations

While this research was successful in producing hybrid membrane material with enhanced separation performance using a high performance polymer matrix, to improve the industrial viability some of the areas still need to be explored and developed. Several of these potential research areas are listed below.

7.2.1. Mixed Matrix Membranes With Higher Loading

The current research was performed with 13-16 wt% AlPO-14 loading in polymer mixed matrix membrane. Although the selectivity obtained from the mixed matrix material was very promising (at 35^0C the mixed gas selectivity was 18.5), yet this selectivity is not enough to generate research grade propylene (>98% pure starting with 70/30 propylene/propane mixed feed, for polypropylene production). At this point, the purity from our mixed gas result is ~95%. Increasing the molecular sieve loading percentage in the polymer matrix is expected to increase the selectivity and permeability. Figure-7.1 shows the modified Cussler model [1] prediction with higher molecular sieve loading. At 30% sieve loading, the selectivity predicted was 32.

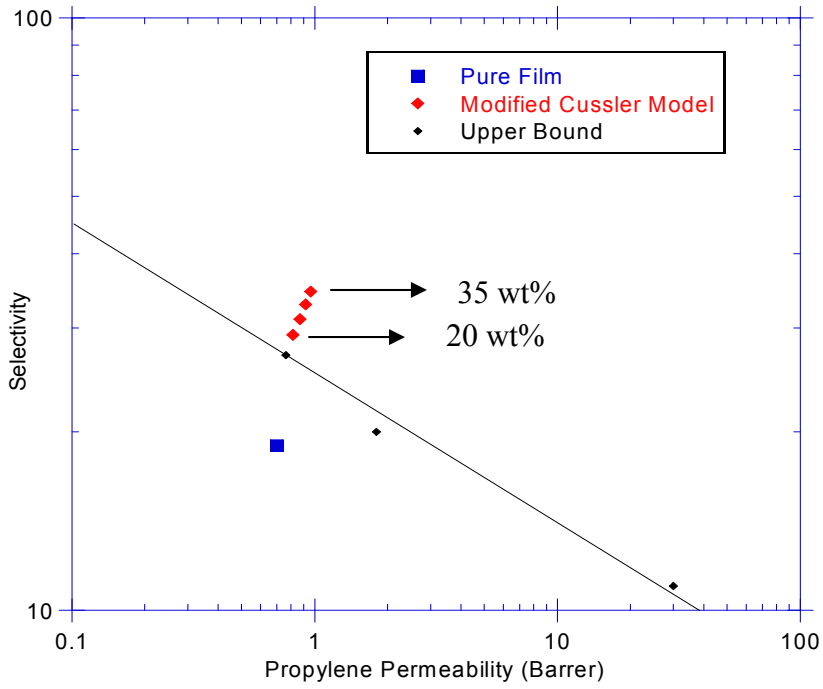

Figure-7.1: Cussler model prediction for high loading mixed matrix membrane with 6FDA-6FpDA-AlPO-14 hybrid material.

As seen from Figure-7.1, it will be really promising to be successfully able to produce high loading mixed matrix membranes.

7.2.2. Pure Polymer Asymmetric Hollow Fiber

One of the final developments of the economically viable membranes is the hollow fiber membranes. There are multiple challenges that are present in hollow fiber spinning process, which are not present in the dense film development work. A significant research has been done to identify some of the key challenges in relatively rigid material hollow fiber spinning, which can use as the starting point [4, 2]. After successful spinning, these fibers must be tested for the transport properties. Since in a

realistic environment, propylene/propane mixed gas enters the column at a high temperature, high temperature testing (~up to 90^0C) should be performed. Although at very high temperature plasticization is expected to be suppressed until higher pressure than observed in 35^0C and 70^0C, mixed gas propylene/propane permeation tests should also be performed at higher pressure also (up to 250 psia) to observe any onset of plasticization. At high feed pressure, covalent crosslinking has been shown to increase plasticization resistance in dense films and asymmetric hollow fibers by suppressing the degree of swelling and segmental chain mobility in the polymer, thereby preserving the selectivity of the membrane for CO_2/CH_4 separation [2, 3]. Since CO_2 is more condensable in nature than propylene or propane, this approach is expected to be even more effective to suppress plasticization in the case of propylene and propane at higher feed pressure.

7.2.3. Hybrid Membranes As Asymmetric Hollow Fibers

There are several important parameters for spinning hybrid asymmetric fibers. Recent work by Husain was able to identify and solve several of these problems successfully, but there are still several areas in need of further development [4]. Since in asymmetric hollow fiber the selective layer is very thin, even small agglomerations of the molecular sieve particles will greatly reduce the selectivity of the membrane. Moreover, the phase separation process that is used to form the asymmetric structure of the hollow fibers can be impacted by the presence of the small sieve particles. In that case although

absent in dense films, new morphological defects especially, voids may form in the hollow fiber. Further work in this area is still needed to spin defect free fibers.

The 6FDA-6FpDA polymer is one of the highest performing polymers for propylene/propane separations; however, the monomers used in synthesizing this polymer are costly relative to some of the lower performing polymers. For industrial application, material cost reduction is important and may be achieved by using dual layer spinning technology. In this technology, hybrid polymer may be used in the sheath layer with an inexpensive polymer (e.g. cellulose acetate) as in the core layer. The main challenge here is the miscibility of the two polymers in dual layer spinning. A simple miscibility test with different polymers may be a good starting point for this objective.

7.2.4. Hybrid Membranes As Asymmetric Hollow Fibers – Surface Adhesion

Although in hybrid dense film work excellent polymer-sieve adhesion was achieved with (6FDA-6FpDA-AlPO-14), for mixed matrix hollow fiber spinning this may be a problem (as mentioned above), thereby possible needing a molecular sieve surface treatment to overcome this problem. Work by Husain showed excellent polymer-sieve matching without any surface treatment of the molecular sieve with SAPO-34 as a molecular sieve in Ultem® polymer matrix due to the low number of acid sites and less hydrophilic nature of SAPO-34 sieves (similar to AlPO-14) [4]. At this point it is believed that no extra surface modification is necessary, but in the case of any lack of polymer-sieve adhesion, work by Shu and Husain may be implemented [4, 5].

7.3. References

1. Cussler E. L., *Membranes containing selective flakes,* JMS, 1990. **52:** p. 275-288

2. Omole, Imona, *Crosslinked Polyimide Hollow Fiber membranes for Aggressive Natural Gas Feed Streams*, 2008, Georgia Institute of Technology, GA.

3. Hillock, A.M.W. and W.J. Koros, *Cross-Linkable Polyimide Membrane for Natural Gas Purification and Carbon Dioxide Plasticization Reduction.* Macromolecules, 2007. **40**: p. 583-587.

4. Husain, S., *Mixed Matrix Composite Hollow Fibers for Gas Separation*, in *Chemical Engineering*. 2003, Georgia Institute of Technology: Atlanta, GA.

5. Shu, S., S. Husain, and J.K. William, *A general strategy for adhesion enhancement in polymeric composites by formation of nanostructured particle surfaces.* The journal of physical chemistry C, 2007. 111(2): p. 652.

6. Laius, L.A., Tsapovestsky, M. I., *Polyamic Acids and Polyimides – Synthesis, Transformations and Structure*, Edited by Bessonov and Zubkov, CRC press, **1993**. p. 47-99.

APPENDIX A

SYNTHESIS PROCEDURE OF 6FDA-6F$_P$DA POLYMER

As Chapter 3 discussed, the 6FDA-6FpDA used in this work was synthesized in the laboratory. 4,4'-(hexafluoroisopropylidene) diphthalic anhydride (6FDA) and 4,4'-(hexafluoroisopropylidene) dianiline (6FpDA) were used to produce a polyimide via polycondensation reaction. Before synthesizing, the monomers were sublimed to gain high purity. In case of small amount of monomer to be sublimed, a small sublimation flask was used. A schematic of the sublimation flask is shown in Figure A.1. The system was held under vacuum. The monomer was then heated in an oil bath with the sublimation flask and the cold finger. The monomers were heated around 15-20^{0}C below the sublimation temperature. The cold finger was maintained at a continuous low temperature by the flow of water. The purified monomers were then used for the polyamic acid formation.

The polyamic acid synthesis was carried out in 1-methyl-2-pyrrolidone (NMP) with ice-water bath for 18-20 hrs. The reaction was performed in a dried environment. All glassware used was dried in a vacuum oven at 200^{0}C overnight and then flame dried three times in alternating nitrogen and vacuum atmospheres prior to the start of the reaction. All solvents used were obtained in anhydrous, sure seal containers, and further dried by storing over dried molecular sieves (Aldrich, Molecular Sieves, 4A, beads, 8-12 mesh). The reaction was performed under positive pressure nitrogen.

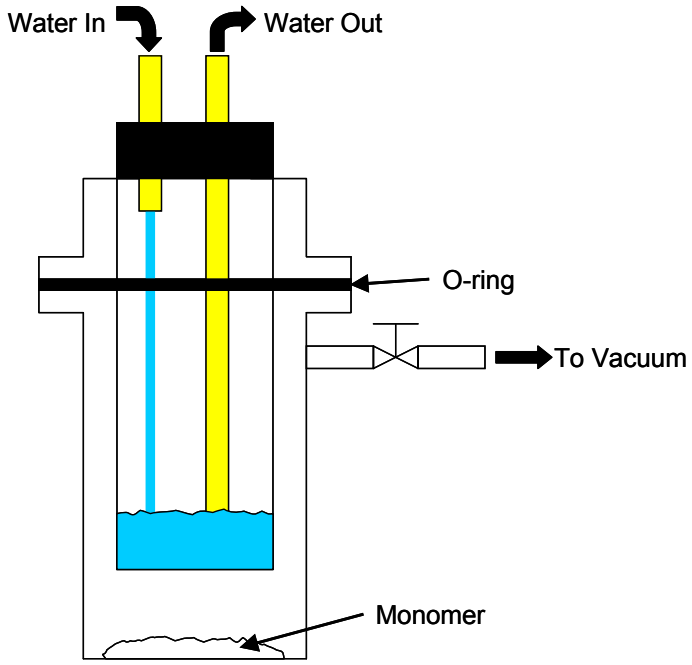

Figure A.1 The monomers were purified by sublimation in a glass sublimation flask as shown. The flask was submerged in a heating oil bath on a hotplate to provide the temperatures necessary for sublimation to occur.

For the synthesis reaction, a pre calculated precise amount of diamine was added to the reaction flask with 80% amount of total required NMP. The solution was stirred with a magnetic egg shaped stir bar. Once all the diamine was dissolved, dianhydride was added portion wise and then the remainder NMP was added to the reaction flask. The reaction was then carried out for 18-20 hrs with continuous low nitrogen purging.

After the polyamic acid formation, the imidization was performed using chemical imidization. A mixture of acetic anhydride and beta picoline was used to complete the imidization reaction. The beta-picoline acted as the catalyst for the imidization reaction whereas acetic acid was the dehydrating agent. Beta-picoline was added with the highly

viscous polyamic acid solution and mixed well before adding acetic anhydride (drop wise). The system was then reacted for 18 hours at room temperature.

The polymer was removed from solution by precipitating into pure methanol. The solution was slowly poured into the methanol bath to facilitate complete phase separation. The resulting polymer was then placed in a blender and just covered with fresh methanol. This solution was then blended thoroughly to produce slurry like mixture. The slurry was then filtered over a Buchner funnel, and the process was repeated three times (until a clear filtered solution was visibly observed). After the final filtration, the polymer was dried in a two step process: 1) dry overnight in a fume hood, 2) dry for ≥ 12 hrs at full vacuum above 200^0C. The polymer was then considered ready for use.

APPENDIX B

STANDARD OPERATING PROCEDURE FOR GAS CHROMATOGRAPH

Starting the GC

- Open the Helium and Air cylinders connected to the GC.
- Start the vacuum pump
- Make sure there is Helium and Air in the cylinder. DO NOT start the GC without Helium.
- Start the GC.
- Adjust the Helium flow to 30 ml/min
- Once the GC starts, then set the temperature to your desired sample test temperature. You can do it by pushing the “oven temp” knob and the entering the desired temp from the keypad followed by “enter”.
- Once the temperature is set, let the GC warm up for about an hour.

Running the GC

- After 1 hour, the GC is ready for any run.
- From the permeation system side, collect enough permeate gas to send to the GC (ideally 5 torr and above). Try to maintain similar permeate pressures with every run.

- Once the GC is ready for run, close the isolation valve between the GC and the vacuum pump.
- Immediately, open the valve connecting the system and the GC (this valve will be right inside/outside of your permeation box near downstream valve.
- Once the valve is opened, wait for around 1 min. 15 secs.
- After 75 secs. Close the valve between system and the GC.
- Immediately hit the start button on the GC.
- You will hear two sounds of pneumatic valves around 5 and 20 seconds after you have started the run.
- Open the vacuum pump right after you hear the second pneumatic sound.
- Wait for the run to be completed.
- Once the GC finishes the run, the paper will print the statistics.
- Note down the numbers and adjust it with the calibration value.
- Wait around one hour before you do the next run. This gives enough time to purge out the gases out of the GC column.

Shutting down the GC

- Set the oven temperature to 30^0C and wait for around 1 hour for the GC to cool down.
- Switch off the GC.
- After 15 mins, turn the regulators of the cylinders off.

Figure B-1 shows the response factor used for this research. Table-B-1 shows the sample RF calculation.

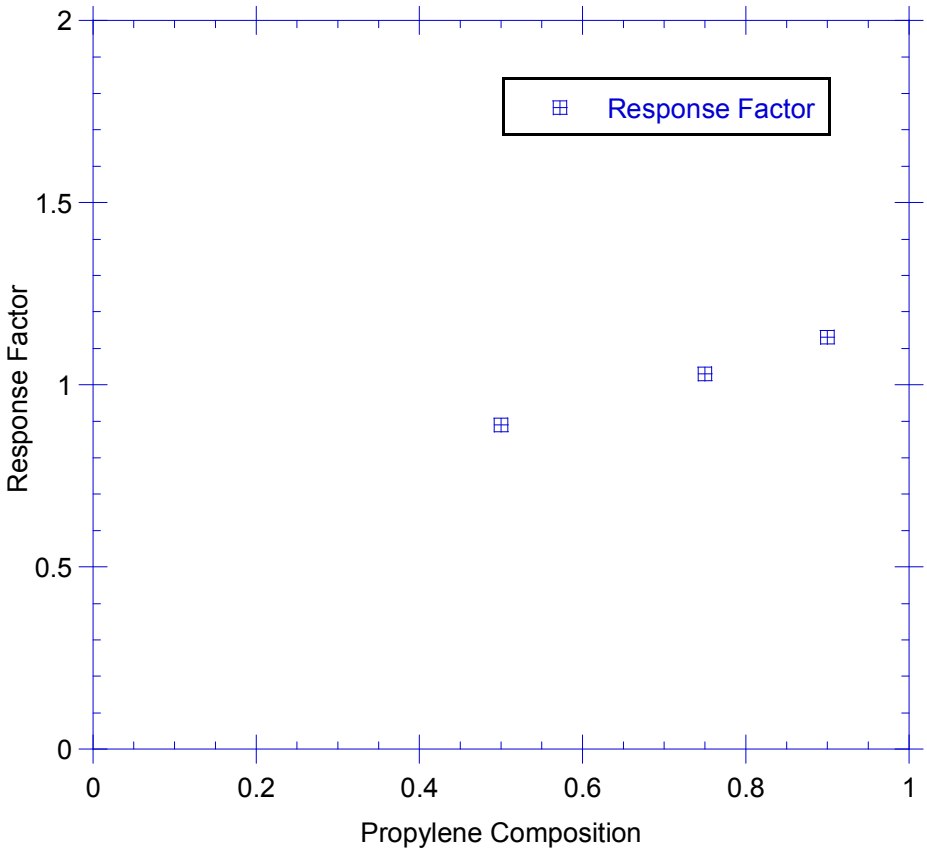

Figure: B-1: Response factor calculated for this study.